April 2015

Actuation Mechanism for a Switch-Mode Continuously Variable Transmission

Deanna Souza
Worcester Polytechnic Institute

Michael Patrick Sweeney
Worcester Polytechnic Institute

Norbert Hector Mongeon
Worcester Polytechnic Institute

Follow this and additional works at: https://digitalcommons.wpi.edu/mqp-all

ACTUATION MECHANISM FOR A SWITCH MODE-CONTINUOUSLY VARIABLE

TRANSMISSION

A Major Qualifying Project Report

Submitted to the Faculty of

WORCESTER POLYTECHNIC INSTITUTE

In partial fulfillment of the requirements for the

Degree of Bachelor of Science

by

Norbert Mongeon

Deanna Souza

Michael Sweeney

Professor Holly Ault, Advisor

April 30, 2015

Worcester Polytechnic Institute
100 Institute Road, Worcester, Ma 01609-2280

Abstract

With greater energy storage and power density than electric and hydraulic systems, a flywheel kinetic energy recovery system may prove to be a viable solution for increasing efficiency in passenger vehicles. A flywheel energy recovery system's primary obstacle is the connection between the high-speed flywheel and a vehicle's relatively low-speed drive train. A Switch Mode Continuously Variable Transmission (SM CVT) may accomplish this connection by using a high-speed clutch operating at a given duty cycle to output a specific torque. Previous research has been limited by the efficiency and wear of the clutch actuation system. The main goal of this investigation was to create a new mechanism for controlling the clutch's high-speed duty cycle with better efficiency, wear characteristics, and reliability.

An actuation method derived from variable valve timing technology was selected. This mechanism uses an eccentric cam to drive a set of linear cams at high speed to engage the clutch with roller followers. Each roller follower has an internal spring system to output the desired clamping force. Duty cycle is varied by changing the position of the eccentric camshaft. Experimental testing was carried out to characterize the performance of the prototype. Tests included clutch closure force, duty cycle, and camshaft acceleration. The device performed to expectations and shows significant improvements over previous designs, with no major wear issues and the ability to run at full speed and at any duty cycle.

Acknowledgements

Table of Contents

Table of Figures

Introduction

Between the pressures of a growing world population on finite fossil fuel resources, the political hotbed of anthropogenic climate change, and the push-and-pull relationship between economic/cultural factors and the new technologies of energy production, one thing is certain: the United States needs to find more efficient ways to use energy. One of the top industries in which there is room for great improvement is transportation. At present, automobile inefficiencies include brakes which lose mechanical energy to friction and heat every time the vehicle decelerates.

Kinetic energy recovery systems (KERS) use several methods to recover braking energy in automobiles. These systems utilize flywheels, batteries, or pressurized fluid to store the recovered energy. Flywheels are particularly advantageous for their high energy and high power densities (Van de Ven and Demetriou, 2011), which do not require as many potentially environment-harming chemicals as batteries or hydraulic systems. This project will focus on the flywheel approach.

Flywheel KERS were first introduced to the market in Formula One racing. KERS was legalized in the 2009 Formula One Season. Relatively few restrictions were placed on the KERS system in order to encourage more designs and create a better basis for implementation in a road car. With the switch from V8 engines to V6 engines in 2014, KERS are expected to play a larger part in Formula One in order to regain some of the lost power (Somerfield, 2014). Though the Flybrid KERS was initially developed for motorsports (Cross and Brockbank, 2009), its applications are now being explored for public transport. Having KERS systems on buses will tremendously improve the fuel economy of their stop-and-go driving patterns. The demand for these systems in civilian automobiles is also increasing, igniting the initiative for this project.

In Formula One, the boost from the KERS is activated when the car is already moving: when the vehicle travels at a high speed, the KERS feeds additional energy into the drivetrain. The KERS boost in a road car would most likely engage when the car accelerates from rest, a period of time during which the combustion engine operates it its least efficient capacity. This poses a problem: how can a fast spinning flywheel transfer power to stationary road wheels? Road cars would require a KERS setup that allowed more control over discharging energy from the flywheel. To achieve this control, researchers at Worcester Polytechnic Institute (WPI) and the University of Minnesota (UMinn) (Van de Ven and others, 2008-2015) developed a flywheel system with an integrated switch-mode continuously variable transmission (SM-CVT). This SM-CVT works by alternating between on and off states with a variable duty cycle, giving it complete control over torque transfer.

As work on the SM-CVT progressed at WPI and UMinn, each successive study focused on a different aspect of the system. First, the system's feasibility was explored with a mathematical model. Then, the necessary parameters for its use in a passenger vehicle were better defined and a small-scale prototype was built, with particular attention paid to the creation of a novel spring to transmit torque into and out of the flywheel, but the prototype's frictional losses were significant. Another mathematical model yielded promising results, but when the next project on the topic created a prototype of an alternative novel spring, it couldn't maintain the necessary torque. The next prototype had a stronger system for dealing with torque, but again, frictional losses were a major problem. There was significant room for improvement in the engagement of the clutch, which led to the intervention of this project.

Literature Review

Flywheel hybrid engines require a continuously variable transmission (CVT) to couple a high energy flywheel, whose angular velocity can be modeled as constant, to a vehicle's drivetrain, whose angular velocity can range from nothing when the vehicle is at rest to the speeds of passenger vehicles. Usually, an engine must produce power to move a vehicle at every state between rest and the engine's maximum RPM. A CVT improves efficiency by taking in the energy produced by an engine at its optimal conditions and outputting only the power needed by the vehicle for whichever velocity or acceleration the operator chooses (Harris, 2005). The variety of CVT's are discussed in more detail below.

This project represents the next step in work started in 2008 by Van de Ven and Forbes. They proposed to couple a high energy density, high power density, high speed flywheel to the wheels of a passenger car with a switch-mode continuously variable transmission (SM-CVT). In this transmission, a clutch, a flywheel and a spring allow the input shaft to maintain a constant angular velocity while the output shaft changes with the needs of a passenger car (Figure 1). Van de Ven and Forbes used a finite difference model to mathematically simulate a passenger car in a standard situation: accelerating from a stop to 13.4 m/s (30mph). The model indicated that with a SM-CVT, a flywheel could store enough energy to accelerate the vehicle even beyond the 13.4 m/s goal without the need for another source of power. Thus, it could be a viable hybrid power source for an internal combustion engine (Forbes and Van de Ven, 2008).
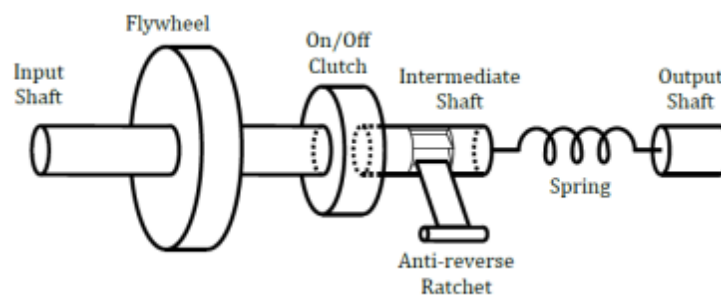
Figure 1 Van de Ven and Forbes's 2008 simple SM-CVT diagram (Forbes, 2008)

The next year, Van de Ven and four WPI MQP students designed a scaled-down prototype for the SM-CVT. For optimal human comfort, the design team determined that the transmission's switching frequency should be 20 Hz. They were able to find an electromechanical clutch by REELL that would operate at this frequency, but its torque transfer could not exceed 6.8 N*m (75 in*lb). The prototype's flywheel was designed not to exceed the clutch's limitations. The main body of Araujo, DeMalia, Lambusta, Morocco and Van de Ven's efforts went into the design of a novel spring for the SM-CVT. It had to have a particular spring constant and the ability to transmit torque both into and out of the flywheel. Their design comprised of rectangular bars arranged in a circle and capped at each end (Figure 2). After building and testing the prototype, they found that the main drawback of the system was its frictional losses (Araujo et al, 2009).

Figure 2 Araujo et al's prototype Torsion Spring (Araujo, 2008)

In 2011, three more WPI MQP students continued work on the SM CVT. They also created a novel spring, this one specifically for low energy loss, high deflection, and a low moment of inertia. After much deliberation, Collins, Rotier and Woodnorth decided upon a Cam Separation Spring that could translate linear motion into rotational motion and torque load into linear compression. They reduced the space used by employing a mirror cam, with symmetrical faces on each side rotating independently from the input and output shafts (Figure 3). Jerk was controlled by the cam's seventh degree polynomial. The system's challenges included axial thrust from the linear springs binding the system, additional torque shearing a pin in the input shaft, and the bicycle disc brake they employed failing to provide constant resistive torque. As with previous work on the SM-CVT, frictional losses were significant; Collins, Rotier and Woodnorth used a roller bearing or sleeve bearing anywhere friction would occur, and still had to resort to the use of molybdenum grease in the trial rig (Collins et al, 2011).

Figure 3 Collins et al's Cam Separation Spring (Collins, 2011)

In the same year, Van de Ven and Demetriou published another mathematical model of the SM-CVT. The goal of the model was to make the torque from the rotation of the spring match the output torque by controlling the switching time. The model indicated that the system would experience equilibrium with the output torque at its desired magnitude when the output shaft had zero velocity-- but in that case, the system could not reach and stay at the desired torque magnitude (Van de Ven and Demetriou, 2011).

The most recent work on the SM-CVT was performed by Cusack (Cusack, 2013; and Van de Ven and Cusack, 2014). The prototypes mentioned above both employed the REELL model EC75 electromagnetic clutch, with its sufficient duty cycle and insufficient capability to transfer torque. Cusack's goal was to design a new clutch to meet the SM-CVT's unique needs. It had to have fast engagement and disengagement; ideally, the clutch would be a binary system between those two states. It also had to be efficient, with a way to control the duty cycle. Cusack's prototype connected

input to output through friction disks, the motion of which was controlled by an axial cam mounted on the flywheel (Figure 4). Unfortunately, frictional losses crippled the testing of the SM-CVT prototype.
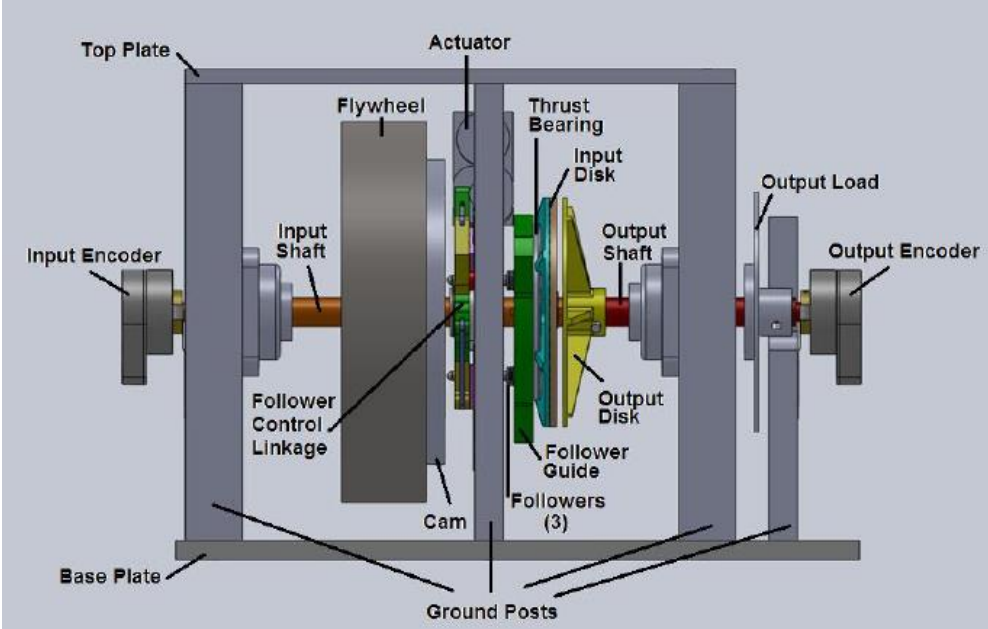
Figure 4 Assembly showing location of components in Cusack's design (Cusack, 2013)

Goal Statement

This project focused on improving the current actuation system of the switch mode continuously variable transmission. The goals of this investigation were to improve the efficiency and feasibility of the switch mode continuously variable transmission. To do this the team designed the actuation system for maximum efficiency and experimentally tested it in prototype form. Success was evaluated by comparing the new system to previous designs.

Background

Continuously Variable Transmissions

Continuously Variable Transmissions (CVT's) are increasingly popular because they allow the car's engine to run at a single speed which can be a specific RPM where the most power and best fuel economy are found. In a regular transmission it is necessary to increase engine speed through a range of RPM's to shift through every single gear. A majority of the time, the engine is not operating at its optimal speed. To solve this problem, designers have created several types of CVT's.

The most common CVT is the variable-diameter pulley (VDP), in which a V-belt which runs between V-belt pulleys. These pulleys increase their gear size by moving their sheaves closer to each other. As the sheaves move closer, their movement squeezes the belt outwards, increasing the radius of the equivalent gear. Figure 5 shows the driving pulley and the driven pulley changing gear ratios.
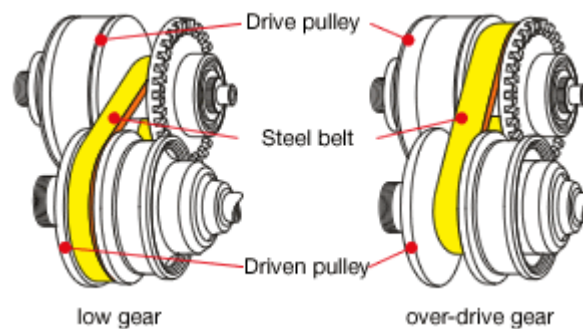
Figure 5 Variable Diameter Pulley CVT (Harris, 2005)

In a toroidal CVT, rollers transfer torque from the input disc to the output disk. By adjusting the angle of the rollers, different gear ratios are achieved. This CVT system is implemented in the Flybrid design and seen in Figure 6. The picture on the left shows the rollers at an angle where the input and output are at a 1:1 ratio while the picture on the right shows the rollers rotated to achieve the largest differences in speed.
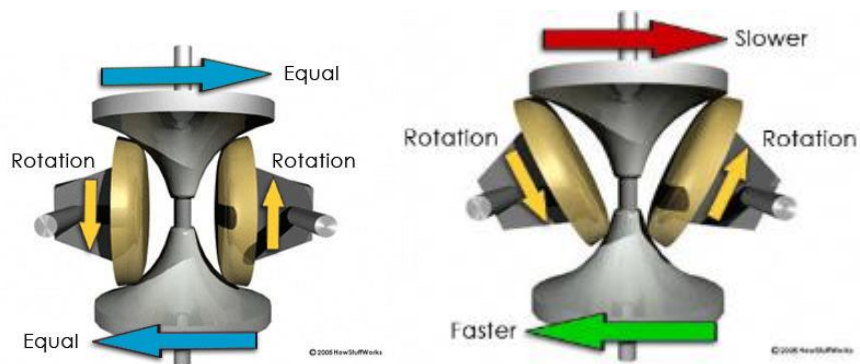
Figure 6 Toroidal CVT (Harris, 2005)

Other types of CVT's include ratcheting, hydrostatic, naudic incremental, cone, radial, and planetary. The major downfall when pairing any of the above mentioned CVT's to a high speed flywheel is that they have a limited range of drive ratios. High rotational speed is required for the flywheel in KERS due to the flywheel kinetic energy equation seen in Equation 1. Since the flywheel geometry is

6

constrained by the size of the vehicle, the only way to increase the kinetic energy is by increasing angular velocity—a squared term with a large effect on the amount of energy the flywheel can store. Therefore, most KERS flywheels spin at 65,000 RPM. To transfer this energy from the flywheel to a stationary car, a high ratio is desirable. For example, a vehicle moving at 5 mph, with a differential ratio of 3.5 and tires that measure 30" in diameter, must have a KERS transmission ratio around 1:331. When the same car is moving at 70 mph, the KERS transmission ratio will be around 1:23. Due to restrictions on component sizes, most existing CVT designs are limited to ratios close to 1:1.These designs rely on clutch slippage when propelling a car from a stop. This clutch slippage is an inefficiency that can be reduced using a SM-CVT.

$$E_F = \frac{1}{2} \cdot I \cdot \omega^2$$

$$E_f = \text{Flywheel kinetic energy}$$

$$I = \text{Moment of inertia}$$

$$\omega = \text{Angular velocity}$$

Equation 1 Kinetic Energy of a Flywheel

The SM-CVT is a promising solution to this problem. It is the mechanical analog of the digital DC-DC boost converter (Forbes and Van de Ven, 2008). It operates in fully on and fully off states. During fully on, 100% of the flywheel's torque is being transferred. During the off state, there is no torque transfer. From switching states at different duty cycles, this system can transmit torque at any desirable ratio ranging from 0:1 to 1:1. This is seen in Figure 7, where each application of the clutch is transferring torque to the output shaft. As seen in Figure 1 above, this clutch is attached to a spring that reduces the vibrations from the rapid switching. The anti-reverse ratchet disables the spring from unwinding when the clutch is disengaged. To charge the system from braking, the clutch is engaged while the output shaft is spinning faster than the flywheel.
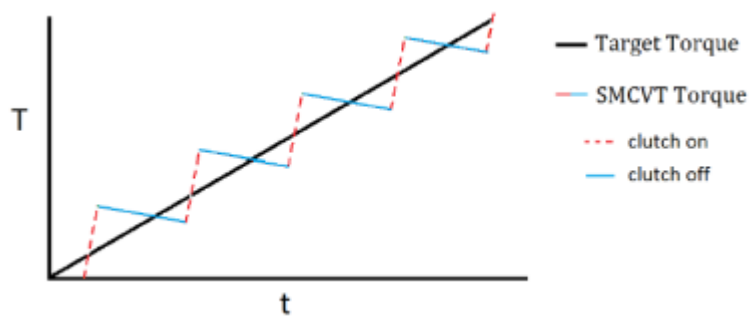
Figure 7 Cusack's Torque vs Time Graph for SM-CVT

Cusack's Work

Cusack's previous work on a SM-CVT transmission included designing, prototyping and testing a system that actuated the clutch through an axial cam that varies radially. The entire design is seen in Figure 4 above**Error! Reference source not found.**. This diagram shows a flywheel that is rotated to a set speed. This provides rotational energy to the input shaft. The actuating system, seen in Figure 8, is composed of three followers that can be adjusted radially. These followers ride on a 3-D cam that is fixed on the flywheel. This eliminates the need for a gear system or electric motors to power a camshaft. The axial cam is beneficial in the SM-CVT because the axial motion is in the direction needed to simply engage the clutch by pushing on the followers. The followers close the clutch by applying a specified force with Bellville Springs. This force translates through a follower guide to the thrust bearing. The thrust bearing pushes against the input disk and clutch as seen in Figure 9. When the clutch is closed, the output shaft becomes coupled to the input shaft through the input disk. A brake rotor and caliper are used to simulate a resistive torque on the input shaft that represents a car accelerating from a stop.
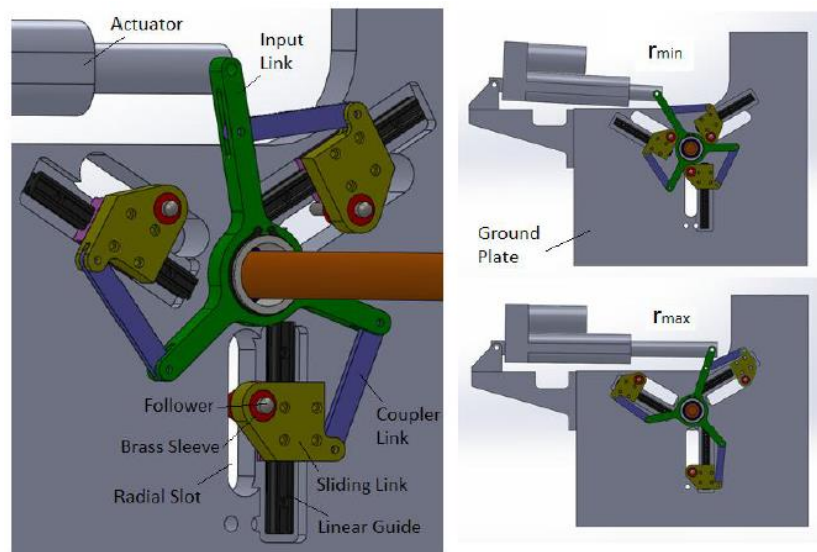
Figure 8 Cusack's Actuating System (Cusack, 2013)
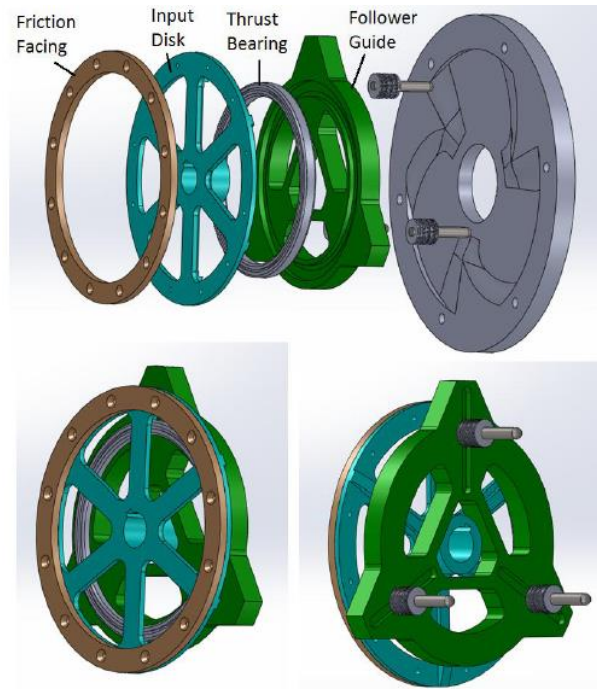
Cusack's system to control the duty cycle utilized the radial characteristics of the cam. Initially the followers started near the center of the axial cam. When the actuating mechanism pulled the followers out radially, the cam profile changed from full low dwell to include a rise, high dwell, and fall. The further the followers moved radially from the center of the cam, the longer the high dwell was and the longer the clutch was applied. The cam layout varied from 0% to 50% high dwell or duty cycle. For every rotation of the flywheel, the clutch engaged three times with each system actuation: once for each of the followers.

Testing showed that, at its maximum, the system was 33% efficient. This low efficiency had several causes. First and foremost, follower wear could be observed on the point followers and on the cam's surface. The HB1 clutch material's deformation under load also resulted in low efficiency. The design did not account for the compliance in the clutch material because the clutch material was thought to be less compressible. This offset the closure force generated by the follower springs and therefore allowed the clutch to slip longer during engagement.

A drawback to Cusack's design was that the cam could not be larger than the flywheel. The distance between the followers and the center of the cam controlled the duty cycle. Since the followers could only move a finite distance away from the center of the cam, the design's duty cycle was limited to a maximum of 50%. Even to achieve the 50%, the shape of the fall segments of the cam had to be adjusted into a spiraling ridge. The fall segment of the spiraling ridge created unwanted forces on the follower, pushing it toward the cam's center. In addition, the follower could only have point contact on the cam's surface because of the geometry that the rises and falls exhibit.

Variable Valve Timing

Variable Valve Timing (VVT) technology incorporates a number of mechanisms that are pertinent to the variable clutch application in the SM-CVT. Therefore it was worthwhile to investigate existing VVT solutions to vary a cam motion program.

Varying the timing of the intake valve in an internal combustion engine can improve the engine's efficiency. VVT mechanisms have the ability to vary the intake valve's phase, when the valve opens relative to the crank angle; lift characteristics, which adjust the distance the valve travels as well as the velocity and acceleration of the motion; and duration, the amount of time the valve remains open. All of these characteristics can be varied to produce more optimum valve motion for a particular angular velocity of the crank shaft. While there are many different systems used in automobiles today, only a few meet the needs of the SM-CVT mechanism (Erdman, 1993).

One of the most common types of VVT systems is the use of multiple cams one at a time. This type of mechanism employs one cam until the crank shaft reaches a certain speed. Then the follower switches to a different cam. Honda's VTEC system uses this method. While this system is relatively simple, it can only have as many motion programs as it does cams. This would not be ideal for the SM-CVT mechanism, because duty cycle must be continuously variable. However, this same principle can be combined into one cam with a profile that varies over its axis. Instead of switching from cam to cam, the cam shaft simply slides along its axis as shown in Figure 10. This method has the benefit of continuity. Unfortunately, manufacturing a three-dimensional surface accurately is considerably more difficult than cutting a standard two-dimensional cam profile.
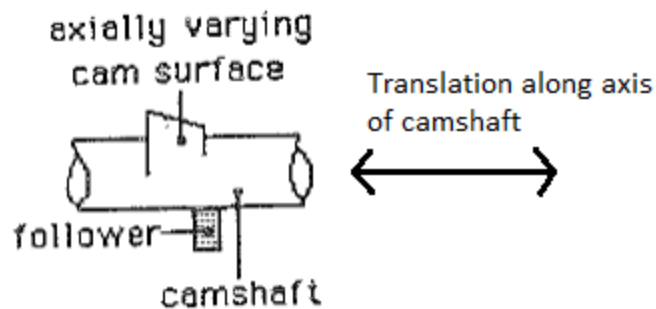
Figure 10- Erdman's Example of an axially varying cam surface (Erdman, 1993)

Another interesting possibility of using VVT technology to vary the dwell time in the SM-CVT is variable motion drive: a system where a valve is driven by an actuating cam which in turn is driven by either another cam or a linkage. Variability is achieved by changing the geometry of the system that is driving the actuating cam.

Figure 11 shows an example of variable motion drive where the valve is driven by a linear cam sliding back and forth. The oscillating motion is achieved through an eccentric cam attached to the face cam via a link. The mechanism is essentially a four bar crank slider. To vary the motion program the position of the eccentric shaft is varied transversely. Varying this position also varies the portions of the cam that are used. To spend more time at the high dwell, the shaft can be translated to the right; to spend more time at low dwell, the shaft can be slid to the left.
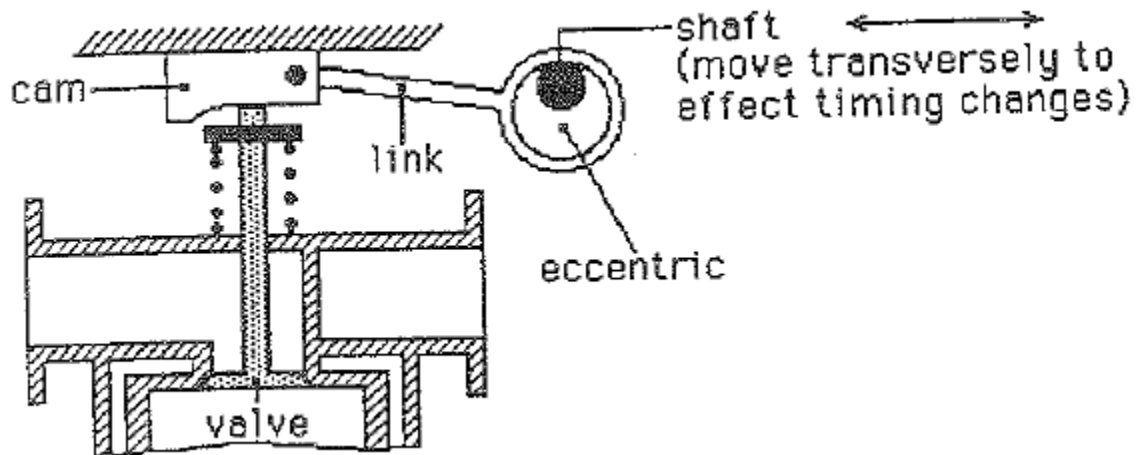
Figure 11 Variable motion drive with an eccentric cam (Erdman, 1993)

A variable motion drive system offers multiple benefits to the SM-CVT that other VVT mechanisms do not. This particular system can vary dwell time without varying the distance of actuation. Furthermore, it offers a great amount of variability limited only to the size of the face cam and the distance the shaft can be translated. The design team for this project deemed this system worthy of further consideration.

Williams's helical cam shaft

The William's helical camshaft is a very recent development in VVT technology. This device was patented in 2004 by Danny Russel Williams. Williams attempted to create a VVT mechanism that varies only the length of time the valve is open or the cam's dwell length. Other VVT technologies can only vary the time the valve is open by opening the valve to greater distances, therefore taking more time. Williams describes his own mechanism as "a new type of mechanical Variable Valve Actuation system (VVA). More specifically it is a camshaft which allows the valve opening duration to be varied over an extremely wide continuous, stepless, range – all the added duration being at full valve lift" (Williams, 2014).

Williams's mechanism itself is simpler than it actually seems. The cam is split into two sections, a stationary rise, shown as 4 in Figure 12 and a variable section of the remaining cam profile shown as part 2. Part 2 is mounted onto the outer portion of the shaft and can be twisted such that the helical slot in which part 4 resides causes part 2 to move transversely. Part 2 is analogous to a thread, while part 4 is analogous to a nut. The helix also allows one side of the variable lobe to have a longer dwell. This can be seen in Figure 12 where figure 1A shows the mechanism at one extreme end, possibly a low length high dwell and figure 1C shows the variable cam lobe translated to the other end at a high length high dwell.
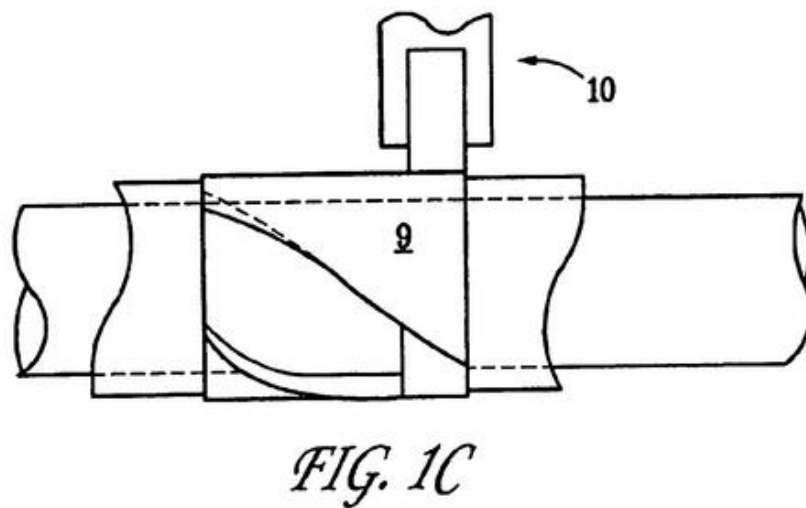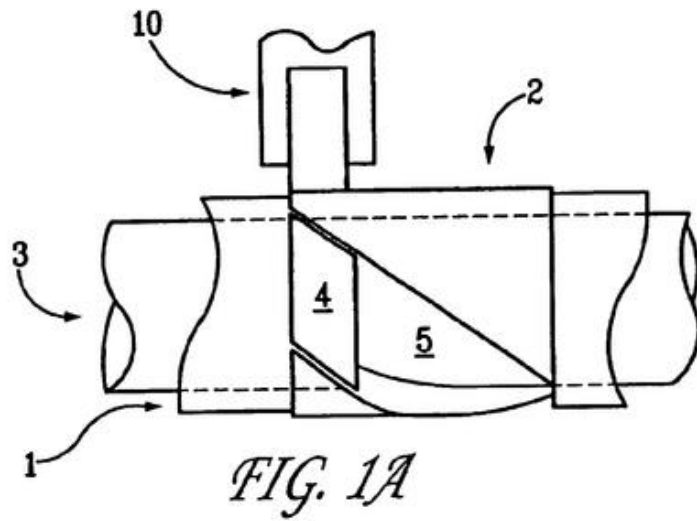
Figure 12 Williams helical camshaft mechanism (Williams, 2004)

It remains to be seen whether this mechanism will be practical to use in automobiles, but it is interesting for the sake of this investigation since it is one of the few VVT technologies that can vary dwell without varying lift. Describing the possible range of dwell, Williams said, "The WHC importantly differs from other members of the general class by having a unique helical movement – a combined circumferential and axial movement of the two profiles. Surprisingly, because of this movement, the WHC in theory has no practical upper limit to its duration range. That is to say, the duration can be increased until the closing flank of the cam lobe reaches the opening flank" (Williams, 2014). Simply put, this mechanism is only limited by the width of the stationary flank. If the stationary flank is a rise with a beta value of ten degrees, then this mechanism could produce a variable high dwell of anything

between zero degrees and 350 degrees. This is one of the few mechanisms this project's design team found which achieves the amount of variability necessary in an SM-CVT.

Design Specifications

Based on the research of previous SM-CVT investigations and variable mechanism concepts the following set of task specifications were developed.

The following task specifications needed to be achieved:

1. **Clutch must be capable of engagement in 0.45ms.**
A 0.45ms engagement time is the worst case condition to limit slip as shown by Forbes et al. (2008). To test this specification, load cells were used to measure the time from when the clutch makes contact until full closure force is applied, thus recording the time for engagement.

2. **The mechanism must apply a uniform clutch closure force of at least 450 lbf.**
Minimum closure force of 450 lbf was necessary to achieve a torque resolution of 51 lbf*ft with a clutch dynamic frictional coefficient of 0.5 and a mean radius of 2.75. This specification was tested with load cells.

3. **The clutch air gap must be near 0.025" for quick engagement.**
In most standard transmissions the clutch has an air gap around 0.04" from the flywheel, while the air gap in Cusack's design was 0.025". To test this task specification, a spark plug gap gauge was used to compare the air gap chosen in the design with the actual air gap in the prototype.

4. **The mechanism should be able to vary duty cycle from 0% to 100% continuously.**
Varying duty cycle from 0% to 100% allowed for complete clutch lock-up, resulting in a higher torque output.

5. **The mechanism must be robust. Forces may not create plastic deformation of parts or cause failures.**
Stress analyses and careful material selection prevented parts from plastically deforming, which would have caused the system to break or malfunction. Compliance could be present as long as it was factored into the design analysis. To test this specification, components were analyzed visually and measurements of deformation were recorded after testing.

6. **Wear must be minimized so it will not interfere with testing. The device should operate for a minimum of 7,000 cycles to complete testing.**
Wear was monitored during testing. Wear of components could create inaccurate test data. Wear was inspected visually after testing and measured. A minimum of 7,000 cycles allowed for testing at 20Hz ranging from 0% to 100% duty cycle, collecting data at 10% increments for tests lasting 30 seconds.

7. **The mechanism must be simple with a minimum number of moving parts and complex geometry. In addition, off the shelf parts are preferred.**
Keeping the mechanism simple will increased reliability, improved test measurements, and aided in manufacturing.

The following task specs were "if possible":

8. **The mechanism should not create resonance in the SM-CVT or the vehicle, and avoid frequencies outside of 20Hz-40Hz.**

Previous work on the SM-CVT referred to a study that showed frequencies below 20 HZ can cause discomfort to vehicle passengers.

9. **The mechanism should be manufacturable and cost less than $480 to prototype.**

Most of the mechanism had to be manufactured on campus with the tools available and under the budget of a three-person MQP.

10. **The mechanism should fit in the SM-CVT with a volume of a 1' long cylinder with a radius of 1'.**

This volume is the rough allowable size of the actuation system within the full system. It should be mounted in a housing that it shares with the flywheel and clutch. Based on the size of regular transmissions, the housing size of 2'x2'x2' is reasonable. The actuation system is allowed to use half of this space. The spring can extend out of the transmission like a driveshaft that will have its own housing. To test this specification, measurements were taken and the volume calculated. This can be accomplished while designing the system.

11. **The mechanism should weigh 20 lb +/- 5 lb.**

The average transmission weighs 150 lb. The flywheel weighs 60lb, 40% of the system. The actuation system is allowed to weigh up to 15% of the entire transmission. The other parts include the housing, clutch, and spring which are 30%, 5%, and 10% of the system respectively.

To test this specification, all the device components were weighed. The mass of the system was calculated in the designing phase but also verified after the prototype was constructed.

Conceptual Design Selection

Several different designs were considered to increase the efficiency of the SM-CVT. These designs were then evaluated based on the task specifications to find the best possible solution to undergo further development.

Axial Cam Varying Radially

An axial cam that varies radially was a proposed solution to the actuation mechanism. This design could incorporate a cam similar to the one used in Cusack's prototype, shown in Figure 13. However, his cam system required several changes in order to reduce wear. The largest change would have to be the follower system, originally regular point followers. Figure 13 also depicts one rise on the cam with a color gradient to show the higher duty cycle at the edge of the cam. It is important to note the angle of approach that the follower made when rising and falling. When the follower contacted the rise section, it moved perpendicular to the outline of the high dwell. A roller follower could have been implemented here if the fall section of the cam had the same characteristics. However, during the fall section the follower exits high dwell at an angle, so a traditional roller follower could not be used in this scenario. As a result, Cusack used regular point followers.
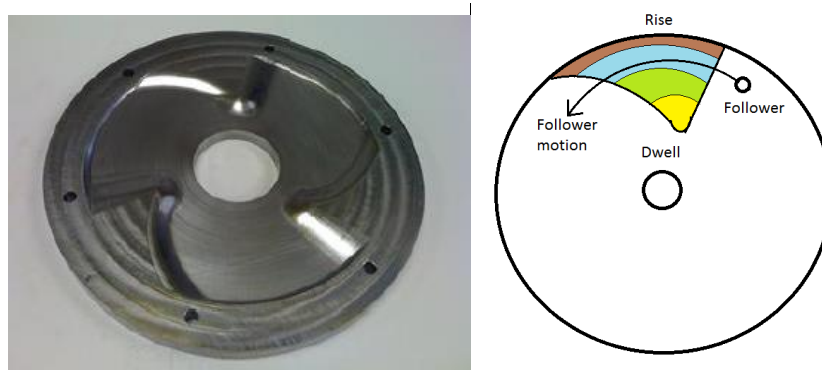
Figure 13 Cusack's 3D Face Cam (Cusack, 2013)

A spherical roller follower could have been an improvement over a point follower. This spherical roller follower would be similar to a ballpoint pen, seen in Figure 14. Lubrication could have been added by channeling oil down the follower to the roller tip (just as a ballpoint pen is lubricated by ink). This is common in pushrod designs on automotive engines. The biggest challenge would have been adding the spherical tip and determining the oil pressure required to allow the follower to roll smoothly.
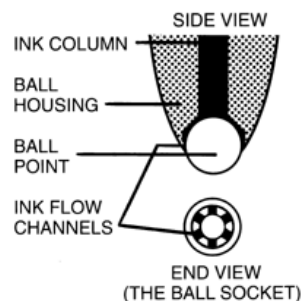
Figure 14 Inspiration from ballpoint pen to make custom followers (Kumar, 2008)

Radial Cam Varying Axially

A radial cam that varies axially could have been used to engage the SM-CVT clutch. This design was also a preliminary in Cusack's work and is seen in Figure 15. When the camshaft is moved in the axial direction, the cam profile's diameter changes where the follower makes contact. This type of cam can provide continuous variation of its profile in a smooth manner.
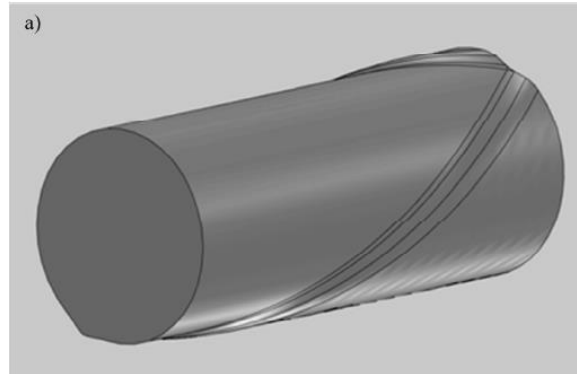
Figure 15 Cusack's proposed radial cam (Cusack, 2013)

When using this design for the SM-CVT, the duration of high dwell would either increase or decrease as the cam moved in the axial direction. The axial cam would start with a low dwell of 0% and end with a high dwell of 100%. Since this cam does not push its followers in the axial direction, it would have to be reoriented. The axis of the radial cam would need to be perpendicular to the input shaft for the clutch. This is seen in Figure 10, above. An electric motor or other power source would drive the camshaft. The cam would push on a follower which would pivot a fork similar to those found in a standard transmission, as seen in Figure 16 and Figure 17. This fork would also give the system mechanical advantage to protect against wear on the cam. However, increasing the mechanical advantage would require a higher rise on the cam.
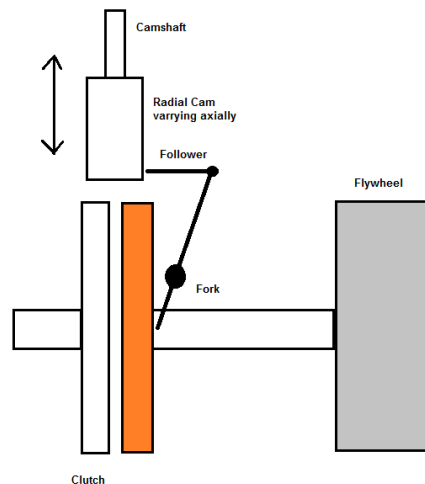
Figure 16 Actuation method for radial cam

Most radial cams that vary axially have large differences in radius from the start of the cam to the end of the cam. The axially varying radial cam for the SM-CVT would not need any difference in the respective radii of the high and low dwell segments, only different durations of high dwell and low dwell. This could reduce the axial pressure that most axially varying radial cams experience.

One disadvantage in this system is that the follower could only have point contact because of the rise and fall geometry of the cam (Erdman, 1993). This disadvantage is also shared with the previously mentioned axial cam.

Multi-cam Multi-phase

A multi-cam, multi-phase system uses phase angle adjustment to create the desired pulse width modulation shown in Figure 18. It is an elaboration on an old valve operation patent (Csandy, 1925). In order to apply the clutch, only one cam would need to be at high dwell, pushing on the follower. In the first pulse, cams 1, 2, and 3 would be at high dwell consecutively. The follower would have to hold its position from when cam 3 entered high dwell until cam 1 left high dwell. In the second pulse, the differences in cam phase angles would cause the high dwell of cams 1, 2, and 3 to overlap. In the last pulse shown, the phase angles would be aligned for all three cams. The duration of high dwell would be the minimum width achievable. In this particular scenario, the torque being transferred from the flywheel would decrease. This mechanism would work equally as well when increasing or applying constant torque transfer.
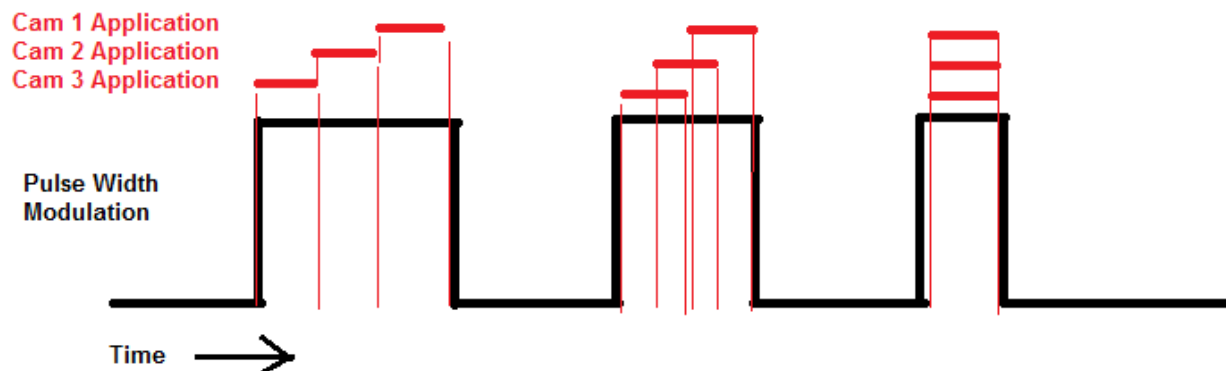
Figure 18 Pulse width modulation with multiple cams

The minimum dwell, shown in the last engagement above should be chosen with respect to the time needed for the clutch to lock up. Maximum dwell is the minimum dwell multiplied by the number of cams in the system or all the dwells added together. This represents the maximum attainable ratio between the flywheel and the output shaft as seen in Figure 19. The difference between the entire period, 100%, and the maximum dwell would be the range of ratios that are attainable between the flywheel and the clutch's output.
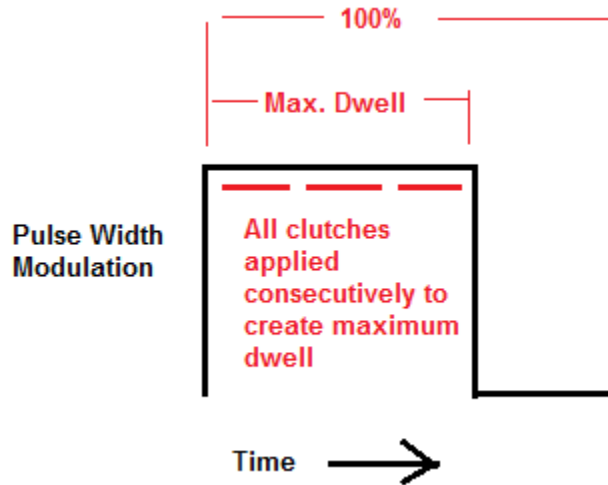
Figure 19 Determining maximum dwell in a multi-cam system

To select the number of cams that an application of this mechanism should have, tabulating several systems is a good place to start. Table 1 shows 2, 3, and 4 cam systems set up with maximum dwells of either 50% or 75%. This table uses Equation 2 and Equation 3: Equations for determining variablity in multi-cam design.

Sample configurations:

Table 1 Sample multi-cam designs

Number of Cams	Max Dwell %	Min Dwell %	Range
2	75	37.50	37.50
2	50	25.00	25.00
3	75	25.00	50.00
3	50	16.67	33.33
4	75	18.75	56.25
4	50	12.50	37.50

$$Range = \max dwell - \min dwell$$

$$\max dwell = \min dwell \cdot number\ of\ cams$$

Equation 2 and Equation 3: Equations for determining variablity in multi-cam design

A minimal number of cams, a large maximum dwell, a small minimum dwell, and a large range would usually be preferred in many designs. However, these variables are dependent on each other and

there is no solution with all these preferences. A design might have to increase the number of cams to increase its range. In addition, increasing the maximum dwell will also increase the minimum dwell.

When designing this multi-cam system for the SM-CVT, the four cam version with maximum dwell of 75% and 50% would be most promising. The 75% maximum dwell offers a large range of 56%, but it would have an undesirable minimum dwell of 19%. The 50% maximum dwell offers a smaller minimum dwell of 13%, but that would come with an undesirable low range of 38%. The original SM-CVT was designed to have a minimum dwell of 0% and a maximum dwell of 50%. This original design is superior in terms of range and minimum dwell but the 4 cam 75% maximum dwell setup could work if clutch lock up takes a relative long time of the 19% minimum dwell. If the clutch were to slip for 10%, a minimum dwell of 0% would not be desirable.

The top view of the system is shown in Figure 20. The first two cams are mounted on a camshaft to the left of the input shaft from the flywheel. This camshaft ends at a bushing which the input shaft goes through. On the other side of this bushing the second camshaft starts and holds cams two and three. The phase angles between all the cams are adjusted by cam phasers. These cam phasers can be either electromagnetic or hydraulic. The cams push on the follower. This follower is constrained to one degree of freedom to engage and disengage the clutch. This follower setup has a hole in the middle to allow the input shaft to continue to the clutch. When one or more of the cams are at high dwell, the follower pushes on the thrust bearing which is mounted on the clutch face. A 3D sketch of the system would show that there are four contact points for the application of the clutch, enabling even engagement. The camshafts can be driven by electric motors or by the flywheel that will turn at a constant velocity. Figure 20 shows the flywheel with a bevel gear that drives two intermediate gears to rotate the two camshafts.
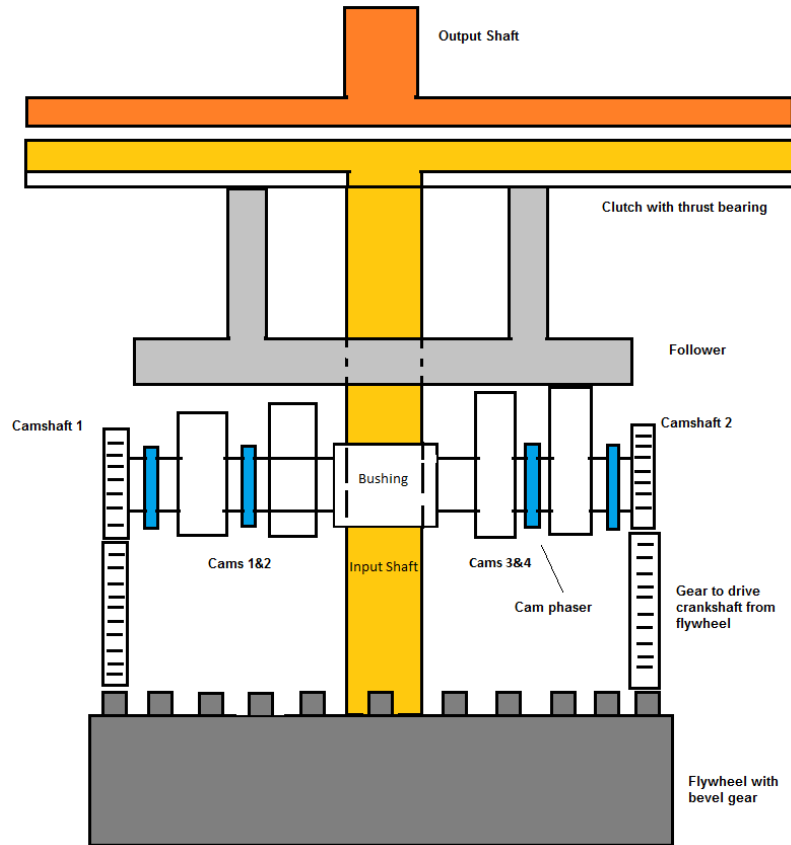
Figure 20 Multi-cam configuration

Variable Motion Drive

This design concept would apply the variable motion drive concept that was discovered through variable valve timing research. To apply this method to the SM-CVT, a separate shaft would be used to drive an eccentric cam and this eccentric cam would be used to drive a linear face cam. This mechanism must also vary the position of the shaft driving the eccentric cam. This will in turn determine the percentage of time the follower spends at the high dwell and low dwell of the linear cam. Figure 21 shows the possible follower positions for a 100% duty cycle and a 0% duty cycle. The 100% duty cycle would occur with the eccentric drive located in an extreme position such that as the cam would continue to oscillate the follower but not leave the high dwell. The opposite extreme position would produce a situation where the follower never left the low dwell. If the eccentric shaft could move to any point between these two extremes, then any duty cycle between these two extreme points could be produced.
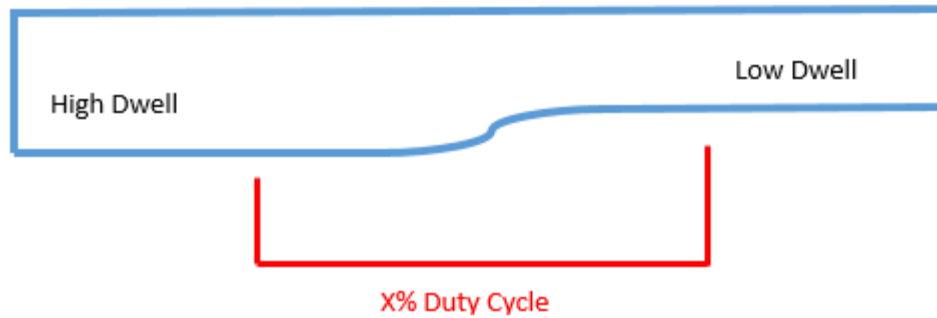
Figure 21-Linear cam with variable duty cycle

The entire system is visualized in Figure 22. The eccentric cam shaft is seen perpendicular to the main shaft of the system and protruding out of the page. By sliding this shaft left and right the follower's path on the linear cam is varied.
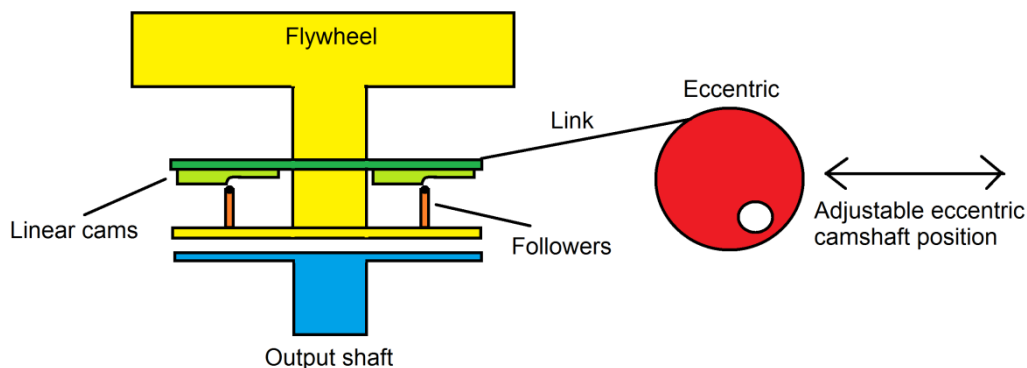
Figure 22-Sketch of variable motion drive applied to the SM-CVT

This system would provide advantages and disadvantages in comparison to Cusack's 3D cam design. Variable motion drive has the potential to vary duty cycle between 0% and 100% continuously while Cusack's system was limited to a maximum of 50% duty cycle. This is an advantage when the context of the SM-CVT is considered. Having a maximum duty cycle of 50% would equate to a maximum throttle of 50% in the vehicle; it is certainly desirable to be able to have more control over throttle percentage for performance reasons. Another advantage of this mechanism is that it is not limited to a specific number of followers. The 3D cam was limited to 3 followers because the number of followers was tied in to the number of cycles per revolution. This compromise produced large forces on individual followers which led to high stress concentration on the cam itself and eventually wore down the cam and followers to such a point that the clutch was no longer functional. This system could conceivably use 4 or more followers and cams to limit stress concentrations. In addition to adding more followers, standard roller followers could be used because the cams would only move in one direction. Roller followers have potential to limit wear and friction at the cam-follower interface and in turn decrease parasitic losses and improve the mechanism's efficiency.

Furthermore, this concept would de-couple the main shaft angular velocity and the switching frequency of the overall mechanism. This would give the design the ability to set the eccentric cam's angular velocity to one specific frequency and remain there as the shaft speeds up and slows down. One of the biggest advantages of this mechanism is the consideration of manufacturing. A 3D cam requires specialized equipment to accurately produce a smooth surface that is essentially a copy of the designed model. In this situation the cams are all two-dimensional profiles that could be cut on a typical CNC mill or other cutting method such as wire EDM.

While there are multiple advantages of this design there are multiple disadvantages as well. Since these cams would oscillate linearly, the cam must use the same section to control the rise and fall of the follower. This may be a disadvantage because it is desirable to engage the clutch and move from low dwell to high dwell as quickly as possible. Since a goal of cam design is to limit unnecessary acceleration it is undesirable to fall from the high dwell too quickly and this design would dictate that the fall is just as quick as the rise. There are also packaging constraints to consider since this design would add an additional sliding shaft and motor to the system and expand the overall footprint of the transmission. There are also vibrational concerns to consider as these cams would be oscillating at 20 – 40 Hz.

Williams Helical Camshaft

A Williams helical camshaft could be used to actuate followers that open and close the clutch with a given duty cycle. The promise of the Williams helical camshaft for the purpose of the SM-CVT can be seen directly, since it is a mechanism designed specifically to vary dwell continuously over a long range. Even the ability to vary a high dwell of zero degrees to 300 degrees would result in a variable duty cycle of zero percent to 83%. While this does not meet the goal of varying duty cycle between 0% and 100%, it would be a significant improvement over the Cusack mechanism which could vary duty cycle a total of 50%.

Similar to other design concepts, this system would require another camshaft added to the entire SM-CVT and possibly be driven by another motor. Decoupling the camshaft and the main shaft would again provide numerous advantages such as choosing one particular switching frequency that is independent of flywheel velocity. Additionally, the Williams helical camshaft allows followers to remain in the same position on the cam. While this concept is similar to the axially varying cam, point contact is not necessary. Standard followers could be used. Standard roller followers would be an improvement towards eliminating the parasitic frictional losses that plagued the efficiency of the SM-CVT in previous research.

However, the consideration of manufacturing poses a challenge to this system since these cams do not have simple two-dimensional profiles. The variable flank requires a helical cut and a variable dwell over its axial length. This would require some advanced machining or other manufacturing process. Despite the manufacturing considerations this is one of the few mechanisms found that is almost a direct application for the needs of the SM-CVT. For this reason it must be considered further.

Electromagnetic Clutch

An electromagnetic clutch uses coils on one side of the clutch to pull two friction plates together. Electromagnetic clutches are commonly used to control the transfer of power from an automobile's engine to its air conditioning compressor. An electromagnetic clutch is an intriguing way to

operate the SM-CVT since it is an existing clutch technology that can be turned on and off without mechanical input.

The biggest advantage of an electronic system like this is the flexibility that can be achieved through programming and electronic control (Norton, 2012). This concept can be thought of as a servo motor with the capacity to easily change its motion program. Changing the motion program of standard cam is far more difficult. Furthermore an electronic clutch would be a very simple addition to the existing SM CVT prototype since it would not involve any additional moving parts. All that would be needed is to replace the existing friction clutch with an appropriate electromagnetic clutch and apply an appropriate control package.

However promising electromagnetic clutches are for this application, there are very limited commercially available options. Previous research by Van de Ven et al. [3] used an electromagnetic clutch manufactured by REELL. This clutch was limited to a maximum torque of 6.8 N*m (75 in*lb). To put this in perspective Cusack's work showed that the required torque of the clutch would be about 400 N*m for reasonable application in a hybrid vehicle. While this clutch from REELL is capable of meeting the engagement time requirements this torque is unacceptable. The work done by Van de Ven and Cusack was done two or three years before this current investigation. As then, there are no current electromagnetic clutches that can meet both the engagement time and torque requirements necessary for the SM CVT. The current limiting factor is latency and maximum transmittable torque. Quickly engaging electromagnetic clutches use smaller coils to charge up quickly and smaller less massive clutch plates (Oberg et al, 2008). The result of this is a smaller maximum torque. This is something to consider since any time between engaged or disengaged is going to result in the clutch slipping and wasting energy. It remains to be seen whether an electromagnetic clutch could have both a quick engagement time and high maximum torque.

Decision Matrix

Not all of the design specifications can be used to judge the design concepts at this point because everything is in the conceptual phase. Judgment must be more qualitative than quantitative. With this in mind the design specifications were translated into qualitative specifications that can be given a score of 1-5 for each design.

1. Ability to vary duty cycle between 0% and 100%
2. Simplicity
3. Ability to generate a large clutch closure force
4. Potential for efficiency
5. Achieve required torque resolution
6. Ability to close the clutch with a force uniformly distributed
7. Can be packaged within the size of 1' x 2' x 2'
8. Weight of the actuation system should be under 20 pounds
9. The system should be simple to manufacture
10. The system should not produce undesirable vibrations
11. The system must exhibit a low potential for wear between components
12. The system must cost less than the team's given budget of $480

With this list of qualitative specifications a pairwise comparison was created to find weights for the design matrix. A score of 1 indicates the specification in the row is more important than the specification in the column, a score of 0.5 indicates equal importance between the row and column and a score of zero indicates the row is less important than the column. The row values are summed and each row is then found as a percent value of all the design specifications. This percentage is the weight that will be used in the design matrix.

	Vary Duty Cycle	Simplicity	Max torque/closure force	Efficiency	Torque Resolution	Uniform clutch application	Packaging	Weight	Manufacturability	Weight balanced	Low wear potential	Cost	Total	Weight
Vary Duty Cycle		0.50	1.00	0.50	1.00	1.00	1.00	1.00	1.00	1.00	1.00	1.00	10.00	15
Simplicity	0.50		0.50	0.00	1.00	0.50	1.00	1.00	0.50	1.00	0.50	1.00	7.50	11
Max torque/closure force	0.00	0.50		0.00	0.50	0.50	1.00	1.00	0.50	1.00	0.50	1.00	6.50	10
Efficiency	0.50	1.00	1.00		1.00	1.00	1.00	1.00	1.00	1.00	1.00	1.00	10.50	16
Torque Resolution	0.00	0.00	0.50	0.00		0.50	1.00	1.00	0.50	1.00	0.00	1.00	5.50	8
Uniform clutch application	0.00	0.50	0.50	0.00	0.50		0.50	1.00	0.50	0.50	0.00	1.00	5.00	8
Packaging	0.00	0.00	0.00	0.00	0.00	0.50		0.50	0.50	0.50	0.00	0.50	2.50	4
Weight	0.00	0.00	0.00	0.00	0.00	0.00	0.50		0.00	0.50	0.00		1.00	2
Manufacturability	0.00	0.50	0.50	0.00	0.50	0.50	0.50	1.00		1.00	0.00	0.50	5.00	8
Low potential for undesirable vibrations	0.00	0.00	0.00	0.00	0.00	0.50	0.50	0.50	0.00		0.00	0.50	2.00	3
Low wear potential	0.00	0.50	0.50	0.00	1.00	1.00	1.00	1.00	1.00	1.00		1.00	8.00	12
Cost	0.00	0.00	0.00	0.00	0.00	0.00	0.50	1.00	0.50	0.50	0.00		2.50	4

Table 2 Pairwise Comparison of Qualitative Specifications

The top five highest weighted design specifications were potential for efficiency, ability to vary duty cycle, potential to minimize wear, simplicity, and ability to generate a large closure force. Efficiency is the primary objective of this investigation and was certainly a hindrance of previous designs. To evaluate a design concept for potential for efficiency the team must consider potential areas for high friction or other parasitic losses. The ability of the design to vary duty cycle is also very important since duty cycle determines how much torque is transmitted from the flywheel. Cusack's prototype struggled to vary duty cycle quick enough to test a large range of duty cycles. It is desirable to have a design concept that can vary over a wide range of duty cycles and change duty cycle quickly. Potential for component wear is also considered a highly weighted design specification. If anything in the actuation system was to wear down the clutch would no longer be closed to its ideal position. This kind of wear could lead to the clutch slipping and wasted energy. Simplicity is the fourth highest weighted design specification. While this specification is not critical to the design's operation it is very important to consider. Simplistic designs tend to be more robust, reliable, and can often provide a better solution. These are all characteristics that are desirable in this system. The fifth highest weighted design specification is the ability of the design to generate a force sufficient to close the clutch properly. A friction clutch is only as good as the force behind it. In the case of Cusack's work, that force was 2045 N (460 lbs.). The clutch closure force is a key to preventing clutch slippage and therefore a key to efficiency. For this reason the clutch closure force was also weighted highly.

With the weightings calculated the designs were evaluated using a design matrix. Designs were given a score between 1 and 5 for each category. This score is then multiplied by its respective weight and then all of these values are summed together. The highest possible score is 500.

	Weight	3D Face Cam	3D Axial Cam	Multi-Cam	Variable Motion Drive	Helical Camshaft	Electromagnetic Clutch
Vary Duty Cycle	15	4	5	2	5	4	5
Simplistic	11	4	4.5	1	4.5	3	4
Max torque/closure force	10	4	4	4	4	4	1
Efficiency	16	2	3	4	4	4	4
Torque Resolution	8	5	5	5	5	5	1
Uniform clutch application	8	5	4	3.5	5	4	5
Packaging	4	5	3	3	3	3	5
Weight	2	4	3	3	3	3	2
Manufacturability	8	2	2.5	3	4	2	1
Low potential for undesirable vibrations	3	5	5	5	2	5	5
Low wear potential	12	2	2	4	5	3	5
Cost	4	4	3	2.5	3	3	1
Score (out of 500)		352	372	325	434	364	350

Table 3 Design Selection Matrix

The 3D Face cam was the first design concept evaluated. This design concept scored poorly in the most important category of efficiency. This is mainly due to the problems that Cusack's prototype exhibited where the flywheel would only remain spinning for very short periods of time. The original design of spherical tipped followers led to high friction at the cam surface. It remains to be seen whether a spherical roller follower could be created to solve this problem. The follower design also created high stresses at the cam surface which lead to the cam and follower wearing down to a point where they could not properly close the clutch. This design also scored poorly in the manufacturability category. Creating this surface very accurately would require some advanced processes such as selective laser sintering. As seen Cusack's previous design, inaccurate parts led to wear problems. The 3D face cam was given high scores for simplicity, ability to vary duty cycle, closure force, and uniform clutch application. This design is fairly elegant in simplicity in the way that it uses the existing spinning flywheel as the energy to power the actuation system. There are not many moving parts in the system other than the follower linkage. This design concept was ranked fourth out of the 6 concepts.

The second design concept evaluated was the 3d axial cam. This system received low grades in the areas of efficiency, manufacturability and wear potential. This system is thought to have poor efficiency because axially varying cams are typically run with point followers. This caused problems in Cusack's face cam so it may not be the best solution for a high speed cam generating high closure forces. This same reasoning led to a low score in the area of wear potential. Manufacturability also received a poor grade because the three dimensional surface would require an advanced manufacturing process to produce an accurate cam. Key areas of this design that were ranked highly include simplicity and torque resolution. This design also exhibits some simplicity since different duty cycles are created by varying the position of the axial cam linearly. Torque resolution was given a high score because it is only controlled by the angular velocity of the cam which can rotate at any speed. This design was ranked second out of the 6 concepts.

The Multi-Cam concept was evaluated next and received low scores in the areas of ability to vary duty cycle, simplicity and manufacturability. The ability of this design to vary duty cycle is dependent on the number of cams used in this design. A design with three cams is limited to the range of 25% to 75%. While 50% is an acceptable range of duty cycle it is essential that the SM CVT can produce a 0% duty cycle or a disengaged position otherwise the flywheel will always be somewhat engaged. Simplicity is perhaps the biggest issue with this concept since it would require three or more cams with independent angular positions. This would be difficult to control at high speeds especially considering the accuracy needed to produce a given duty cycle. Manufacturing this system would certainly be a challenge especially when considering how it must be controlled. This design scored well in the key areas of closure force, efficiency, torque resolution, and wear potential. Closure force is thought to be adequate since this design uses standard cams which tend to have high values of mechanical advantage. Efficiency was given a high score because these cams are not three dimensional and therefore are not limited to a point contact. The use of roller followers would help to eliminate large frictional forces at the cam surface which was most likely the largest parasitic loss in Cusack's prototype. Like the other cam concepts, this design is not limited to a specific torque resolution. Wear potential is thought to be a non-issue with this design since standard followers could be employed. This would help reduce areas of high stress at the cam follower interface and reduce areas of wear. Due to the very low scores in ability to vary duty cycle and simplicity this design received the lowest overall rating.

The fourth design ranked was the Variable Motion Drive concept. This design scored high in many areas including the top three heaviest weighted specifications of efficiency, ability to vary duty cycle, and potential for low wear. This design is thought to be more efficient and have a low wear potential because it can employ standard roller followers and eliminate areas of high friction and stress on the cam surface. The ability to vary duty cycle was given high score because this concept can vary duty cycle by simply moving a shaft translationally and should be able to produce any duty cycle desired. The simplicity of this design also led to a high score in manufacturability. This is an area where other designs fell short. This design can use two dimensional cams which are much cheaper and easier to make. Additionally, this design has a simple control system to adjust duty cycle. The one area where this design received a low grade was the area of vibrational concerns, due to the cam's oscillation. This is an area that would have to be addressed if this design was to be built. This design concept received the highest of these designs and outscored the second design by 62 points.

The Williams helical camshaft was evaluated next. This design is mainly plagued with complexity and manufacturability issues. This cam has the complexity of a 3D surface but also has the complexity of a helical slot. The efficiency was given a score of a four because it is believed that this cam could be integrated with a standard roller follower and partially eliminate the frictional parasitic losses. Since this design involved a cam it was also given a high score in the area of closure force and torque resolution. This design was evaluated to be the third best option.

The final design evaluated was the idea of using an electromagnetic clutch. This concept scored very poorly in the areas of torque resolution, closure force, and manufacturability. These three areas were given low scores because an electromagnetic clutch with fast engagement time and a high closure force does not exist. Any commercially available electromagnetic clutch would not be able to meet the torque resolution requirement of operating between 20 Hz and 40 Hz and the torque requirement 400 N*m. However, this concept received a high score for ability to vary duty cycle since it is entirely programmable. This concept also has no potential for component wear since the actuation is performed

electronically. Despite these advantages this design cannot be built with current technology. For this reason this design was considered the second worst option.

Through this evaluation process the Variable Motion Drive concept is considered to be the most promising. This concept promises reduced wear and increased efficiency in comparison to Cusack's design, with comparable simplicity. Furthermore this system requires no three dimensional cams to be made which makes it a much more manufacturable solution. For these reasons the team pursued the variable motion drive concept to control the actuation of the SM CVT.

Design Overview

Following the design selection matrices, a variable motion drive SM CVT was developed. Two models of the SM CVT were designed. The first was a full scale model which included all of the sub-systems. The second was a smaller model that mainly focused on the actuating system. The full scale model was important to have in order to design the actuating system that was developed for this MQP. In addition, the actuating system was designed to be easily incorporated into the full scale model for later development.

The full scale model includes rotating input and output shafts, a clutch, and the actuating system. As seen in Figure 23, the mechanism starts with a spinning flywheel. This flywheel stores the energy from regenerative braking and rotates the input shaft on which it is mounted. The actuating system is connected by a belt drive (not shown in diagram) to the input shaft. This eliminates an additional power source to run the actuating system. The belt drive spins an eccentric cam that is housed in the u-block on a steel camshaft. The u-block enables adjustment of the duty cycle because it is designed to slide toward and away from the drivetrain. The geometry of the u-block and its support stands allow this translational sliding adjustment. When the u-block is pulled out, away from the drivetrain, a higher duty cycle is obtained and vice-versa. The eccentric cam's camshaft rests on two steel roller needle bearings which are pressed into the u-block. Spinning the camshaft and eccentric translates four linear bearings back and forth via the eccentric strap. The eccentric strap has a press fit brass bushing to reduce friction with the aluminum eccentric. The strap shares a double pin joint with the cam holder. This cam holder sits on four linear bearings that support the four linear cams. The cam profiles were designed to decrease engagement time, to limit clutch slippage, apply the correct closure force, and prevent follower jump. Profile selection is explained in detail later. The motion of the cams is applied to four roller followers. These roller followers translate back and forth, parallel to the drivetrain, to apply the clutch. Each of these roller followers has its own spring system made out of arrangements of Bellville springs. The Bellville springs create a constant predetermined spring force to engage the clutch. The spring configuration and force are explained in detail later. In order to apply the clutch the followers push against the thrust plate. The thrust plate rides on the input shaft but does not spin because it is mounted on a roller bearing. A thrust bearing is placed in between the output disk with the thrust plate, allowing the output disk to rotate. The output disk is rotated by the input shaft with a keyway that still allows the output disk to translate along the input shaft to engage and disengage the clutch. The clutch material is attached to the output disk. When the clutch is engaged, it couples the input and output shafts. To disengage the clutch, an additional spring system is composed of wave springs to return the followers to low dwell. Design details follow. The output shaft has a brake rotor and caliper that simulates an automobile starting from a stop. This system incorporates the flywheel and clutch. Since this project is focused on the actuating system and because of budgetary and time constrains, several components were deemed unneeded, simplifying the system.
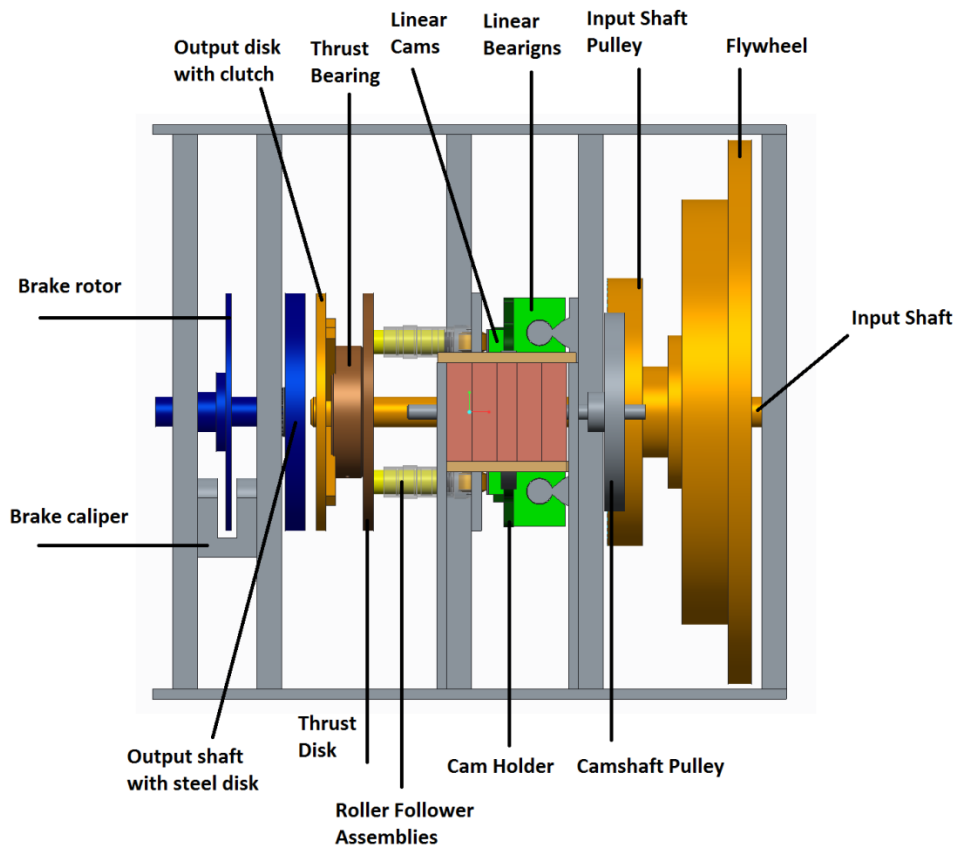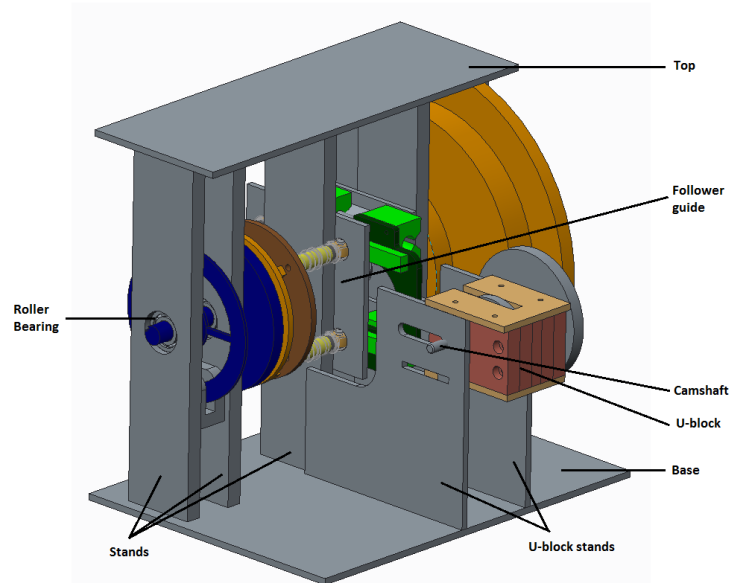
Figure 23 Full Scale Design

The actuation method model was prototyped for this project. This design is seen without the motor in
Figure 25.The model is very similar to the full scale design's actuating system in order to encourage

further work on the transmission. The cam shaft is chain driven by a permanent magnet electric DC motor. The sprocket on the end of the camshaft creates a 5:7 ratio to the drive motor. The camshaft is held in a similar u-block that can translate toward or away from the drivetrain. Shoulder screws attached to the u-block slide in machined slots on the u-block's stands to enable this motion. The camshaft has its own flywheel to overcome the resistance of compressing the follower springs and changing the direction of the linear cams. The eccentric translates the linear cams in the same manner as the full scale model and engages the clutch. The follower spring and wave spring systems are the same and will also be explained later in this paper. This design incorporates a leadscrew to adjust the duty cycle while testing. The biggest difference is that the clutch in this model is represented by a plate that does not spin. This clutch representation is adequate because closure force and duty cycle can be measured through load cells. Four load cells are located between the trust plate and the front stands. For further testing a torque transducer is mounted on the flywheel.
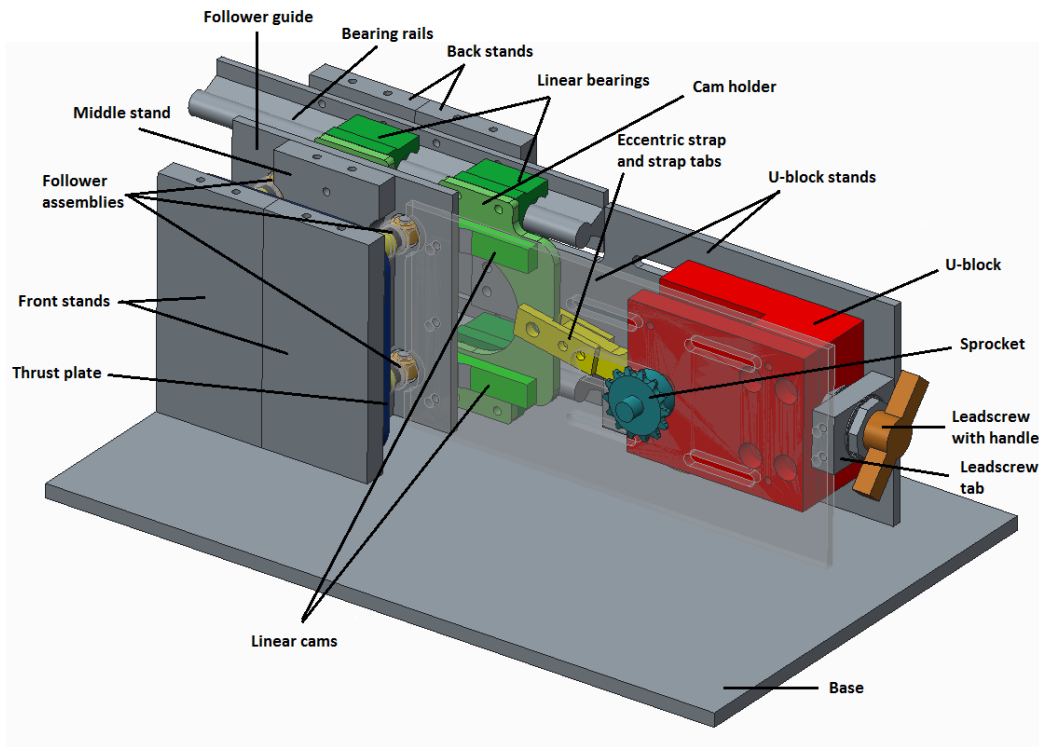

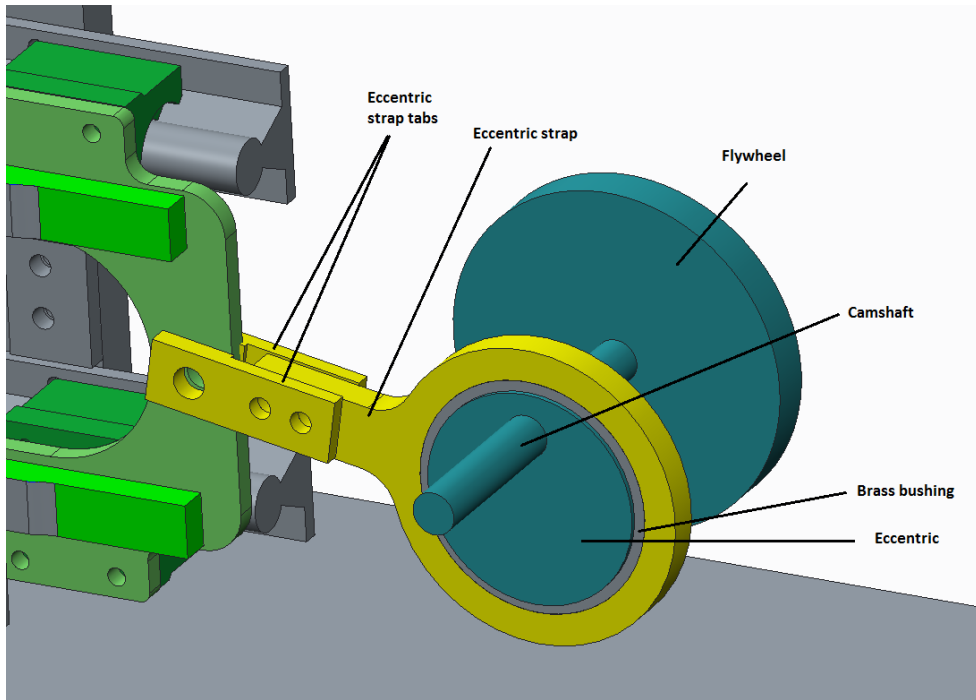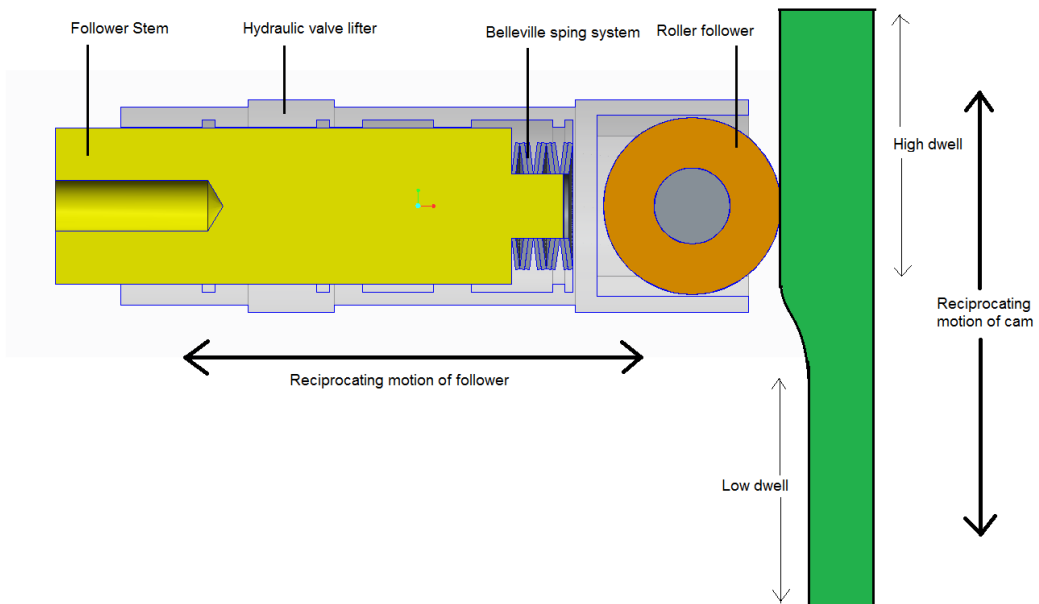Figure 24 Actuating system full model

Figure 25 Eccentric cam

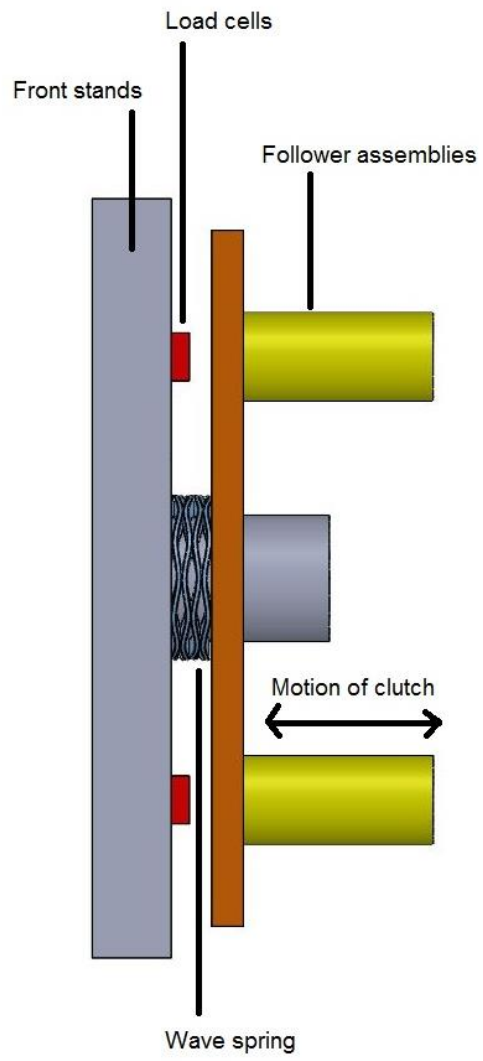
Figure 26 Follower system

Figure 27 Theoretical clutch

Design Refinement

There were many areas that design was critical for the success of the prototype. The cam needed to fulfill several requirements to operate correctly. Furthermore, the cam motion ultimately depends on the eccentric design and the speed of the camshaft. Each spring system, return and closure springs, were designed to output a specific force under a given compression from the cams. Torque needed to drive the camshaft was calculated to size the motor, assist stress analysis, and size the flywheel. Gearing of the camshaft was calculated to obtain the correct cycle frequency. Stress analysis was performed the cam holder, eccentric strap, lead screw, and camshaft, among other components to prevent failures.

Cam and Eccentric Design

As the detailed design of the actuation system began one problem with the linear cams quickly emerged. The concave portion of the rise on the cam did not have a sufficient radius of curvature to accommodate the diameter of the roller followers. A small radius of curvature would have resulted in multiple problems such as high stress on the cam surface due to small contact area as well as high deformation in the pins the support the roller followers.

In order to achieve a satisfactory cam design numerous variables had to be manipulated including the eccentric offset, rise height, the rise length and the polynomial that controlled the rise. Much of the work was iterative in the way that variables were changed incrementally in the CAD model until the desired curvature values were reached.

The iterative eccentric offset values ranged from 0.25 offset to a maximum of 0.75. The effect of increasing the eccentric offset is similar to that of increasing the prime radius of a regular radial cam. A larger eccentric offset will lead to a larger overall motion of the linear cam, which means that the entire cam will be stretched out and the rise section of the cam will be flatter and require less curvature. However, a larger eccentric offset would lead to higher accelerations and velocities for the linear cams. Ideally the smallest offset would be selected.

The rise height was manipulated and influenced by previous research. The original rise height of Cusack's 3D cam was 0.125". This rise height proved to be too tall for the linear cam to have sufficient curvature values and a rise height of 0.0625" was selected. This divided the rise into approximately equal portions of closing the clutch air gap and compressing the follower springs.

The rise duration was selected as well. The rise duration was defined as a percent of one cycle of the total motion. With an eccentric offset of 0.75" the total motion is 1.5".The rise duration was initially 10% of the cycle but this was increased to 21% to create an acceptable curvature value.

The polynomial that defined the curvature was optimized. Originally a 3-4-5 polynomial was used, but this meant that the polynomial was symmetric about its midpoint. This symmetry resulted in the concave curvature equaling the convex curvature. This is not ideal. The convex curvature can be higher than the concave curvature because undercutting to accommodate the follower occurs only on the concave portion of the cam. In order to improve this, an asymmetric polynomial was chosen. Asymmetry in the profile will also lead to asymmetry in the velocity and acceleration plots. A lower follower acceleration will occur on the concave portion and a higher acceleration will occur on the

convex portion. This high acceleration is not concerning since the spring force will be around 400 pounds. To achieve asymmetry a 5-6-7 polynomial was used.

In order to find the optimum polynomial, a Matlab code was set up to calculate one million different polynomials, each with two randomly assigned points in the middle. The other six control points were position equal to zero at the beginning and 0.0625 at the end, velocity equal to zero at the beginning and end, and acceleration equal to zero at the beginning and end. The program then searched through all of these different polynomials for the one with the best curvature. The final result of this optimization was a curvature value of 2.08 in^{-1} or a radius of 0.48", acceptable for use with our roller followers, which have a diameter of 0.35". The ratio of the cam radius to the follower radius is 1.35. The commonly used ratio is 2, but given the extreme accuracy with which these cams will be cut, a ratio of 1.35 was deemed acceptable. The constraints of the polynomial are detailed in **Error! Reference source not found.** and the coefficients are shown in Table 5. The Matlab code can be found in Appendix D - Matlab Cam Optimization.

Table 4-Cam Timing Constraints

Beta (Inches)	0	0.082	0.2434	0.315
Position (Inch	0	0.00522	0.0522	0.0625
Velocity	0			0
Acceleration	0			0

Table 5-Cam Profile Polynomial

C_0	0
C_1	0
C_2	0
C_3	22.335
C_4	-253.191
C_5	1484.000
C_6	-4177.5
C_7	4341.4

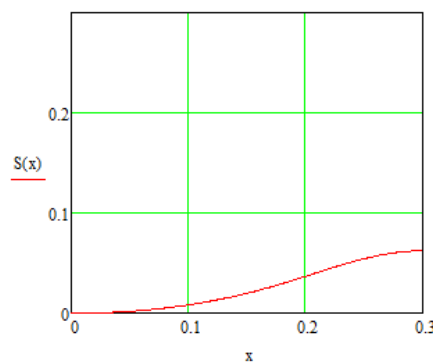The resulting curve path of the rise is shown below in Figure 28.

Figure 28-Optimized Polynomial Rise

Follower and Spring Design

The roller follower design is quite elegant. This system incorporates both the follower and spring system. The roller is a hydraulic valve lifter which is used in many older cars as an adjustment in the pushrod valve train. These rollers have tight tolerances and can support well over 100 lbf. Our system does not use the hydraulic part and replaces the inside with a Bellville Spring configuration that has a spring constant of 3068 lbf/in. When all four follower spring systems are compressed in parallel by 0.038", the follower system will apply 466 lbf. This amount is just above the 450 lbf needed for clutch lockup as calculated from the friction coefficient, clutch radius, and desired torque of 70Nm to meet the required torque resolution. The springs are stacked with four sets in series. The first set has three in parallel while the next three sets are composed of two in parallel. This is illustrated as setup 1 in the table below. The cylinder that slides into the valve lifter holds the springs in position. The back of this cylinder is tapped and is bolted onto the thrust disk. The gap between the other end and the inside bottom surface of the lifter is just a little larger than the spring's deformation at high dwell.
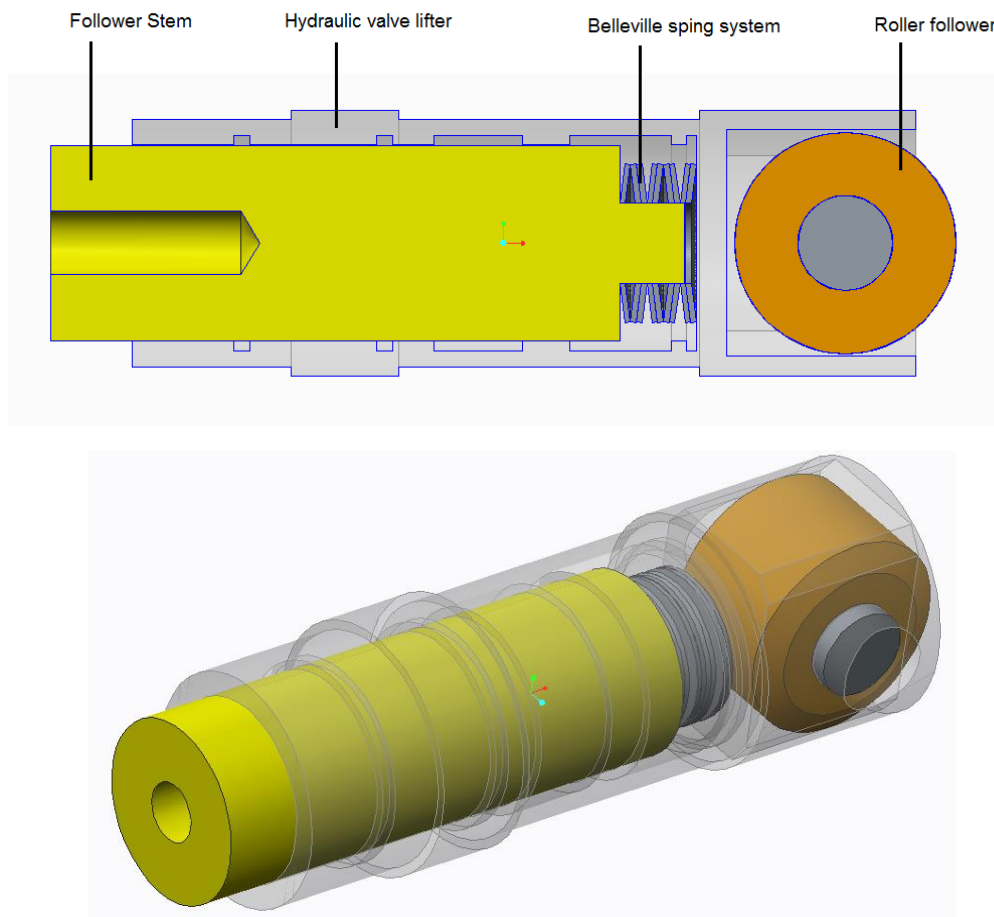

Figure 29 Follower System

The setup of the Bellville Springs can be adjusted by different combinations of series and parallel which create a range of spring constants. The ability to adjust the spring rate by altering their setup will be beneficial during testing if the mechanism does not perform efficiently at first.

Below is a table showing Belleville spring constants in several combinations. These were calculated from McMaster-Carr #9712K61 with a spring constant of 5625 (lbf/in). Our desired spring constant for the entire follower system is 12075.5 (lbf/in). The difference column of the table shows how much we are exceeding our desired spring constant while the combination column visually shows how the springs are configured in parallel and series. Calculations can be seen in the appendix B.

Table 6 Belleville spring selection

Setup #	Spring Constant of follower system (lbf/in)	Difference (lbf/in)	Combination
1	12273	197	>> << >> <<<
2	12857	782	>> << >> <<<<
3	13235	1160	>> << >> <<<<<
4	13500	1425	>> << >>> <<<
5	14211	2135	>> << >>> <<<<
6	15000	2924	>> << >>>> <<<<

The purpose of the wave spring is to return the follower assembly to low dwell. As with the Belleville springs, the wave springs in our mechanism can be reconfigured to apply a range of spring constants allowing us to adjust them during testing and find the least amount of force needed to return the follower system. Table 7 shows the spring constants for multiple setups calculated from McMaster-Carr #9714K33 with a spring constant of 360 (lbf/in). Figure 30 shows 4 wave springs in series. Calculations can be seen in the appendix B.

Table 7 Wave spring options

Setup #	Force at high dwell (lbf)	Number of springs in series
1	4.14	4
2	10.44	5
3	14.64	6

Figure 30 Wave spring

Force and Torque Analysis

An analysis was performed to solve for the dynamic forces experienced by the system due to inertia and the spring compression. A free body diagram of the cam plate is shown below with the eccentric strap force included as a reaction.
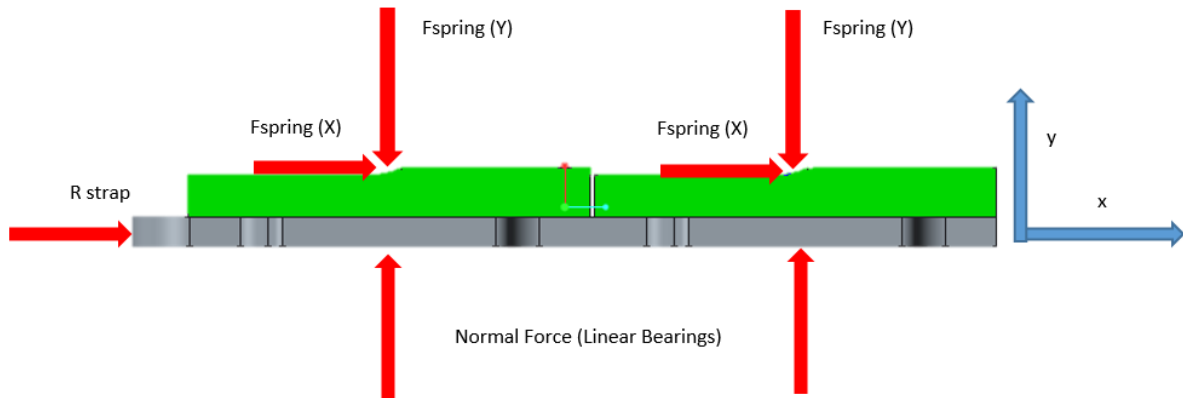

Figure 31-Cam Plate Free Body Diagram

To calculate the inertial forces of the cam plate sliding back and forth a kinematic analysis of the four-bar slider mechanism was performed.

The angle of the eccentric over time is found to be

$$\theta_2(t) := \omega \cdot t$$

Equation 4-Angular Position of the crank

where ω is the angular velocity of 125.664 radians per second as given by the 20 Hz duty cycle.

The angle of the eccentric strap is know from kinematics to be

$$\theta_3(t) := asin\left(\frac{a \cdot sin(\theta_2(t))}{b}\right)$$

Equation 5-Angle between the eccentric strap and the horizontal

where a is the eccentric offset of 0.75 inches (19.05 mm) and b, the length of the eccentric strap, is 4.6 inches (116.84 mm).

The position over time of the cam plate is found from kinematic analysis to be

$$d(t) := -\left[\left(a \cdot \cos\left(\theta_2(t)\right) - b \cdot \cos\left(\theta_3(t)\right)\right) + 0.098m\right]$$

Equation 6-Position of the cam plate over time

The second derivative of this function yields the acceleration at the cam plate. This acceleration can be multiplied by the cam plate sub assembly total mass of 0.907 kg. The total inertial force is found to be

$$F_{inertia} = MassCam * accel(t)$$

Equation 7-Inertial Force required to translate the cam plate

This inertial force can be graphed over a cycle. This graph is shown in Figure 32.
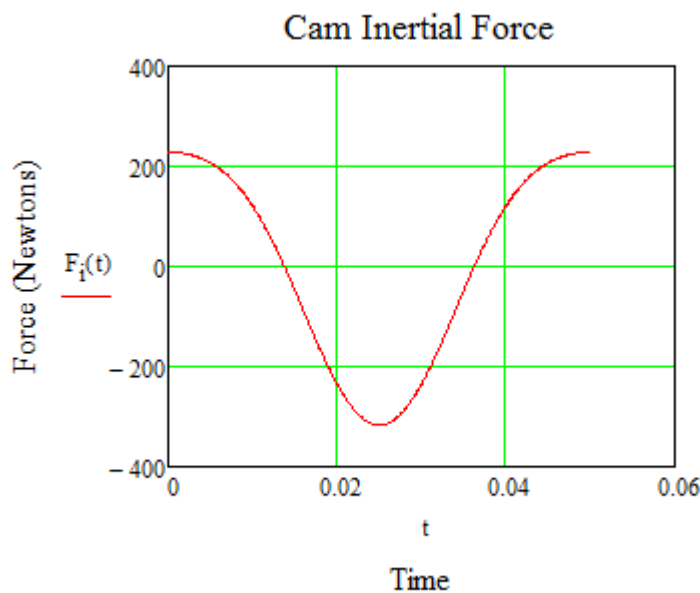
Figure 32-Inertial Force of the cam plate over one cycle

The maximum force occurs at 180 degrees of the eccentric's position and has a value of 71 lbf (315 N).

The next force that must be calculated is the force of the cams compressing the springs. The spring compression is found to be the rise height of the cam multiplied by the spring coefficient. The preload is neglected since it is merely a few pounds and is insignificant compared to 400 pound clutch closure springs. The horizontal (x) component of this is the interesting part that is needed. The horizontal component is equal to the spring compression multiplied by the tangent of the normal vector of the cam profile minus 90 degrees.

Equation 8 displays how the normal vector was obtained. The C values represent the cam profile constants as shown in the cam design section. X(t) is a step function of the follower height over time, where it is equal to zero at low dell, the cam profile during the rise section, and finally the total height at high dwell. Further detail on this function can be seen in

Appendix E – Force & Torque Dynamic Analysis.

$$\text{Norm(t)} := \left(\text{atan}\left(3C3 \cdot x(t)^2 + 4 \cdot C4 \cdot x(t)^3 + 5 \cdot C5 \cdot x(t)^4 + 6 \cdot C6 \cdot x(t)^5 + 7 \cdot C7 \cdot x(t)^6 \right) + \frac{\pi}{2} \right)$$

Equation 8- Normal vector of cam profile over time

$$Xspring(t) = SpringCompression(t) * \tan\left(Norm(t) - \frac{\pi}{2}\right)$$

Equation 9-Horizontal component of spring compression

A graph of the horizontal component of the spring compression is shown below in Figure 33.
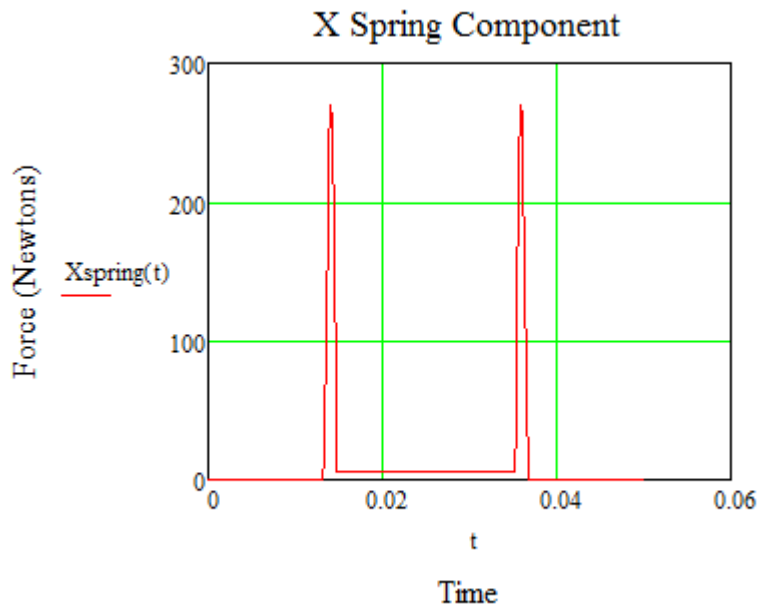
Figure 33-Horizontal Force needed to compress the springs

The sum of the horizontal spring compression and the cam's inertial force is the total force on the eccentric strap when multiplied by the cosine of the angle between the horizontal and the eccentric straps center line. This graph is shown below in Figure 34. The maximum force occurs when the cam is changing direction and the crank is at 180 degrees. The force here is 70 lbf (311 N). The other maximums are when the springs are being compressed. This force is 58 lbf (260 N).
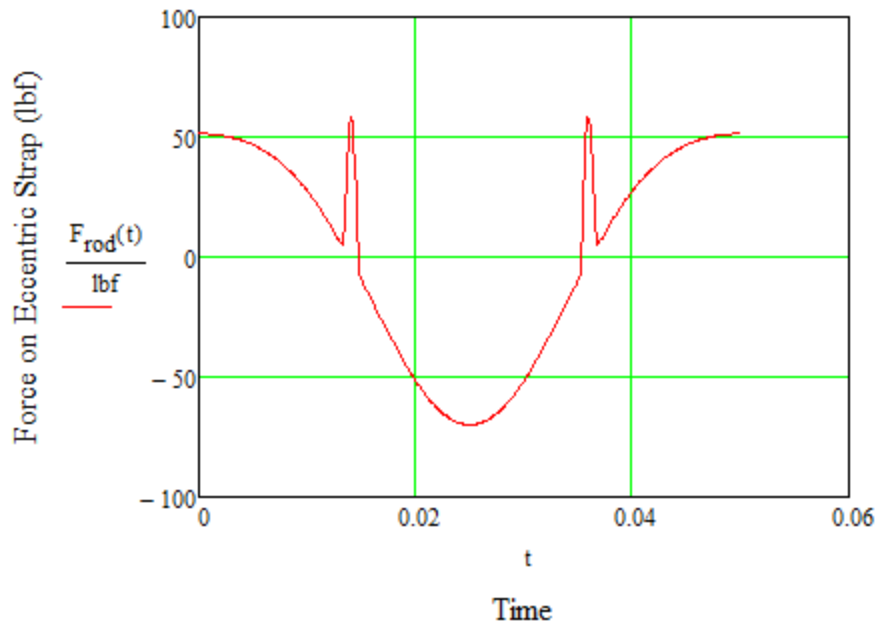
Figure 34-Total Horizontal Force of the cam plates inertia and spring compression

The axial force on the eccentric is computed as

$$F_{rod}(t) := \frac{F_T(t)}{\cos\left(\theta_3(t)\right)}$$

Equation 10-Total axial force on the eccentric strap

With the axial force on the rod now known the torque needed to drive the eccentric can be found. The torque is equal to the eccentric offset total force multiplied by the sine of the difference in the crank angle to the eccentric. The torque needed to drive the eccentric is shown in Figure 35. Further details of the dynamic force analysis can be found in

Appendix E – Force & Torque Dynamic Analysis

$$T\theta(t) := \pi - \theta2(t) - \theta_3(t)$$

Equation 11-Angle between the crank and eccentric strap

$$T(t) := F_{rod}(t) \cdot \sin(T\theta(t)) \cdot 0.75in^{\blacksquare}$$

Equation 12-Torque needed to drive the eccentric
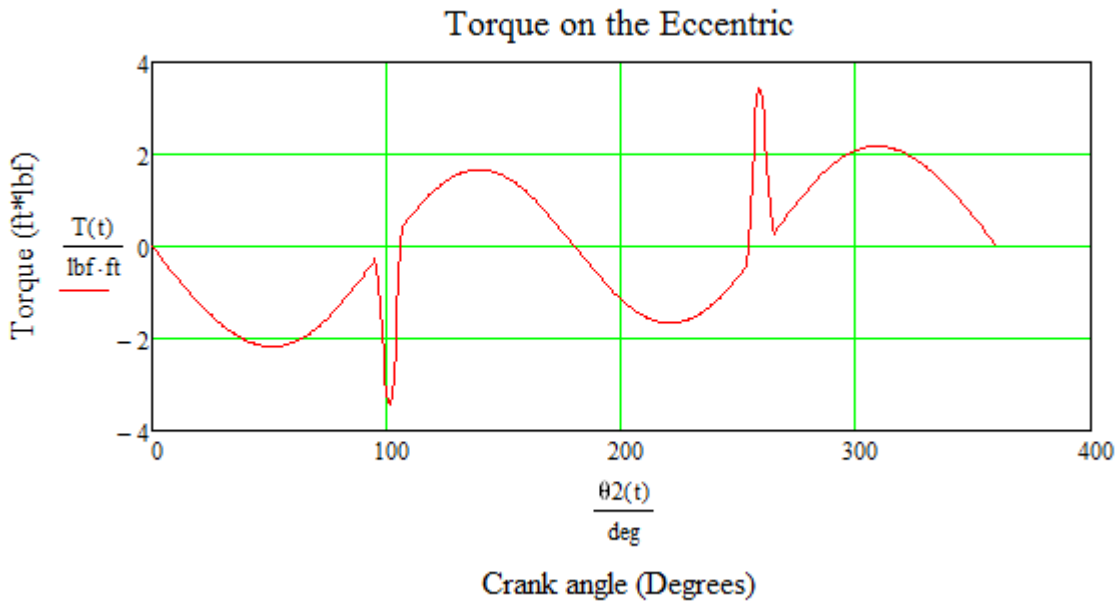
Figure 35-Torque needed to drive the eccentric

Figure 35 shows that the maximum torque occurs when the springs are compressed. The torque needed to pull the cams past the springs is 3.419 ft*lbf (4.635 N*m).

In order to confirm this analysis a dynamic mechanism analysis was performed in Creo with the eccentric rotating at 20 Hz. Figure 36 and Figure 37 show the simulated results for two cycles. Both the inertial forces matched very closely with the calculated values having a maximum of 71 lbf (315 N) and a minimum of -51 lbf (226 N) and the simulated values having a maximum of 79 lbf (351 N) and a minimum value of -56 lbf (249 N).
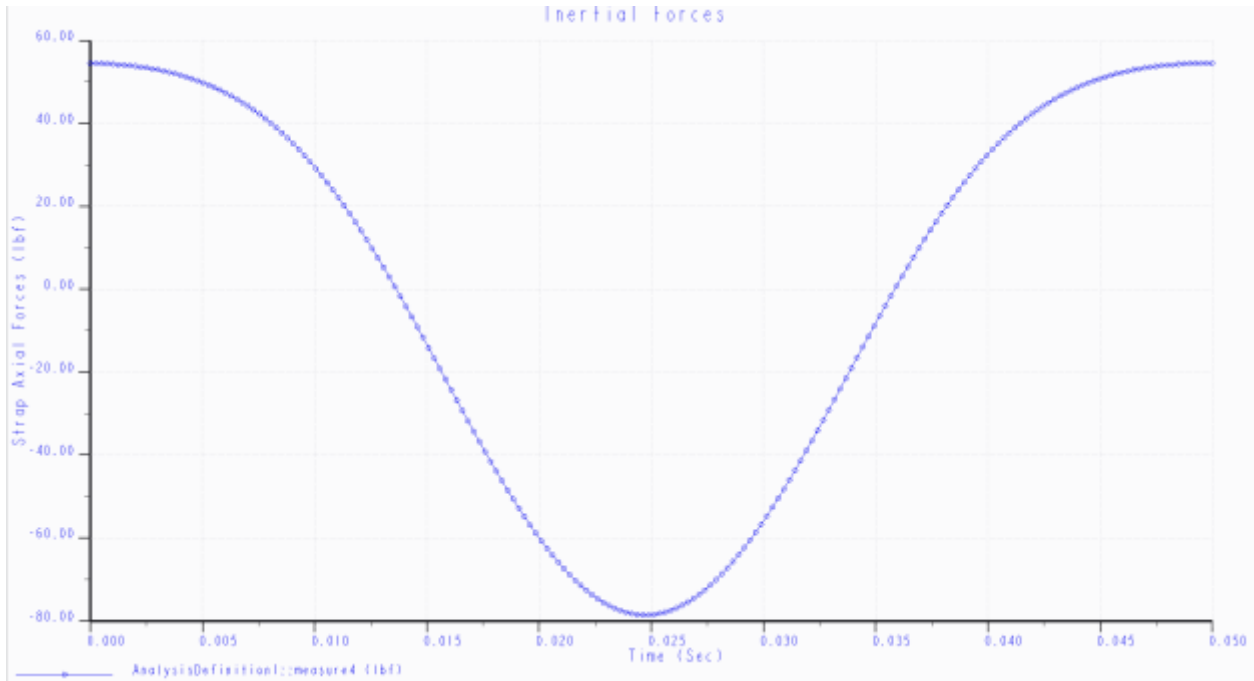
Figure 36-Simulated Inertial Forces

The simulated torque also matched closely with the calculated torque varying from 2.1 ft*lbf to 2.1 ft*lbf and the simulated torque varying from a maximum of 2.5 ft*lbs to 2.5 ft*lbs.
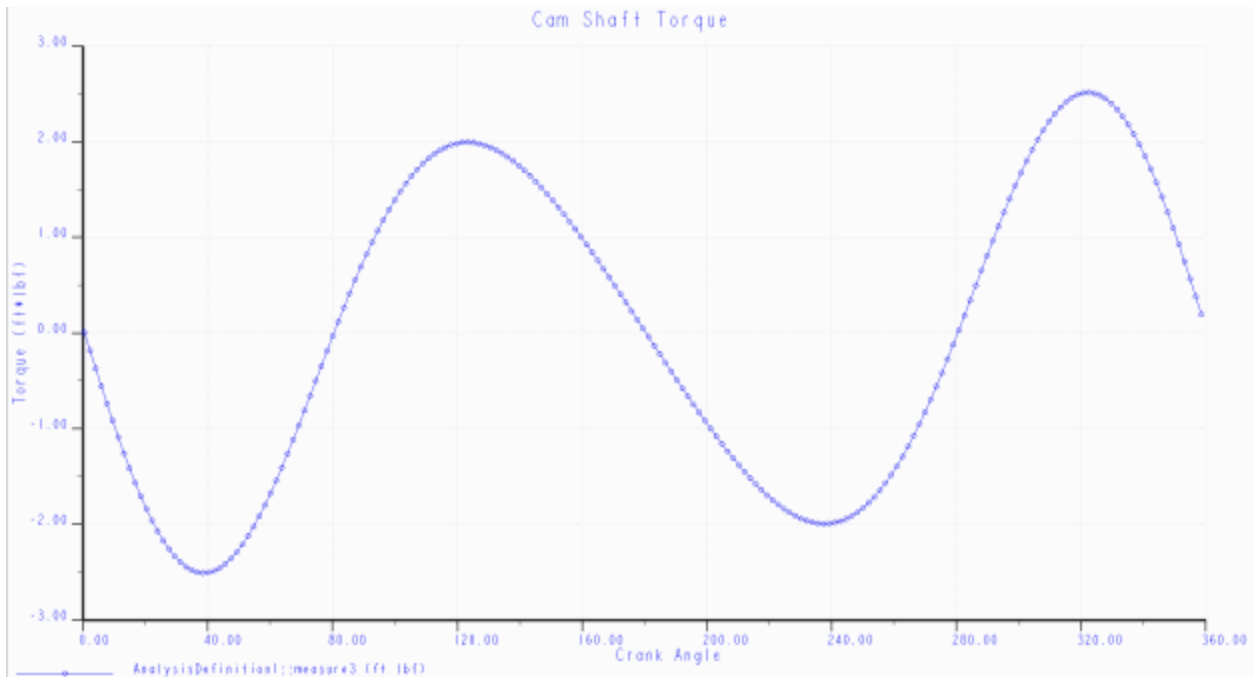
Figure 37-Simulated torque from inertial forces

With the forces needed to drive the cam back and forth both verified and understood this data can now be used to calculate stresses in other components.

Cam Holder and Eccentric Strap

As indicated from above, the linear cam holder was designed to withstand up to 71 lbs (315 N). It was connected to the eccentric strap by an 18-8 stainless steel clevis pin with a diameter of 3/8" and a cotter pin. This led to three possible methods of failure: tearout of the connecting hole on the cam holder, which was in double shear; tearout of the connecting holes on the tabs of the eccentric strap tabs, which were each in double shear; and deformation or breakage of the pin itself, which faced all six shear forces.
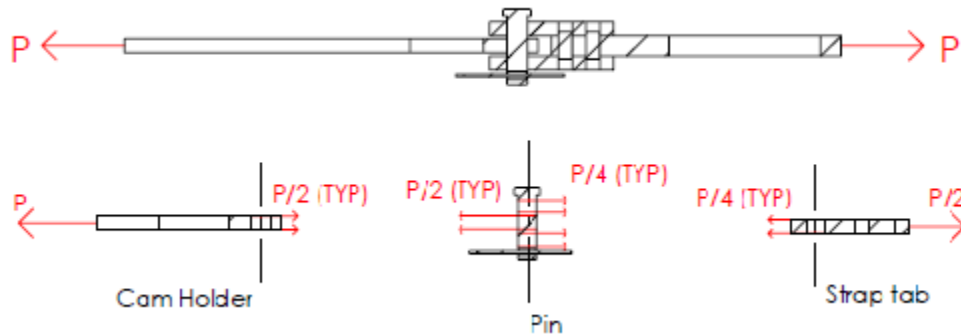
Figure 38: Shear forces on the cam holder and eccentric strap (P = 71 lbs)

Five equations were necessary to determine the safety factors of the camshaft and eccentric strap tabs:

$$A_{bearing} := \frac{\pi}{4} \cdot Diameter^2$$

$$stress_{bearing} := \frac{Force}{A_{bearing}}$$

$$A_{tearout} := 2 \cdot PartlThickness \cdot \frac{PartWidth - Diameter}{2}$$

$$stress_{tearout} := \frac{Force}{A_{tearout}}$$

$$SafetyFactor := \frac{MaterialYieldStrength}{stress}$$

Figure 39: Safety Factor equations for bearing and tearout stresses

It was found that the cam holder had a bearing safety factor of 62.2 and a tearout safety factor of 435.5. The strap tabs' safety factors were 62.2 and 52.8, respectively. As a safety factor of 2 can be considered conservative (Norton, "Machine Design"), the possibility of bearing or tearout failure of the cam holder and strap tabs was considered negligible.

The clevis pin's maximum load, shear stress, bending moment and deflection were analyzed to find its maximum Von Mises stress. After all calculations were complete, it was concluded that the pin

would have a safety factor of 9.7. Furthermore, from the clevis pin's material, finish, load, and size, along with an assumed operating temperature under 840°F (449°C) and reliability of 99%, it was calculated to have an endurance strength of 30.1 ksi (207.5 MPa).
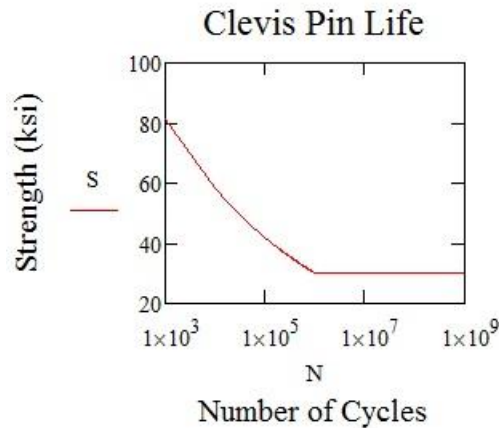

Figure 40: Expected life span of Clevis Pin

Together, the cam holder, the eccentric strap and their mutual clevis pin were deemed safe for use in the prototype.

Camshaft

The camshaft analysis was similar to the analysis of the clevis pin connecting the cam holder to the eccentric strap, but its loads were more numerous, and torque provided by the motor had to be taken into account. Maximum load, shear stress, bending moment and deflection were calculated at two times in the rotation cycle: 0.027s, when the camshaft experienced the maximum load from the eccentric; and 0.014s, when the camshaft felt its maximum torque. The load and moment analyses indicated that two sections along the camshaft could be critical: 3.235 inches from the flywheel end, where the camshaft experienced maximum shear forces; and 5 inches from the flywheel end, where the camshaft experienced maximum moment.

An analysis of points at the top of the shaft, which experienced maximum bending, and the side of the shaft, which experienced maximum shear stress, at both of the indicated times and both of the necessary lengths, showed that the shaft experienced the greatest stress at the 0.027s, 5 inches, at the top of the shaft (indicated in Figure 41 as point e).
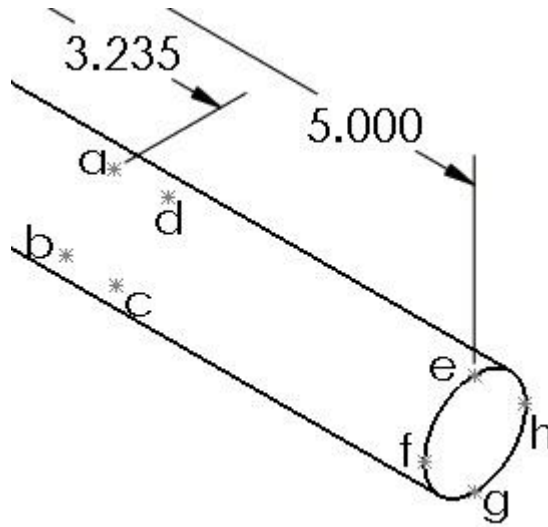
Figure 41: Potential critical points of the Camshaft

The Von Mises stress at this point is 17.75 ksi, leaving the part with an acceptable safety factor of 2.37. Finally, the camshaft's material, finish, load, and size, along with an assumed operating temperature under 840°F (449°C) and reliability of 99%, led to the calculation of an endurance strength of 23.8 ksi (164.1 MPa).
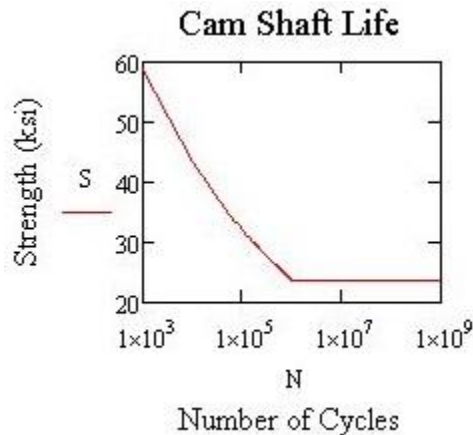

Figure 42: Expected life span of Camshaft

Lead Screw

The lead screw's safety factor was the easiest to calculate. With such a wide thread a 1"-8, and a minor diameter of 0.8492 in (Odberg et al), the part can reasonably be modeled as cylindrical steel in compression. The maximum compressive force equal to the maximum force equal to the maximum force on the eccentric: 71 lbf.   Under these conditions, the safety factor of the lead screw was found to be 837.6; assurance that the part should not fail under its anticipated circumstances. Additionally, the screw's material, finish, load, and size, along with an assumed operating temperature under 840°F (449°C) and reliability of 99%, it was calculated to have an endurance strength of 38.3 ksi (264.1 MPa).
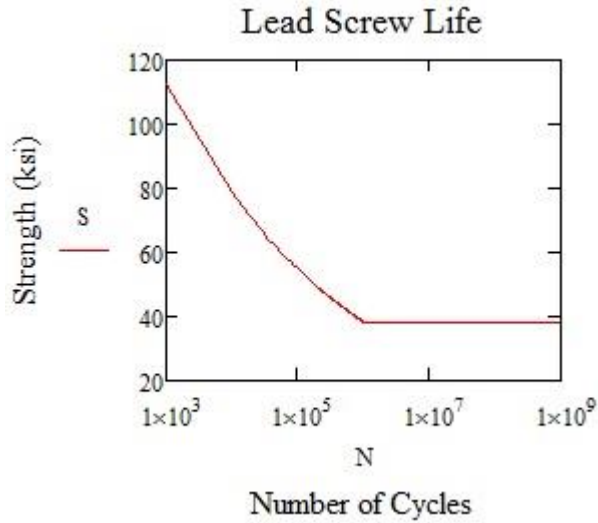
Figure 43: Expected life span of Lead Screw

Lead Screw Tab

Like the cam holder and eccentric strap tabs, the lead screw tab faced the possibility of bearing and tearout failure, but its safety factors in these cases were 357.5 and 799.4, respectively. The tab's most vulnerable region was at its exact center, where the 71 lbf force of the lead screw acted on the smallest cross-sectional area of the solid tab. A complete analysis of the load, shear stress and moment confirmed that the critical section was centered on the 2.375 in length. The principal stresses were used to calculate the maximum Von Mises stress of 670 psi, which lead to the calculation of a safety factor of 59.6. Beyond this strong safety factor, the tab's material, finish, load, and size, along with an assumed operating temperature under 840°F (449°C) and reliability of 99%, led to the calculation of an endurance strength of 14.5 ksi (99.97 MPa); a strength far greater than was necessary for the component's expected stresses.
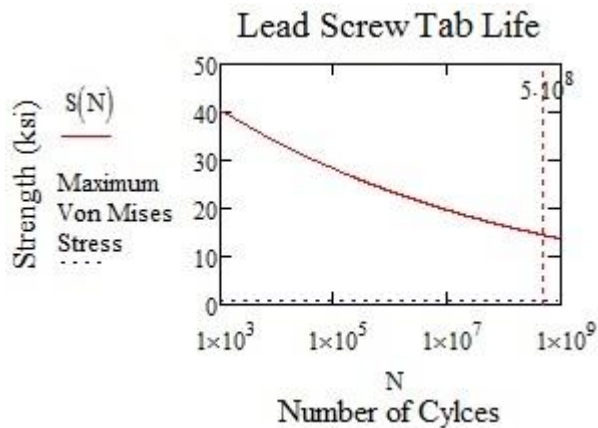

Figure 44: Expected life span of Lead Screw Tab

Motor and Gear Sizing

The motor for this project is rated as a ½ HP motor at 1700 RPM. The motor was chosen since it was readily available and incorporated the necessary features of power, speed, and a driver to vary speed. A chain driven system was chosen over a belt system since it is guaranteed not to slip. Converting the motor's power to torque results in an output of 1.545 ft*lbs. This is less than the required 2.1 ft*lbs needed to drive the eccentric. Since the motor can run at full power at 1700 rpm gearing can be used to increase the motors torque. The motor uses a sprocket with 10 teeth and the camshaft uses a sprocket with 14 teeth. This means the eccentric spins at 1214 RPM while the motor rotates at 1700 RPM. The torque on the camshaft is now 2.164 ft*lbs of torque.

Another problem encountered is that the motor must produce 4 ft*lbs of torque to compress the springs. To solve this problem a small flywheel was attached to the eccentric shaft. To find the size of the flywheel the spring energy was compared to the flywheel's energy. The potential energy of the springs is shown in Equation 13.

$$U_s := \frac{1}{2} \cdot 12273 \, \frac{lbf}{in} \cdot (0.038in)^2 = 1.001 \, J$$

Equation 13-Spring Potential Energy

Steel round bar with a 4" diameter and 1/2" thickness was selected for the flywheel as it fits into the available space and has a kinetic energy storage capacity of 8 joules at 1200rpm. This calculation is shown in Equation 14.

$$I := \frac{1}{2} \cdot m_{fw} \cdot r^2 = 1.03 \times 10^{-3} \, m^2 \cdot kg$$

$$U_{Fw} := \frac{1}{2} \cdot I \cdot \omega_{shaft}^2 = 8.324 \, J$$

Equation 14-Flywheel energy

Final Design

After the design refinement was complete, the working model could be updated and prepared for manufacturing. This final design reflects the conclusions made from analysis to give the prototype the highest chance of success.

In this final design the eccentric offset was set at 0.75". This creates a total motion of the linear cams to be 1.5". The cam's rise high was 0.0625". The rise is controlled by a 5-6-7 polynomial that represents 21% of the cam's face and creates a 1.35 ratio with the follower's curvature. The Bellville spring system was designed to output a force of 466 lbf when the system is applying the clutch. The return spring system could be adjusted by switching wave spring configurations. The return force ranged from 4-15 lb. To create the torque needed to rotate the camshaft a Boston Gear ½ HP permanent magnet DC electric motor was used and a steel flywheel to overcome the additional torque from engaging the clutch was sized with a diameter of 4". The motor would run at 1700 RPM with a gear reduction through the chain sprockets of 10:14 to create the required 20Hz. The current design of the

cam holder and eccentric strap passed tearout analysis while the camshaft was show to reach its endurance limit.

Materials used include 6061 aluminum and low carbon steel. The aluminum was used as stock for most of the machined components. Steel was used if a weld was required or significant weight was desired, as with the flywheel and base. Needle roller bearings were selected for the camshaft and a brass bushing was used for the eccentric. The linear bearings were selected mostly for budgetary reasons, they are not the highest quality but they were rated highly enough to achieve the design specs. The drawings for all major parts are included in Appendix A - Part Drawings. A final bill of materials was created to order the parts and can be seen in Appendix B – BOM.

Manufacturing

The manufacturing component of this MQP included 29 parts, most with multiple operations that were performed in the CNC mills available in Washburn. To convert the CAD model into a program that would instruct the CNCs to cut the parts, Esprit was used to create tool paths, select tools, adjust speeds and feeds, and generate NC code which could be uploaded to the machine. Setup and machine run time for the CNCs totaled more than 45 hours. Other manufacturing tasks such as cutting stock, welding, sandblasting, pressing, assembly, polishing, and tapping were also carried out to create our final prototype.

While designing the machining procedure in Esprit, particular attention was paid to critical holes and tolerances. In order to get the correct sliding fit or press fit on holes, ANSI specifications and cutter compensation were used. The tolerances from the ANSI charts and measuring tool wear with cutter compensation allowed us to get acceptable results for sliding and press fits. The limiting factor for any error in any of the parts can be attributed to machine tolerances, although error was eliminated by machining, measuring, and then adjusting tool radius in order to run additional passes and achieve the correct fit.

Cams

Each cam required four operations. Facing the ends of the cam was done manually and with a program. The profile was cut with an endmill which included a finish pass. The side of the end mill was used to cut the cam profile in order to obtain a smooth surface finish as seen in Figure 45. In this part, the location of the mounting holes, height of low and high dwell, and shape of the rise section were all critical. After machining the ¼"-20 UNC holes were used to mount the cams onto the cam holder and a pin was pushed through the cam holder into the cam to protect from the bolts shearing. These holes are seen in Figure 46.
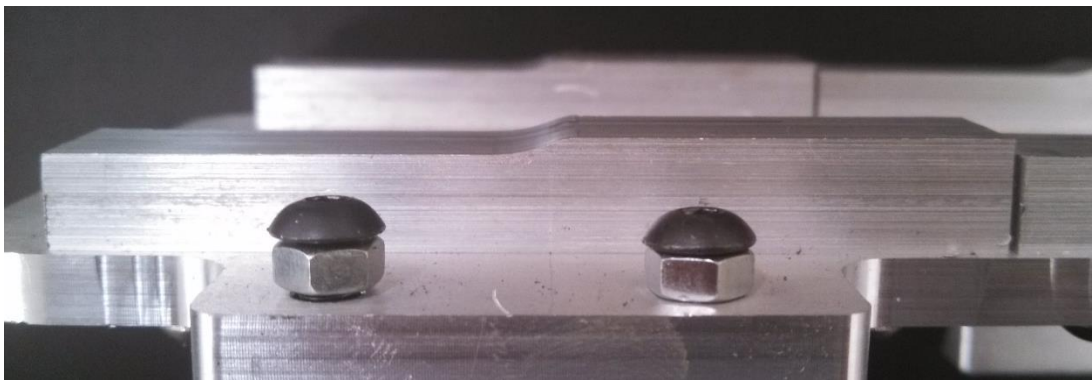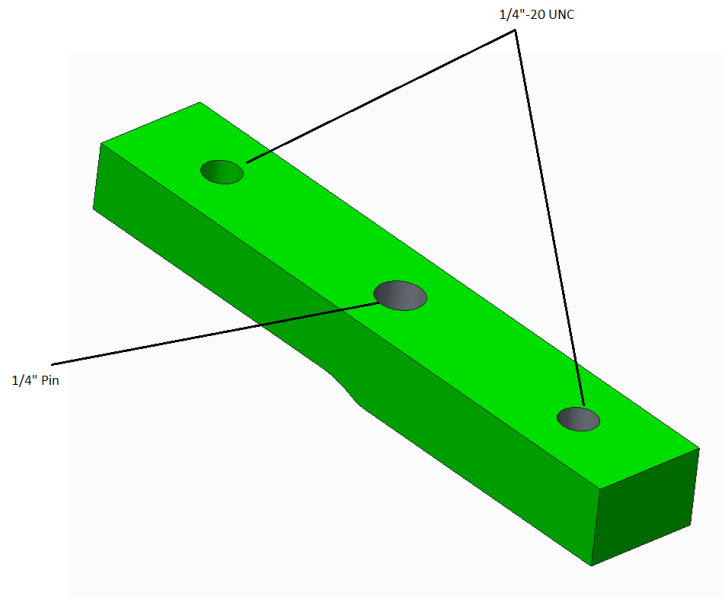

Figure 45 Linear cam on cam holder

Figure 46 Bottom of linear cam

Follower Stems

The follower stems in Figure 47 were made from 1" aluminum rod. The outside diameters were turned using a lathe. In order to get snug sliding fit, this part was made several times with different tool offsets. These follower stems were designed to have a sliding fit inside the hydraulic valve lifters. These lifters are steel castings with machined features. The follower stems that fit the best into the back of the valve lifters were collected and clamped in a collet for drilling the #7 hole on a Minimill. The ¼"-20 threads were tapped by hand and the outer diameters were polished. Every dimension on this part is critical except the depth of the hole.

Figure 47 Follower Stems

U-Block

The U-block was designed as a two component part in order to facilitate mounting the eccentric strap. These two parts are connected using counterbored 3/8"-16 UNC bolts. There is a 1"-8 UNC tapped lead screw hole for adjusting duty cycle in the back piece. ¼"-20 shoulder screws to support the U-block are located on both the front and back pieces. Each hole for the needle bearings has a flange for the bearings to sit against.

The holes that support the bearings for the camshaft and the shoulder screw holes were the most critical features in this part. They must line up with each other and their designated slots on the u-block stands.
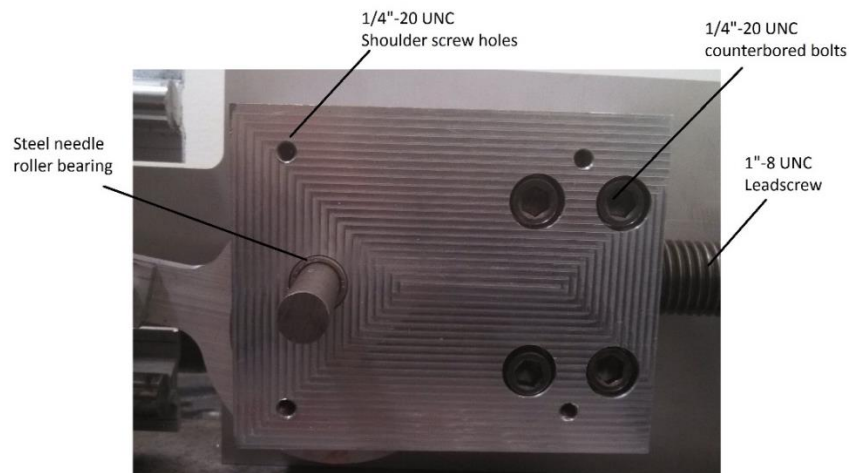
Figure 48 U-block

Eccentric Strap

The eccentric strap is a 4 component sub-assembly. It consists of the strap itself, a brass bushing, and two tabs designed for its connection to the cam holder.

The strap was machined in the VM2 on a sacrificial plate. Bolting the stock to the sacrificial plate enabled us to create the holes in the strap. Then bolting the strap down through those holes enabled us to contour the part and mill the bushing's hole to a press fit tolerance. An additional bolt on the u-block side of the strap was used as a precaution to prevent the part deflecting during the contouring operations. The tab that contained its hole was removed later. Placement of both ¼" holes and bushing hole diameter were critical in this part.

The two strap tabs were milled in a Minimill as one part and then separated. The critical dimensions in this part were the differences two surface heights and each hole which measure 0.052".
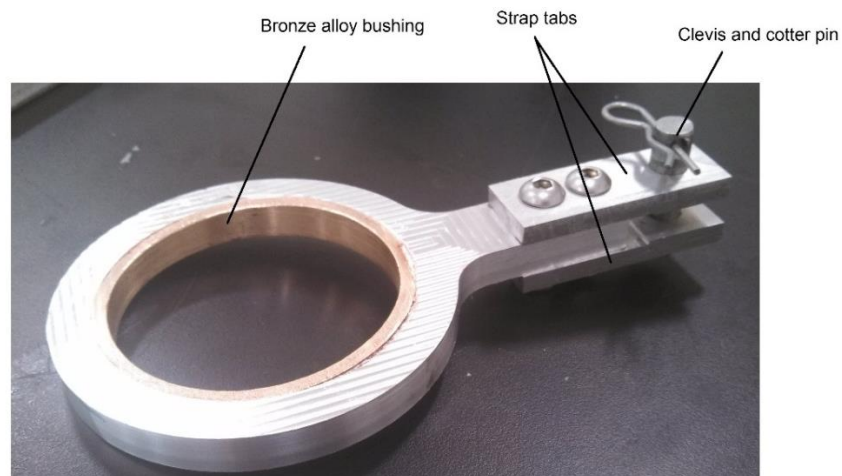
Figure 49 Eccentric Strap

Cam Holder

The cam holder was machined out of ¼" aluminum plate. The processes of fixturing were the same as the eccentric strap. The diameter of the clevis pin hole was dimensioned to provide a fit that allowed sliding with no play. The locations of the mounting holes for the cams were critical dimensions. These holes, for each cam, included two #7 holes to screw the cams on with ¼"-20 UNC and one ¼" hole for a pin to protect the bolts from shearing. These are seen in Figure 50 while the finished cam holder is shown in Figure 51.
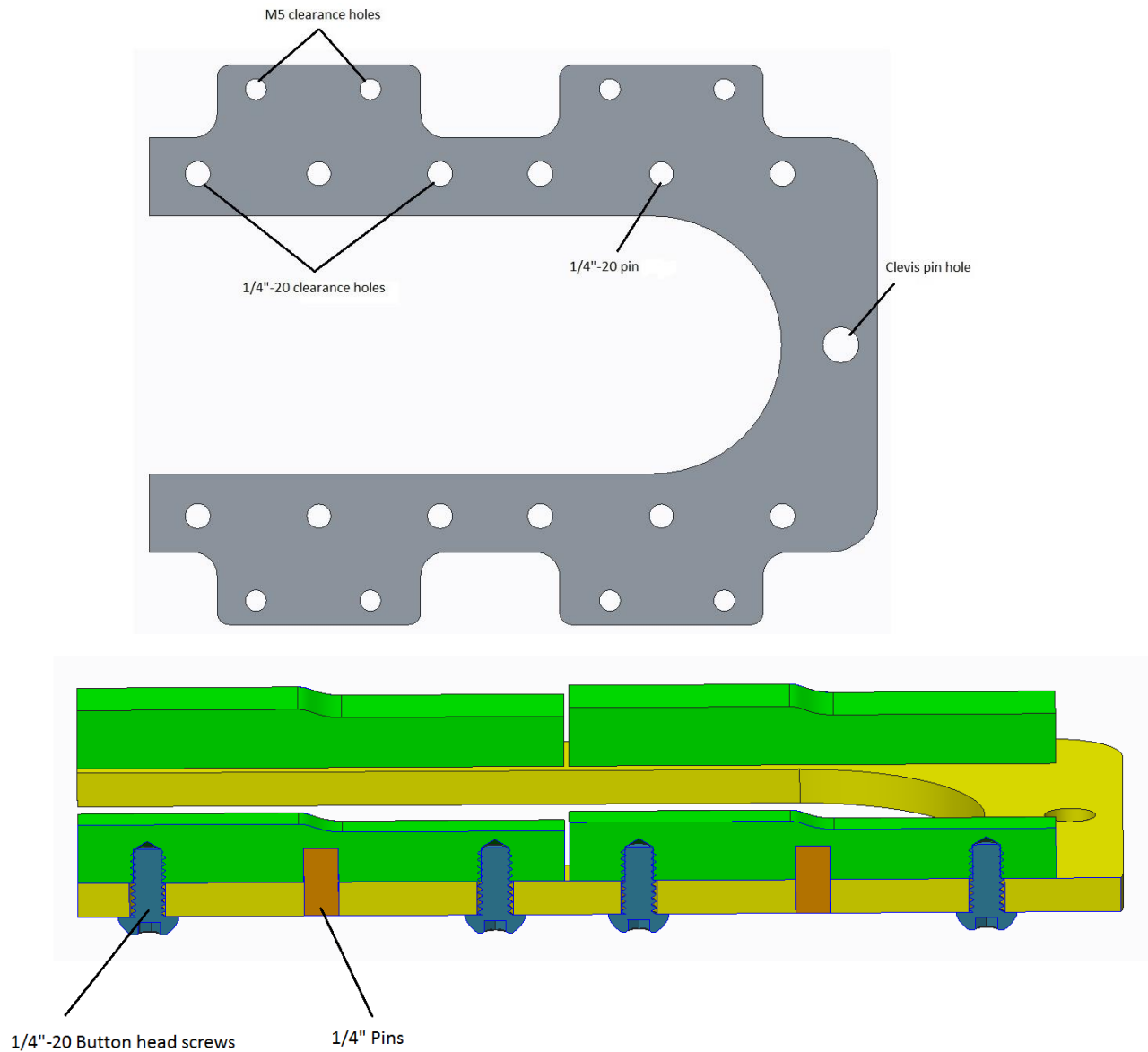
Figure 50 Cam holder critical holes
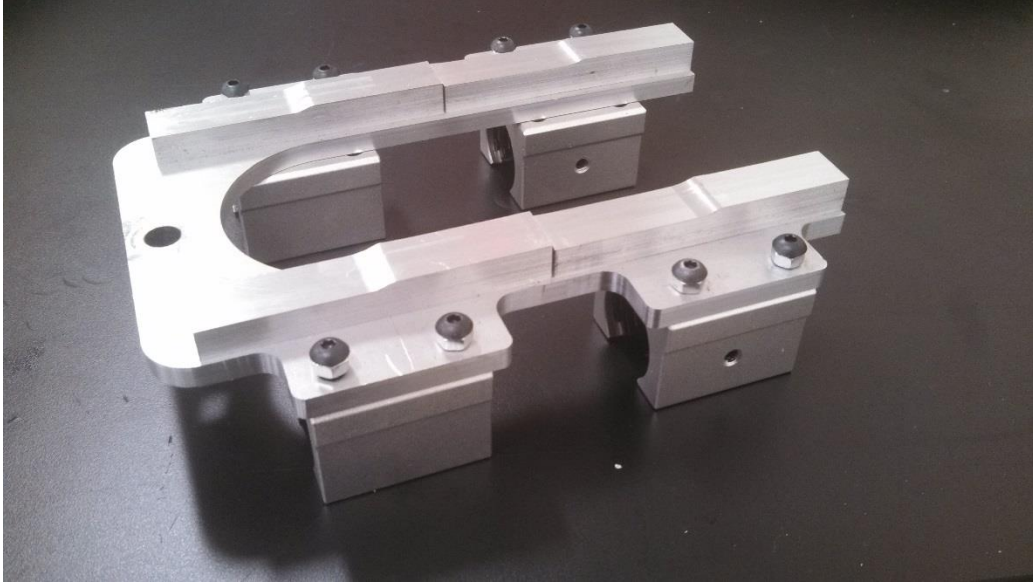
Figure 51 Cam holder with cams and bearing blocks

Eccentric

The eccentric was made in a lathe with radial tooling to make the setscrew hole and the off-center camshaft hole. This was the first MQP part made on Washburn Shop's ST30. The location and size of the cam shaft hole was critical. Later the eccentric was polished.
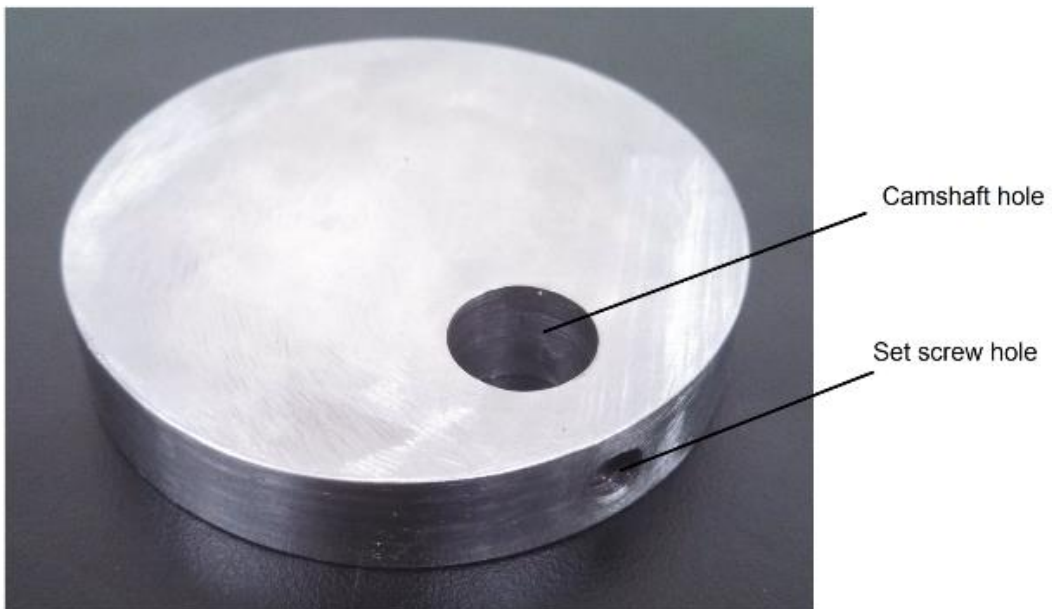
Figure 52 Eccentric

System pictures

After manufacturing was completed, assembly began. Pictures were taken in order to document the prototype. Figure 53 shows the full system supported by anti-vibrational pads on a granite base before testing. The wiring is for the strain gages and will be discussed in the testing section.

Figure 53 Mechanism on granite base for testing

Figure 54 shows the front of the mechanism. It shows how the chain is connected to the crank shaft and how the u-block stands are connected to the rest of the system.
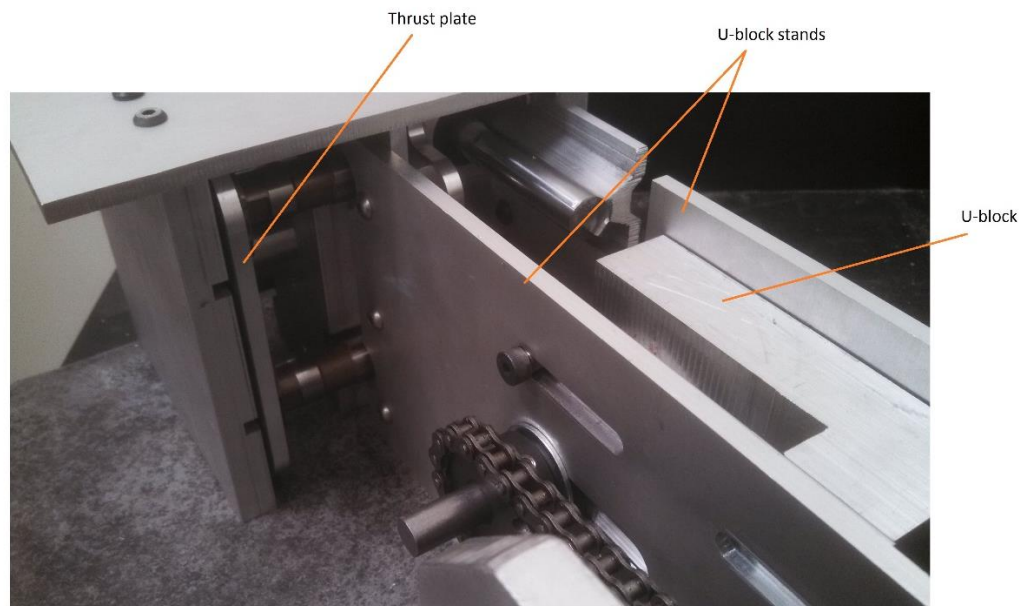
Figure 54 Front of mechanism

Figure 55 shows the placement of components from the left side of the system. This is a good view because many components are visible. When the mechanism is running, the thrust plate can be seen translating at the adjusted duty cycle.
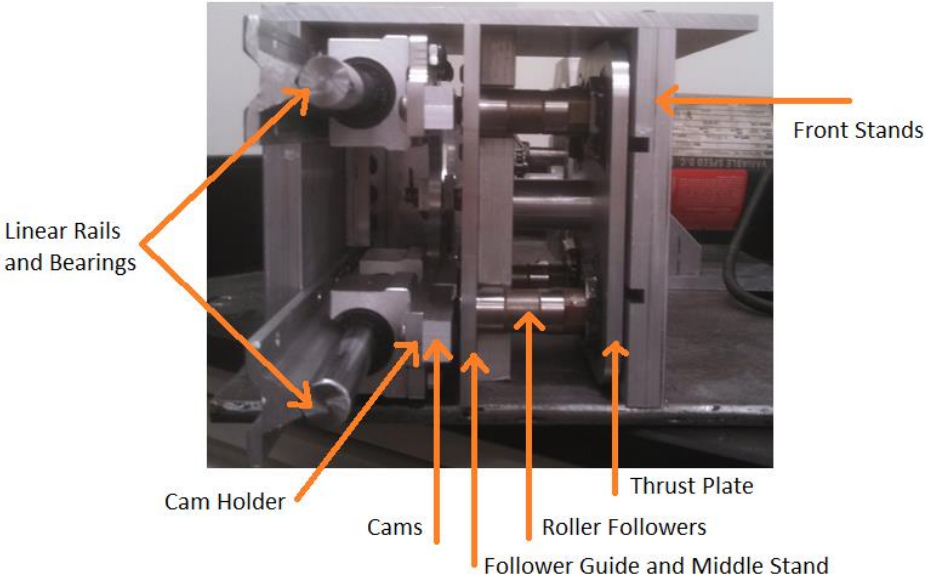
Figure 55 Left side of mechanism

To check for wear on the cams the follower system can be removed, making the cams, cam holder, and linear bearings visible, as seen in Figure 56.
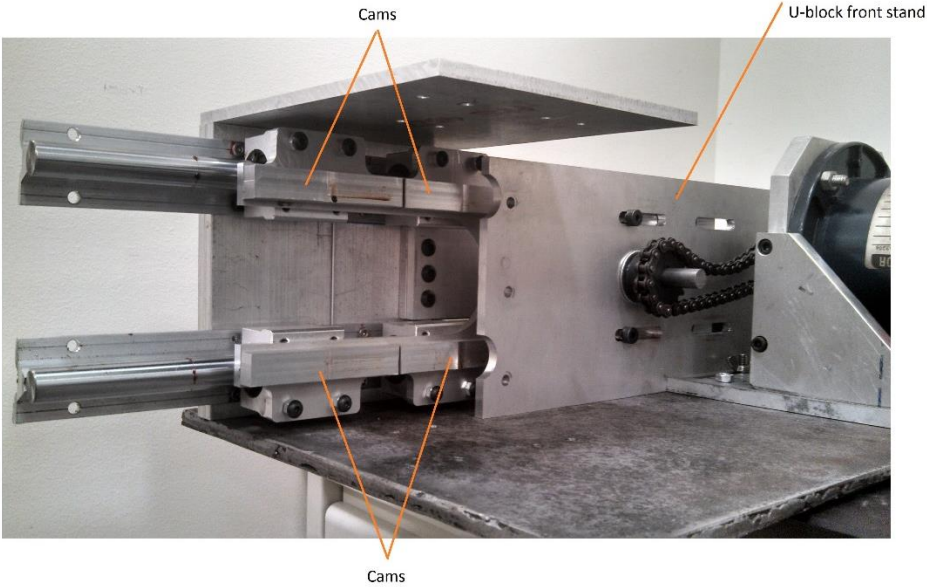

Figure 56 Mechanism front

Testing

To test the prototype two tests were performed. The first test measures the simulated clutch closure force. This is the force exerted by the cams on the followers which compress the internal Bellville springs and push against the thrust plate. The second test records the angular vibrations of the camshaft.

load vs time data were measured using two strain gage based loadcells located on each front stand. These four loadcells can measure up to 441 pounds of force (1960 N). Each test stand contained two half-bridge strain gauges so together they make one full bridge. This configuration can be processed by one amplifier so a total of two signal conditioning amplifiers were used. Each signal conditioning amplifier was fed into one channel of the National instruments 16 bit DAQ. The lab view program details are in Appendix F - LabVIEW Program.

Figure 57-Load cell configuration with nest milled into back stand

The voltage was recored by the DAQ over a period of 0.2 seconds while sampling at 10000 Hz or 500 samples per cycle. Since such high rate measurements are needed the conversion of volts to force was applied during post processing in excel. To convert volts to force a mechanical calibration was performed for each bridge.

To calibrate the load cells, multiple weights were applied up to 110 pounds. The weight was applied to all four load cells through a flat aluminum plate. For each weight applied the weight and force were recorded and graphed as shown in Figure 58. A line can be fit to these points which results in the force voltage conversion equation shown in Equation 15.
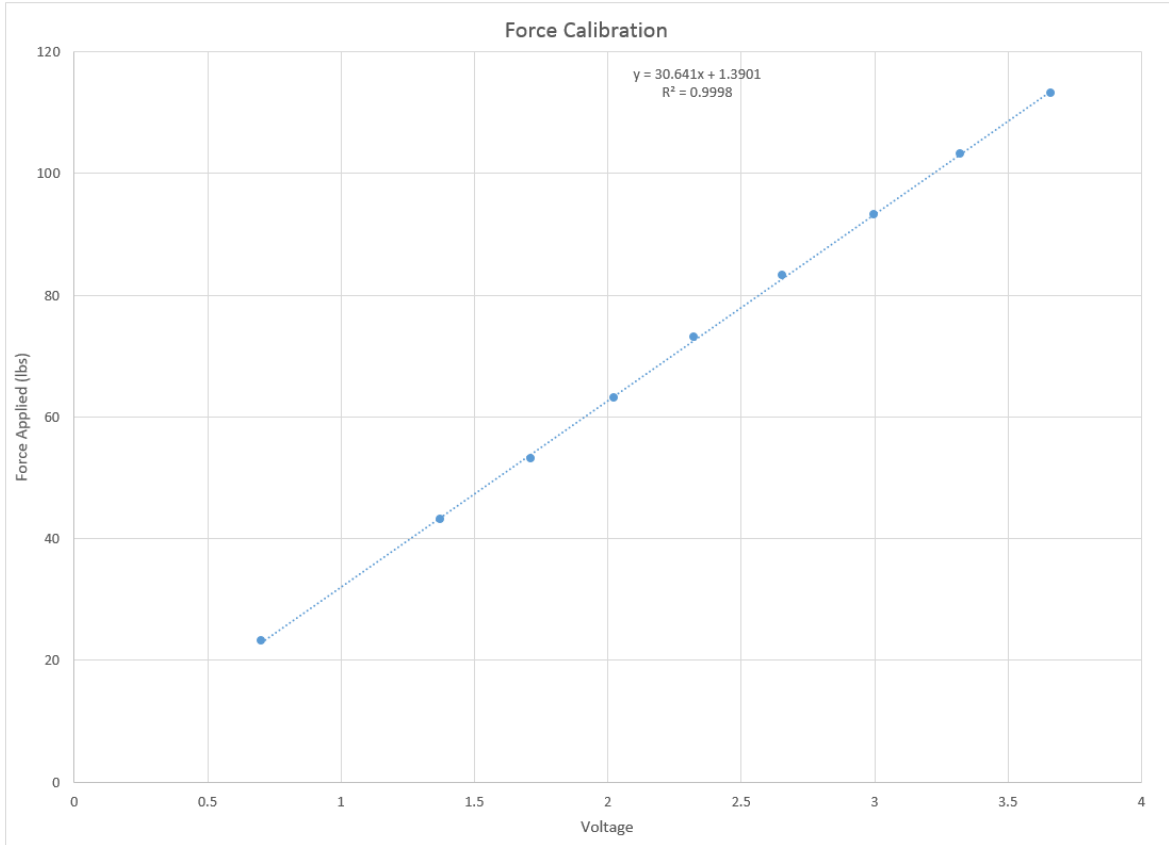
Figure 58-Graph of Force versus voltage

$$Force = 30.641 * voltage + 1.3901 pounds$$

Equation 15-Conversion of voltage to force

Torsional vibration in the eccentric camshaft was measured with a torque transducer. The torque transducer measures torsional vibrations of up to 3 degrees in the direction of positive rotation or negative rotation. Calibration is accomplished with a calibrated magnet. This magnet corresponds to 3 degrees of rotation. This can then be compared to the output voltage. With an observed output voltage of 6 volts the calibration is 2 volts per degree. The voltage output of the transducer fed into an external amplifier and from the amplifier the signal fed into a signal analyzer.

Figure 59 HBM Drehschwingungus Aufnehmr Torsional Vibration Transducer

Test Protocol

       The following method was used to test the prototype actuation system. The system was tested at every 10% interval of duty cycle. During each test the load cell force and the angular acceleration of the cam shaft were recorded as a function of time. The steps for each test were as follows:

1. Set the device in approximate position by adjusting the lead crew and the position of the U-Block to achieve the desired duty cycle.
2. Ensure there are no obstructions of the moving parts and place the protective enclosure over the mechanism.
3. Check multimeters to ensure both wheatstone bridges are zeroed, if not re-zero that bridge.
4. Turn the power on the box to the "ON" position.
5. Slowly increase the speed to 100%
6. Wait 5 seconds to allow the device to reach a steady state
7. Record test data over a minimum of 3 cycles.
8. Stop recording, turn off the motor and reposition the U-Block for the next test.

Results

Torsional Vibration Measurements

After compiling the data, graphs were made in excel. Figure 60 is a graph of the torsional vibration voltages (orange) compared to the load cell voltages (blue). Unfortunately, the torque transducer was not able to fully measure the vibrations in the camshaft. The torsional transducer reached its mechanical limit recording torsional vibrations of the camshaft at plus and minus 3 degrees. Measurements were limited to avoid damaging the instrument. In this situation the internal accelerometer is essentially bouncing between two hard stops. Due to this it is not possible to make any useful observations or measurements from this data other than the fact that the cam shaft is undergoing large angular accelerations.
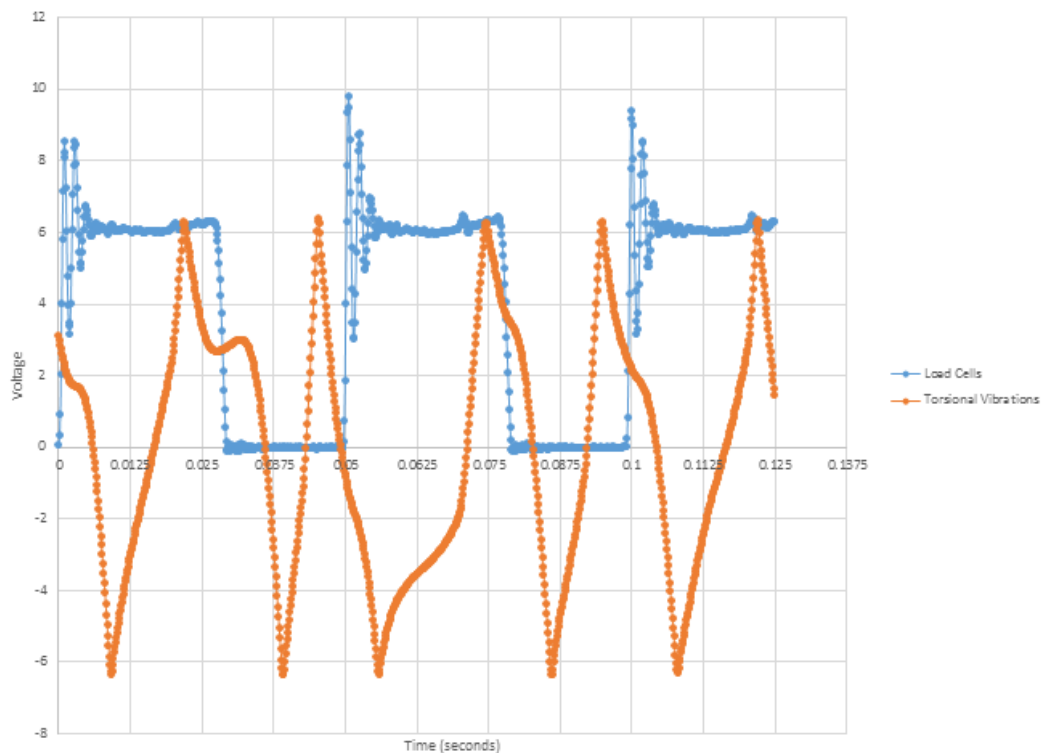
Figure 60-Torsional Vibrations Compared to Clutch Duty Cycle

Although the torsional vibration measurement scheme was insufficient to acquire data it is known that the camshafts angular velocity was not consistent. In a full transmission system the camshaft would be coupled with a large high speed flywheel. Coupling a larger rotational mass to the camshaft would lead to a more consistent rotation through the systems cycling.

Load Cell Measurements

Despite the limitations of the torque transducer a large amount of data was collected successfully via the load cells. Measurements obtained from the load cell include closure force, cycle frequency, engagement time, and duty cycle. Other observations include the system ringing as well as inconsistencies in the 0% duty cycle as well as the 100% duty cycle. Figure 61 shows a load cell response

graph for a 10%, 50%, and 90% test, all of the load cell graphs are available in Appendix G – Load Cell Response Graphs.
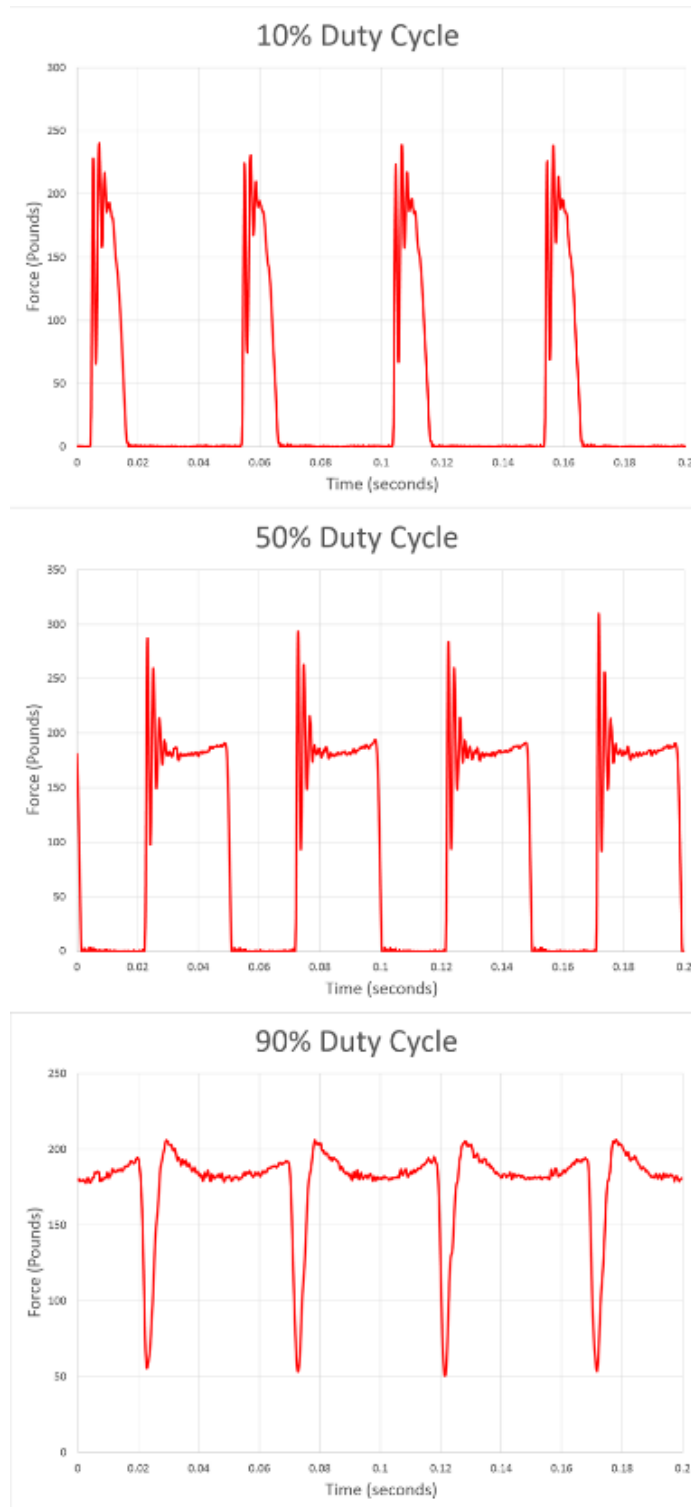

Figure 61-Sample of duty cycle load cell measurements

Closure force was consistent across all tests. Excluding the ringing oscillations the average closure force was 185 pounds. This was measured visually across all tests by taking the average of all the points at high dwell after the vibrations were gone. This is concerning since it is 265 pounds below the design spec of 466 pounds. Further analysis of this will be discussed in the results evaluation section.

Cycle frequency was another characteristic that was consistent across the duty cycles tested. Cycle frequency was measured by taking the first point of two rise sections and finding the time between them. This is the cycle's period, the frequency can be found by taking the inverse. The average frequency across all tests was 20.243 Hz. The design spec was for a minimum switching frequency of 20 Hz and the gearing of the cam shaft was designed for a frequency of 20.233 Hz.

Two variables that were not as consistent across tests were engagement time and the accuracy of the predicted duty cycle. Engagement time was measured as the time until a force of 185 pounds was reached. The observed duty cycle was measured as the percent time of a cycle the force was 185 pounds or greater. Table 8 summarizes both variables across all duty cycles.

Table 8- Desired duty cycle compared to engagement time and observed duty cycle

Desired Duty Cycle	Engagement Time (Sec)	Observed Duty Cycle
10%	0.001	11%
20%	0.0005	29%
30%	0.0005	37%
40%	0.0004	44%
50%	0.0006	54%
60%	0.0004	61%
70%	0.0006	69%
80%	0.00345	73%
90%	0.0065	82%

Engagement time ranged from 6.5 milliseconds to 0.4 milliseconds. This is expected since the cam speed relative to the follower is not constant. Duty cycles near the ends of the spectrum (10%, 20%, 80% and 90%) engage the clutch when the cam is near the end of its stroke. This means that the cam is slowing down so more time is spent on the rise section. The opposite is true for duty cycles near the middle of the spectrum (40%, 50%, 60%), the cam is moving faster so less time is spent on the rise section. The design spec of engagement time was specified as 0.45 milliseconds. This was achieved on only the 40% and 60% duty cycles. By this logic it would follow that the 50% would be the fastest engagement time. It is unclear why the engagement time was slower by 0.2 milliseconds. However, the cycle time was ensured to be correct during this test. The 20%, 30%, 50%, and 70% were all still less than a millisecond. The 10%, 80% and 90% were all above 1 millisecond.

The duty cycles achieved were not as accurate as desired. The worst difference was at 20% with an error of 9%, the 90% duty cycle was off by 8%, the 80% was off by 8% and the rest of the duty cycles were within 3% or 4%.

Another design spec that can be analyzed was the wear of the components. The only components that exhibited noticeable wear were the top two cams. This is seen in Figure 62 and Figure 63. It can be seen that the follower was not riding perfectly tangent on the surface. This likely resulted in stress concentrations at the top of both cams. The total wear was measured with a dial indicator and is close to 10 thousandths of an inch. The bottom two cams did not exhibit any visible wear and the paths were much more evenly distributed on the surface. This is shown in Figure 64. Ideally these cams would be made out of a hardened steel instead of aluminum which was chosen for manufacturability.
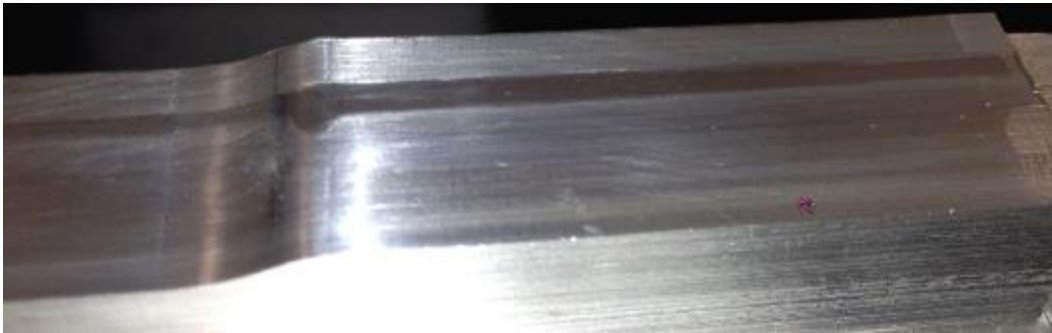
Figure 62-Wear on top right cam
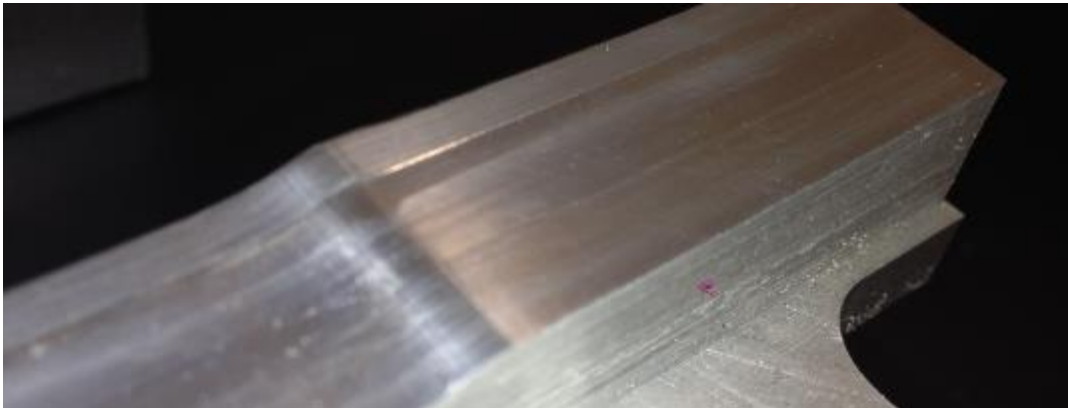
Figure 63-Wear on top left cam
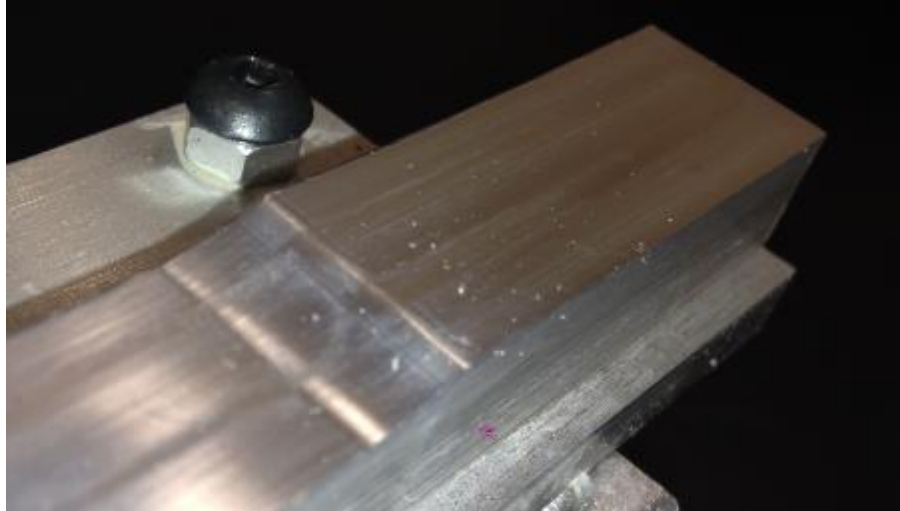
Figure 64-Bottom cam exhibiting relatively no wear

Another point of interest was the ringing in the follower system exhibited in the load cell measurements. Due to the short rise time the thrust plate is impacting the load cells with a large force and causing the system to oscillate for a short period. This is shown in detail in Figure 65. The resonance last for 8 milliseconds and oscillates between a peak of 325 pounds and 76 pounds. The highest frequency of vibration observed was 500Hz which underwent damping until it evened out.
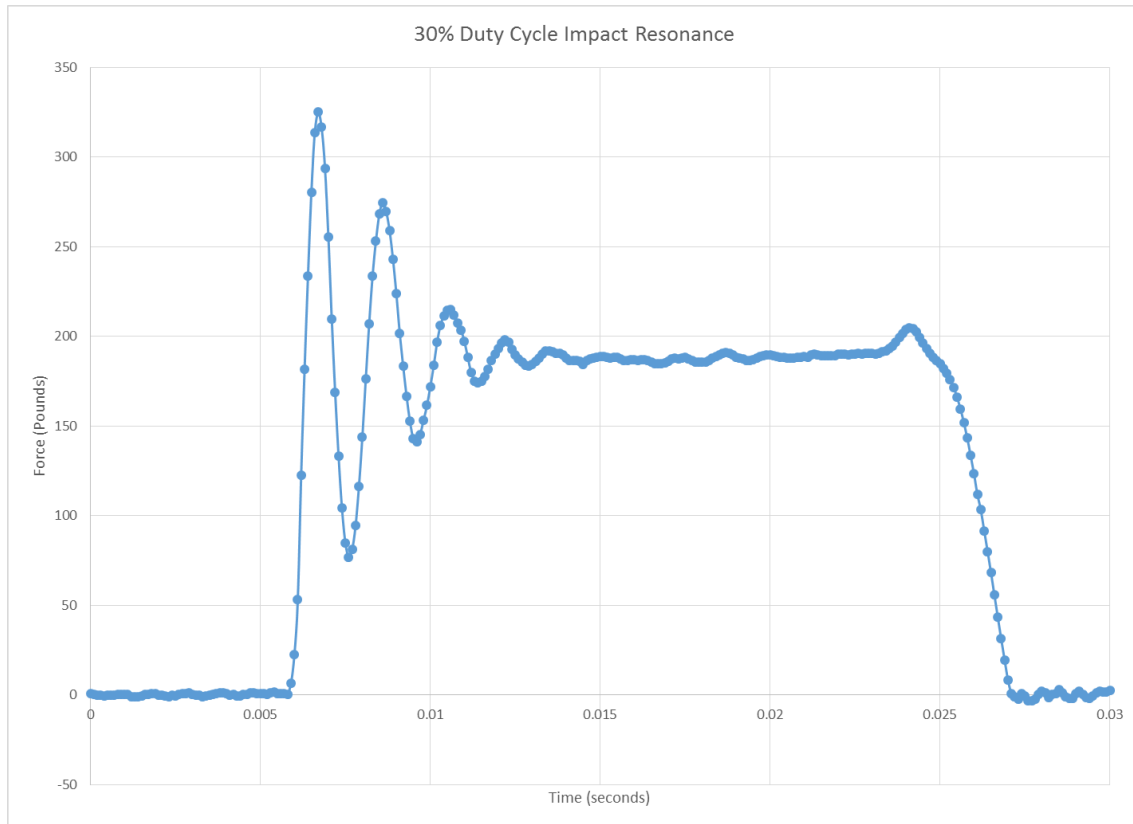
Figure 65-Impact Resonance of thrust plate and load cells

Two of the more interesting graphs occurred during 0% and 100% duty cycle tests. The 0% Duty cycle graph is shown in Figure 66. During this test it was surprising to see the clutch actually create a measurable force. The reason for the sharp force is that the cam does somewhat close the clutch but not enough to close the clutch under static conditions. When the system is running at speed the follower gets thrown outwards and the thrust plate jumps into the load cells. This could be fixed by allowing the U-Block to move forward further so that there is no rise during a 0% duty cycle.
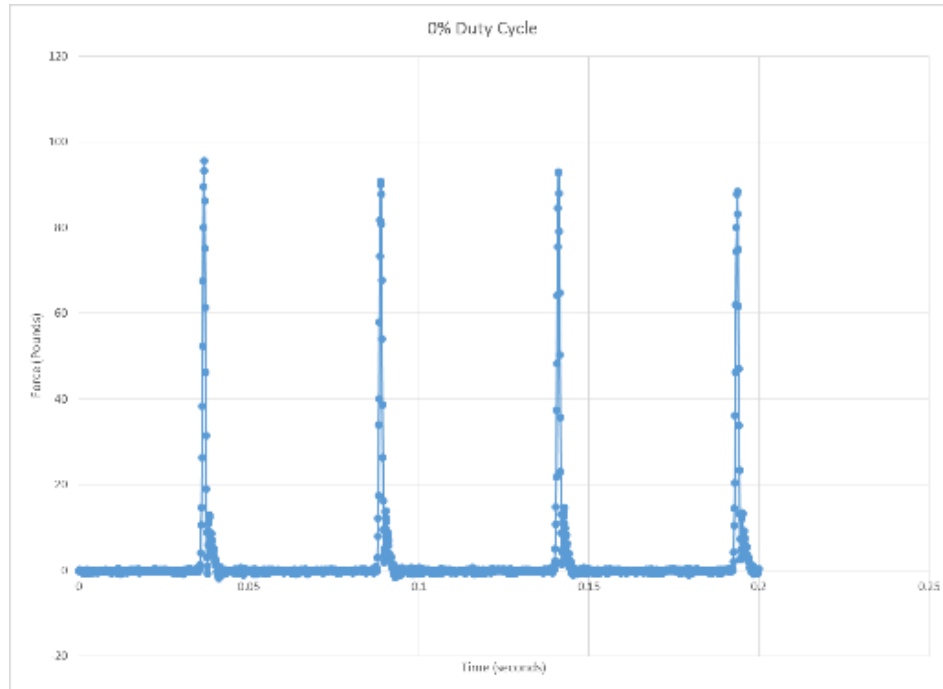
Figure 66-0% Duty Cycle Response Graph

The 100% duty cycle is more confusing since the follower never leaves the high dwell in this position. However, the load was inconsistent, the graph is shown in Figure 67. The load varied from 171 to 193 pounds. A slight irregular frequency can be seen through this graph. By measuring the time between two bottom points this frequency can be found. Interestingly enough, the frequency is 20Hz which is the same as the translation of the cams. It is very likely that this motion is travelling through the entire device even though the forces are occurring in different directions. It is also certainly happening during other duty cycle tests as well.
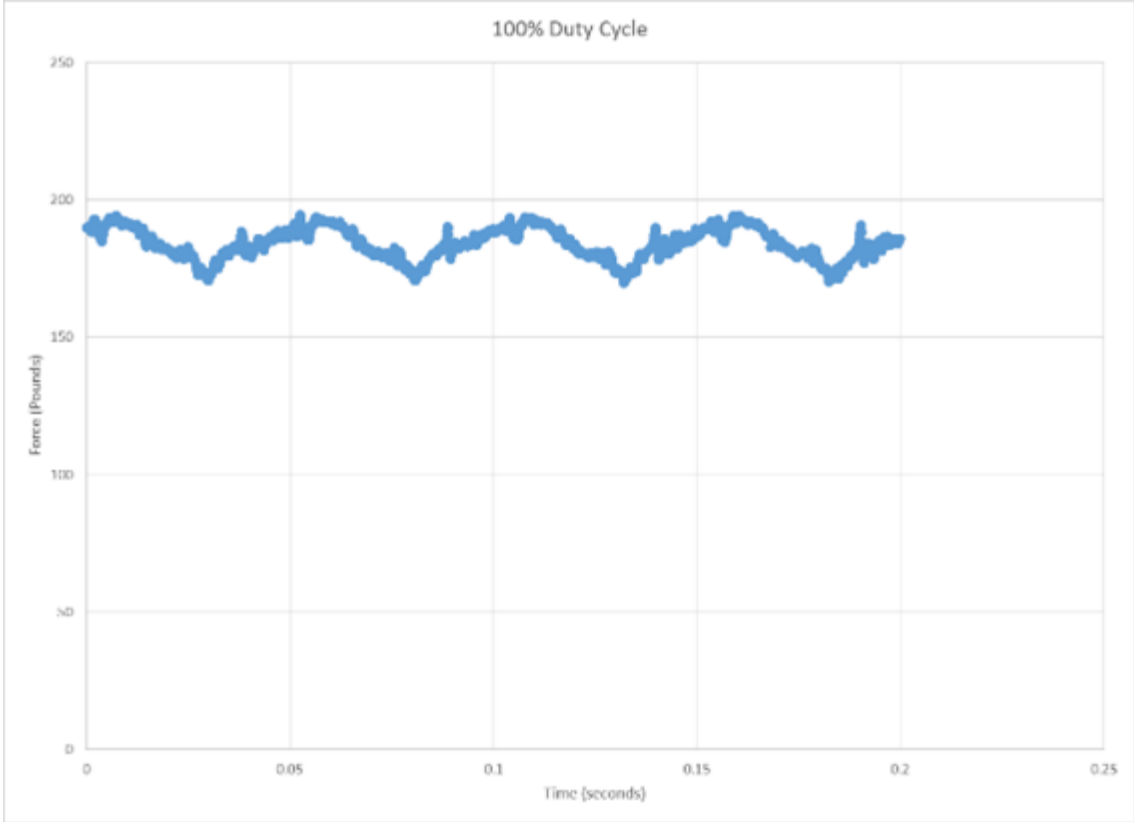
Figure 67-100% Duty Cycle response graph

Results Evaluation

The largest error in the results was perhaps the lack of a sufficient closure force. This error was investigated further to understand the cause. Since the loadcells rely on deflection to create a strain in the strain gauges they can be thought of as another spring in the system. Any deflection in the loadcells is essentially deflection that did not happen in the follower springs and therefore limited the final force measurement.

This theory was proven by finding the total spring coefficient of the follower springs and the load cells. Figure 68 shows a basic FEA analysis done through Solidworks Simulation tool.
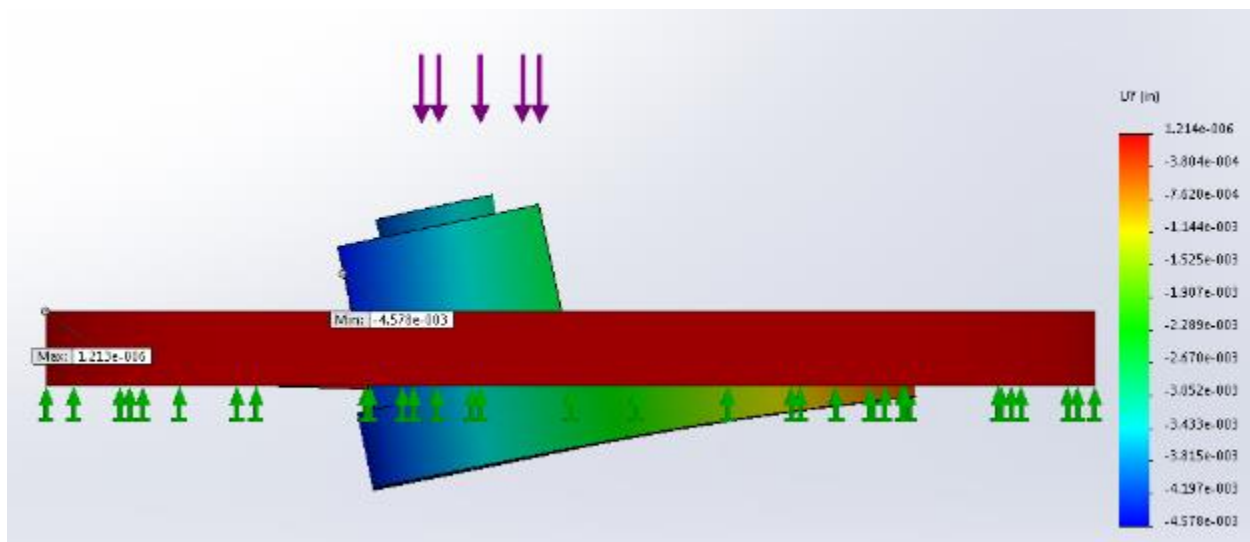
Figure 68-Load Cell FEA Analysis, deflection due to a 10 pound force

With a force of 10 pounds applied the load cell deflected 0.00458 inches downward. This results in a spring coefficient of 2184.36 Pounds per inch. The four load cells are in parallel with a total spring coefficient of 8737.44 lbs/in. The loadcells happen to be softer than the follower Belleville spring systems which have a combined spring coefficient of 12272 lbs/in. This equivalent spring can be combined with the equivalent spring of the four follower springs for a total equivalent spring coefficient of 5103.7 lbs/in. With an applied load of 185 pounds the equivalent spring would deflect 0.0362 inches. If the follower springs were to push against something much more rigid then all of this deflection would be present in the follower springs, provided the clutch gap was the same. The four follower springs have a combined spring coefficient of 12272 lbs/in. With this deflection the follower springs would push with 444 pounds of force, only 5 pounds short of the design spec. Through this analysis it is clear that due to the fact that the loadcells are softer than the follower springs the measured force was severely limited.

Another limitation in the prototype was the accuracy of achieving a given duty cycle. Due to the fact that the leadscrew was not aligned properly the U-Block could not be pulled or pushed by turning the handle. Instead the two locking nuts were loosened and the block was manually positioned based on the markings in Figure 69. Due to this the positioning was not very accurate and resulted in the errors discussed in the results section. A better positioning scheme could include a well aligned lead screw as well as an incorporation of the motor or power system into the linear motion.
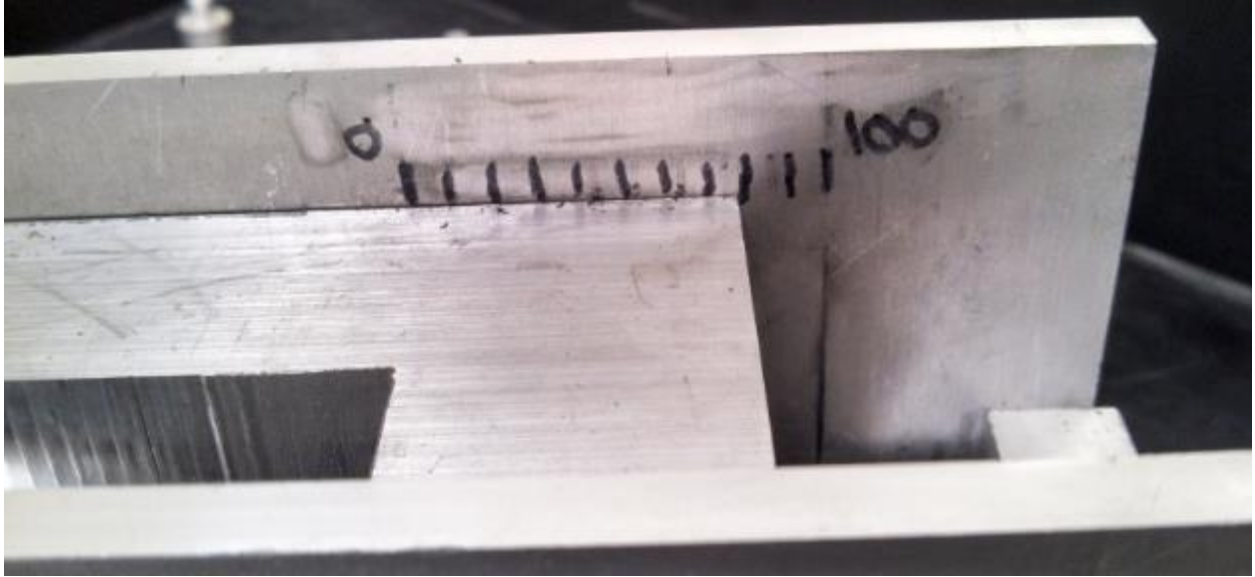
Figure 69-Duty Cycle adjustment markings

Conclusions

The goal of this project was to improve the actuation of a switch mode CVT. The project meets this goal by not only satisfactorily completing the task of engaging a theoretical clutch, but doing so in areas where the previous prototype fell short. Although there is room for some improvements, this MQP has shown that a cam based switch mode CVT's can be a viable solution for pairing a high speed flywheel with an output clutch for a vehicle.

The success of this system can be accredited to the entire design process which began with background research. Understanding current CVT and VVT technology in addition to previous work specifically on switch mode CVTs permitted foresight during preliminary designs and a selection of the best design. Analysis was carried out to prove that the chosen design could work and improve its operation. Areas of analysis included selecting the eccentric offset, cam profile, stress analysis, and spring system setup. After analysis and the design work completed, prototyping started. The system is comprised primarily of unique parts that required work with CAM software and operation of CNC machinery. After the prototype was assembled, testing began. Testing include determining duty cycle, closure force, and engagement time. Testing demonstrates where future work needs to be performed. Although some results from tests did not reach the task specs, most of the causes are understood and can be improved in future designs.

This project resulted in the desired 20Hz cycle frequency. Forces for clutch lock up were 150 lb lower than expected, due to load cells deflections and a slightly larger air gap due to tolerancing. Duty cycle achieved was reasonable. It would be easy to make an extension on this project to tune this actuating system and obtain almost perfect results. This prototype represents significant improvements over previous designs, with no major wear issues and the ability to run at full speed and at any duty cycle.

One of the underlying values of this project was what was learned along the way. Many of the topics that were touched upon during this MQP were new to the student team. Exposure to new and practicing old material has benefitted all members.

Recommendations

There are several recommendations for future work on the actuation mechanism to fine tune the system. In addition, there are many other aspects of the SMCVT that need further research.

1. Modifications can be made to the current prototype to replicate the full scale model that was designed in the initial phases of the project.
2. Testing the full system can determine effective clutch lockup, the correct size flywheel to drive the system, and the efficiency of taking the stored energy in the flywheel and transfer it through the transmission.
3. Stiffer loadcells can be installed to show that the closure force will increase proportionally.
4. The clutch air gap can be corrected.
5. A counterbalance system can be designed to dampen vibration.

References

Araujo, Jeffrey J., Michael A. DeMalia, Christopher M. Lambusta, Anthony J. Morocco, and James D. Van De Ven, Ph.D. *Switch-mode continuously variable transmission prototype design and testing*. Report. Denver, CO: International Energy Conversion Engineering Conference (IECEC), 7th International Energy Conversion Engineering Conference, 2008. Web.

Bernsau, Tim. *hotrod*. 29 July 2013. Web. 15 April 2015.

Collins, Michael. S., Matthew A. Rotier, and Scott R Woodnorth. *Switch-Mode CVT: Torsion Spring*. Undergraduate Major Qualifying Project No. 042711-231644. Worcester, MA: Worcester Polytechnic Institute, 2011. Web.

Cross, Douglas and Chris Brockbank. "Mechanical Hybrid System Comprising a Flywheel and CVT for Motorsport and Mainstream Automotive Applications." Technical Paper. 2009. Web.

Csandy Dejoe, and Edward Woydt. Valve-operating means. United States: Patent US1527456 A. 24 February 1925. Web.

Cusack, Jessy C. *Switch-Mode Continuously Variable Transmission Prototype Design and Testing*. Master's Thesis. Worcester, MA: Worcester Polytechnic Institute, 2013. Web.

Ding, Caihong and Yang Yanzhu. "Analysis and Improvement Method of the Dynamic Response of Electromagnetic Clutch Used in the Tufted Carpet Jacquard." *International Conference on Computer and Electrical Engineering*. Phuket, Thailand: International Conference on Computer and Electrical Engineering, 2008. Web.

Erdman, Arthur G. *Modern Kinematic*. Hoboken, NJ: Wiley-Interscience, 1993. Print.

Forbes, Tyler D and James D. Van de Ven, Ph.D. "Switch-Mode Continuously Variable Transmission with Flywheel Energy." *IMECE2008-67685*. Boston, MA: ASME 2008 International Mechanical Engineering Congress and Exposition, 17, 2008. Web.

Harlow, Nathan, and Robert Scott Johnson. "A new Spin on Hybrids." 2012. *Integrating Flywheel-Based Kinetic Energy Recovery Systems in Hybrid Vehicles.*

Harris, William. "HowStuffWorks.com." 27 April 2005. *How CVTs Work.* Web. 15 April 2015.

Kumar, Sunil S. *A study on working of Ball Pen*. 2008. Web. 15 April 2015.

Mitsubishi. "Mitsubishi-Motors.com." 2014. *CVT continuously controls the O-pulley diameter and changes the gear change ratio.* Web.

Norton, Robert L. *Design of Machinery*. New York, NY: McGraw Hill, 2012. Print.

—. *Machine Design: An Integrated Approach*. Upper Saddle River, NJ: Prentice Hall, 2014. Print.

Oberg, Erik, Holbrook L Horton, Franklin D Jones, Henry H Ryffel, Christopher J McCauley, and Riccardo M Heald. *Machinery's Handbook, 28th Ed.* New York, NY: Industrial Press, Inc., 2008. Web.

Somerfield, Matthew. *MattSomersF1*. 2014. Web. 15 April 2015.

Van de Ven, James D., and Jessy Cusack. "Synthesis and Baseline Testing of a digital-pulse-width-modulated clutch." *Mechanism and Machine Theory* August 2014: 81-91.
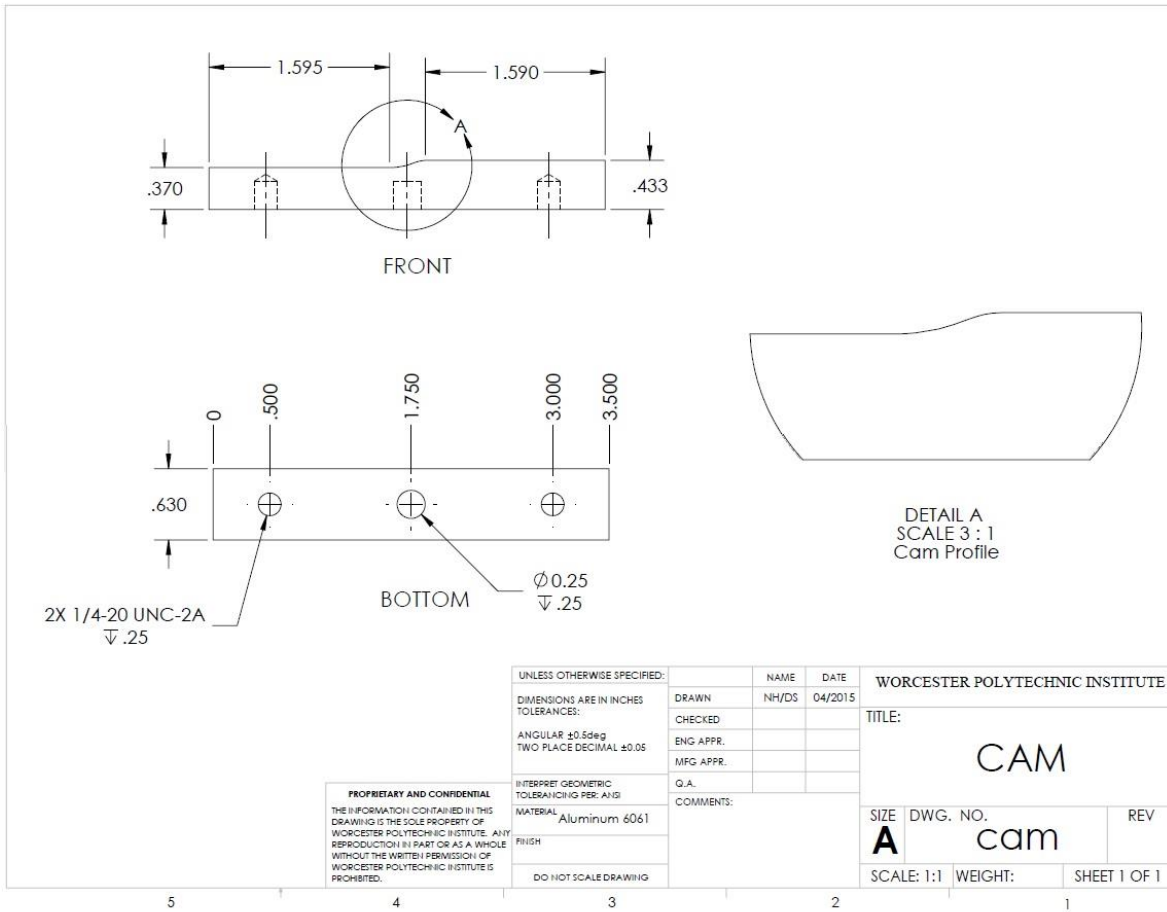
Van de Ven, James D., and Michael A. Demetriou. "Switch-Mode Continuously Variable Transmission: Modeling and Optimization." *Journal of Dynamic Systems, Measurement and Control* 2011: 031008-1 - 031008-7. Web.

Williams, Danny. Variable duration camshaft. United States: Patent US6832586 B2. 21 December 2004. Web.

—. *Williams Helical Camshaft Details*. 2014. Web.

Appendices

Appendix A - Part Drawings

1.700

.286

Ø.624

Ø.255

UNLESS OTHERWISE SPECIFIED:		NAME	DATE	WORCESTER POLYTECHNIC INSTITUTE
DIMENSIONS ARE IN INCHES TOLERANCES:	DRAWN	NH/DS	04/2015	
	CHECKED			TITLE:
ANGULAR ±0.5deg TWO PLACE DECIMAL ±0.05	ENG APPR.			FOLLOWER STEM
	MFG APPR.			
INTERPRET GEOMETRIC TOLERANCING PER: ANSI	Q.A.			
MATERIAL	COMMENTS:			
Aluminum 6061				
FINISH				SIZE A	DWG. NO. follower_stem	REV
DO NOT SCALE DRAWING				SCALE: 1:1	WEIGHT:	SHEET 1 OF 1

5   4   3   2   1

75

PART THICKNESS: 0.602

4X 3/8-16 UNC-3A THRU ALL
⌴ ⌀.650 ⤓ .440

⌀ .560 THRU ALL
⌴ ⌀ .688 ⤓ .500

4X 1/4-20 UNC-2A
THRU ALL

UNLESS OTHERWISE SPECIFIED:		NAME	DATE	WORCESTER POLYTECHNIC INSTITUTE		
DIMENSIONS ARE IN INCHES TOLERANCES:	DRAWN	NH/DS	04/2015	TITLE:		
	CHECKED			U BLOCK FRONT		
ANGULAR ±0.5deg TWO PLACE DECIMAL ±0.05	ENG APPR.					
	MFG APPR.					
INTERPRET GEOMETRIC TOLERANCING PER: ANSI	Q.A.					
	COMMENTS:			SIZE	DWG. NO.	REV
MATERIAL Aluminum 6061				A	U_Block_front	
FINISH				SCALE: 1:1	WEIGHT:	SHEET 1 OF 1
DO NOT SCALE DRAWING						

PART THICKNESS: 0.375

5.259

3.509

.750

.250

.750

⌀2.750

R1.750

2X ⌀.257
THRU ALL

UNLESS OTHERWISE SPECIFIED:		NAME	DATE	WORCESTER POLYTECHNIC INSTITUTE
DIMENSIONS ARE IN INCHES TOLERANCES:	DRAWN	NH/DS	04/2015	TITLE:
	CHECKED			ECCENTRIC STRAP
ANGULAR ±0.5deg TWO PLACE DECIMAL ±0.05	ENG APPR.			
	MFG APPR.			
INTERPRET GEOMETRIC TOLERANCING PER: ANSI	Q.A.			
	COMMENTS:			
MATERIAL Aluminum 6061				SIZE A / DWG. NO. eccentric_strap / REV
FINISH				
DO NOT SCALE DRAWING				SCALE: 1:1 WEIGHT: SHEET 1 OF 1

5   4   3   2   1

Ø.50
THRU ALL

.75

Ø2.50

UNLESS OTHERWISE SPECIFIED:		NAME	DATE	WORCESTER POLYTECHNIC INSTITUTE
DIMENSIONS ARE IN INCHES TOLERANCES:	DRAWN	NH/DS	04/2015	TITLE:
	CHECKED			
ANGULAR ±0.5deg TWO PLACE DECIMAL ±0.05	ENG APPR.			ECCENTRIC
	MFG APPR.			
INTERPRET GEOMETRIC TOLERANCING PER: ANSI	Q.A.			
	COMMENTS:			
MATERIAL Aluminum 6061				SIZE **A**	DWG. NO. eccentric	REV
FINISH					
DO NOT SCALE DRAWING				SCALE: 1:1	WEIGHT:	SHEET 1 OF 1

5   4   3   2   1

PART THICKNESS: 0.25 INCHES

7.52
7.02
6.42
5.77
5.24
4.52
3.48
2.76
2.32
2.23
1.58
.98
.38
0

5.78
5.53
5.03
4.66
4.22

8X ⌀.25
THRU ALL

4X ⌀.257
THRU ALL

2.89

⌀.37

1.56
1.12
.75

0

8X ⌀.22
THRU ALL

2X R.50

8X R.25

UNLESS OTHERWISE SPECIFIED:		NAME	DATE	WORCESTER POLYTECHNIC INSTITUTE		
DIMENSIONS ARE IN INCHES TOLERANCES:	DRAWN	NH/DS	04/2015	TITLE:		
	CHECKED					
ANGULAR ±0.5deg TWO PLACE DECIMAL ±0.05	ENG APPR.			CAM HOLDER		
	MFG APPR.					
INTERPRET GEOMETRIC TOLERANCING PER: ANSI	Q.A.					
	COMMENTS:					
MATERIAL Aluminum 6061				SIZE	DWG. NO.	REV
FINISH				A	cam_holder	
DO NOT SCALE DRAWING				SCALE: 1:4	WEIGHT:	SHEET 1 OF 1

5   4   3   2   1

.25

0
.44
1.36
3.13
4.90
6.25

0
.63
.79
1.36
2.13
2.79
4.13
4.79
4.90
5.63
6.25

3X 1/4-20 ANSI 2A
THRU ALL

4X ⌀.257
THRU ALL

4X ⌀.84
THRU ALL

UNLESS OTHERWISE SPECIFIED:		NAME	DATE	WORCESTER POLYTECHNIC INSTITUTE
DIMENSIONS ARE IN INCHES TOLERANCES:	DRAWN	NH/DS	04/2015	TITLE:
	CHECKED			
ANGULAR ±0.5deg TWO PLACE DECIMAL ±0.05	ENG APPR.			FOLLOWER GUIDE
	MFG APPR.			
INTERPRET GEOMETRIC TOLERANCING PER: ANSI	Q.A.			
MATERIAL Aluminum 6061	COMMENTS:			
FINISH				

SIZE **A** DWG. NO. follower_guide   REV

SCALE: 1:4 WEIGHT: SHEET 1 OF 1

5   4   3   2   1

3.00

1.00

1.00

.31

.63

4X 1/4-20 UNF-2A
0.88▼

.25
(ALL OTHER SLOTS)

.31
(R.50 SLOT)

6.25

2X 2.25

2X 1.50

R.50

R.81

8X R.15

2X 1.13

2X 1.75

2X 2.00

2X 2.63

UNLESS OTHERWISE SPECIFIED:		NAME	DATE	WORCESTER POLYTECHNIC INSTITUTE
DIMENSIONS ARE IN INCHES TOLERANCES:	DRAWN	NH/DS	04/2015	
	CHECKED			TITLE:
ANGULAR ±0.5deg TWO PLACE DECIMAL ±0.05	ENG APPR.			FRONT STAND
	MFG APPR.			
INTERPRET GEOMETRIC TOLERANCING PER: ANSI	Q.A.			
	COMMENTS:			
MATERIAL Aluminum 6061				
FINISH				

SIZE **A**

DWG. NO. cam_stand_left_front

REV

SCALE: 1:2 WEIGHT: SHEET 1 OF 1

DO NOT SCALE DRAWING

5   4   3   2   1

81

Appendix B – BOM

Quantity	Part	Part Description/Stock Material	Supplier
2	1"-8 nuts	Hex Nut, Grade 2,1"-8	Grainger
1	1/2 HP-Electric Motor	Boston Gear PM DC motor, 1700 RPM, 1/2 Horsepower	WPI ME Department
3	back stand bolts	1/4"-20 UNC button head screws	Rockys Ace Hardware
1	Base	3/8" fabricated low carbon steel	Exeter Scrap Metal
8	Bearing Block Screws	M5 button head socket screws	McMaster-Carr
4	Bearing Blocks	SBR16UU 16mm Aluminum open linear bearing	Ebay
2	bearing races	Washer for 1/2" Shaft Diameter Steel Thrust Needle-Roller Bearing	McMaster-Carr
36	Belville springs	High-Carbon Steel Belleville Disc Spring	McMaster-Carr
1	Bronze Alloy Bushing	2 1/2" bronze alloy bearing bushing	Grainger
1	Cam Holder	1/4" Aluminum 6061 plate	Onlinemetals
8	Cam Screws	1/4"-20 UNC button head socket head screws	Rockys Ace Hardware
4	Cams	3"x5/8" Aluminum 6061 rectangle	MSC
1	Camshaft	1/2" Steel Rod	
2	camshaft bearings	Steel Needle-Roller Bearing	McMaster-Carr
1	Camshaft Sprocket	Steel Machinable-Bore Sprocket for ANSI Number 35 Roller Chain	McMaster-Carr
2	camshaft thrust bearings	Cage Assembly for 1/2" Shaft Diameter, 15/16" OD Steel Thrust Needle-Roller Bearing	McMaster-Carr
1	chain	Roller Chain, ANSI Number 35	McMaster-Carr
1	chain connector	Connecting Link for ANSI Number 35 Roller Chain	McMaster-Carr
1	Clevis pin	18-8 Stainless Steel Clevis Pin with Cotter Pin 3/8" diameter	McMaster-Carr
1	Eccentric	2 1/2" Aluminum 6061 rod	Washburn Shops
1	Eccentric Strap	3"x5/8" Aluminum 6061 rectangle	MSC
2	Eccentric Strap Tabs	1/4" Aluminum 6061 Plate	Onlinemetals
1	Flywheel	Low Carbon Steel Rod, 4" Diameter, 1/2" Length	McMaster-Carr
4	Flywheel Bolts	M5x10 Socket Head Cap Screws	Washburn Shops
1	follower guide	1/4" Aluminum 6061 Plate	Onlinemetals
3	follower guide bolts	1/4"-20 UNC button head screws	Rockys Ace Hardware
1	granite base	21"x25" granite slab	New England Industrial Recycling
1	handle	1"-8 Hex nut and steel scrap	Grainger/Washburn Shops
1	lead handle screw set screw	1/4"-20 UNC set screw	Washburn Shops
1	lead screw	ASTM A193 Grade B7 Steel Threaded Stud	McMaster-Carr
2	leadscrew thrust bearing	Steel Thrust Needle-Roller Bearing	McMaster-Carr
4	lifter guides	Hyraulic valve lifter guides 5.7L GMC/Chevrolet	Mongeon's Auto
4	load cells	4 pcs Body Load Cell Weighing Sensor Resistance strain Half-bridge	Ebay
1	Motor Sprocket	#35 Chain 10 Spoke Sprocket	WPI ME Department
1	motor stand	1/2" aluminum 6061 Plate	WPI ME Department
2	motor stand screws	1/4"-20 UNC Flathead 1/2"	Rockys Ace Hardware
4	Pins	1/4" Black-Oxide Alloy steel pins 1/2" Length	McMaster-Carr
16	rail screws	M5 button head socket screws	McMaster-Carr
2	Rails	linear bearing rail SBR16-350mm	Ebay
3	Set Screws	1/4"-20 UNC set screws 3/8" long	Rockys Ace Hardware
1	shaft	1"OD Aluminum Round Rod	MSC
6	Shoulder Screws for U-Block	1/4"-20 UNC shoulder bolts	McMaster-Carr
1	spacer	1/4" Aluminum 6061 Plate	Onlinemetals
10	Stand Bolts to Base	1/4"-20 UNC Flathead 1 1/8"	Rockys Ace Hardware
10	Stand Bolts to Top	1/4"-20 UNC button head screws 1 1/8" lenght	Rockys Ace Hardware
5	Stands	3"x5/8" Aluminum 6061 rectangle	MSC
2	Strap Tab Bolts	1/4"-20 UNC	Rockys Ace Hardware
1	test hood	Plywood, acrylic, LED lights	Donation
1	thrust plate	1/4" Aluminum 6061 Plate	Onlinemetals
4	thrust plate bolts	1/4"-20 UNC Flathead 1/2"	Rockys Ace Hardware
1	Top	1/4" Aluminum 6061 plate	Onlinemetals
4	U-Block Bolts	3/8"-16 UNC socket head cap screws	Washburn Shops
2	U-block pieces	Aluminum Rectanglar bar 6061	MSC
2	U-Block stands	1/4" Aluminum 6061 Plate	Onlinemetals
4	valve lifter stems	1" Aluminum 6061 rod	MSC
4	valve lifters	Hyraulic valve lifter 5.7L GMC/Chevrolet	Mongeon's Auto
4	vibration pads	Vibration damping rubber	WPI ME Department
1	Vibrational Tourqe Transducer	HBM Drehschwingungus Aufnehmr	WPI ME Department
5	wave springs	Wave Disc Spring, High-Carbon Steel	McMaster-Carr

Bellville Spring Options

$$k_b := 5625 \cdot \frac{lbf}{in}$$

McMaster-Carr Belleville Dic Spring
#9712K61

Option 1

$$k_{follower} := \frac{1}{\frac{1}{k_b \cdot 2} + \frac{1}{k_b \cdot 2} + \frac{1}{k_b \cdot 2} + \frac{1}{k_b \cdot 3}} = 3068 \cdot \frac{lbf}{in}$$

>> << >> <<<<
Spring configuration

$$k_{sys} := k_{follower} \cdot 4 = 12273 \cdot \frac{lbf}{in}$$

$$difference := k_{sys} - 12075.5 \cdot \frac{lbf}{in} = 197 \cdot \frac{lbf}{in}$$

Option 2

$$k_{follower} := \frac{1}{\frac{1}{k_b \cdot 2} + \frac{1}{k_b \cdot 2} + \frac{1}{k_b \cdot 2} + \frac{1}{k_b \cdot 4}} = 3214 \cdot \frac{lbf}{in}$$

>> << >> <<<<<
Spring configuration

$$k_{sys} := k_{follower} \cdot 4 = 12857 \cdot \frac{lbf}{in}$$

$$difference := k_{sys} - 12075.5 \cdot \frac{lbf}{in} = 782 \cdot \frac{lbf}{in}$$

Option 3

$$k_{follower} := \frac{1}{\frac{1}{k_b \cdot 2} + \frac{1}{k_b \cdot 2} + \frac{1}{k_b \cdot 2} + \frac{1}{k_b \cdot 5}} = 3309 \cdot \frac{lbf}{in}$$

>> << >> <<<<<<
Spring configuration

$$k_{sys} := k_{follower} \cdot 4 = 13235 \cdot \frac{lbf}{in}$$

$$difference := k_{sys} - 12075.5 \cdot \frac{lbf}{in} = 1160 \cdot \frac{lbf}{in}$$

Option 4

$$k_{follower} := \cfrac{1}{\dfrac{1}{k_b \cdot 2} + \dfrac{1}{k_b \cdot 2} + \dfrac{1}{k_b \cdot 3} + \dfrac{1}{k_b \cdot 3}} = 3375 \cdot \dfrac{lbf}{in}$$

>> << >>> <<<<

Spring configuration

$$k_{sys} := k_{follower} \cdot 4 = 13500 \cdot \dfrac{lbf}{in}$$

$$difference := k_{sys} - 12075.5 \cdot \dfrac{lbf}{in} = 1425 \cdot \dfrac{lbf}{in}$$

Option 5

$$k_{follower} := \cfrac{1}{\dfrac{1}{k_b \cdot 2} + \dfrac{1}{k_b \cdot 2} + \dfrac{1}{k_b \cdot 3} + \dfrac{1}{k_b \cdot 4}} = 3553 \cdot \dfrac{lbf}{in}$$

$$k_{sys} := k_{follower} \cdot 4 = 14211 \cdot \dfrac{lbf}{in}$$

>> << >>> <<<<

Spring configuration

$$difference := k_{sys} - 12075.5 \cdot \dfrac{lbf}{in} = 2135 \cdot \dfrac{lbf}{in}$$

Option 6

$$k_{follower} := \cfrac{1}{\dfrac{1}{k_b \cdot 2} + \dfrac{1}{k_b \cdot 2} + \dfrac{1}{k_b \cdot 4} + \dfrac{1}{k_b \cdot 4}} = 3750 \cdot \dfrac{lbf}{in}$$

$$k_{sys} := k_{follower} \cdot 4 = 15000 \cdot \dfrac{lbf}{in}$$

>> << >>>> <<<<

Spring configuration

$$difference := k_{sys} - 12075.5 \cdot \dfrac{lbf}{in} = 2924 \cdot \dfrac{lbf}{in}$$

Wave Spring Options

$$SpringF := \frac{18 \cdot lbf}{0.05 \cdot in} = 360 \cdot \frac{lbf}{in}$$

$$height := 0.099 \cdot in$$

$$gap := 0.35 \cdot in$$

$$SpringC := \frac{1}{\dfrac{1}{SpringF} + \dfrac{1}{SpringF} + \dfrac{1}{SpringF} + \dfrac{1}{SpringF}} = 90 \cdot \frac{lbf}{in}$$

$$SpringC \cdot (height \cdot 4 - gap) = 4.14 \, lbf$$

$$SpringC := \frac{1}{\dfrac{1}{SpringF} + \dfrac{1}{SpringF} + \dfrac{1}{SpringF} + \dfrac{1}{SpringF} + \dfrac{1}{SpringF}} = 72 \cdot \frac{lbf}{in}$$

$$SpringC \cdot (height \cdot 5 - gap) = 10.44 \, lbf$$

$$SpringC := \frac{1}{\dfrac{1}{SpringF} + \dfrac{1}{SpringF} + \dfrac{1}{SpringF} + \dfrac{1}{SpringF} + \dfrac{1}{SpringF} + \dfrac{1}{SpringF}} = 60 \cdot \frac{lbf}{in}$$

$$SpringC \cdot (height \cdot 6 - gap) = 14.64 \, lbf$$

Appendix D - Matlab Cam Optimization

```
%Optimize Cam Curvature Hopefully
clear all;
ecc=0.75;
cam=0.2;
rh=0.0625;

x1=0;    y1=0;

x4=cam*2*ecc;    y4=rh;
%r = a + (b-a).*rand(100,1);

step=0.1;

for j=1:5000000;
    x2(j)=0.069+(0.082-0.069).*rand;
    y2(j)=0.003+(0.006-0.003).*rand;
    x3(j)=0.23+(0.26-0.23).*rand;
    y3(j)=0.048+(0.058-0.048).*rand;
    B=[y2(j);y3(j);y4;0;0];
    Poly=[x2(j).^3, x2(j).^4, x2(j).^5, x2(j).^6, x2(j).^7;
        x3(j).^3, x3(j).^4, x3(j).^5, x3(j).^6, x3(j).^7;
        x4.^3, x4.^4, x4.^5, x4.^6, x4.^7;
        3.*x4.^2, 4.*x4.^3, 5.*x4.^4, 6.*x4.^5, 7.*x4.^6;
        6.*x4, 12.*x4.^2, 20.*x4.^3, 30.*x4.^4, 42.*x4.^5;];
    C=inv(Poly)*B;
```

```
    x=0:0.003:0.3;

v=3.*C(1,1).*x.^2+4.*C(2,1).*x.^3+5.*C(3,1).*x.^4+6.*C(4,1).*x.^5+7.*C(5,1).*
x.^6;

a=6.*C(1,1).*x+12.*C(2,1).*x.^2+20.*C(3,1).*x.^3+30.*C(4,1).*x.^4+42.*C(5,1).
*x.^5;
    k=a./((1+(v).^2).^(3/2));
    kmax(j)=max(k);
end

temp=10;

for j=1:5000000;
    i=kmax(j)-2;
    if i>0 && i<temp;
        temp=i;
    end
end

temp=temp+2;
I=find(kmax==temp);

x2opt=x2(I);
y2opt=y2(I);
x3opt=x3(I);
y3opt=y3(I);


B=[y2opt;y3opt;y4;0;0];
Poly=[x2opt.^3, x2opt.^4, x2opt.^5, x2opt.^6, x2opt.^7;
      x3opt.^3, x3opt.^4, x3opt.^5, x3opt.^6, x3opt.^7;
      x4.^3, x4.^4, x4.^5, x4.^6, x4.^7;
      3.*x4.^2, 4.*x4.^3, 5.*x4.^4, 6.*x4.^5, 7.*x4.^6;
      6.*x4, 12.*x4.^2, 20.*x4.^3, 30.*x4.^4, 42.*x4.^5;];
C=inv(Poly)*B;

x=0:0.003:0.3;
    s=C(1,1).*x.^3+C(2,1).*x.^4+C(3,1).*x.^5+C(4,1).*x.^6+C(5,1).*x.^7;

plot(x,s);
```

Eccentric Offset $a := 0.01905 m$

Strap Length $b := 0.117 m$

Angle offset $c := 0 \cdot m$

$fac := \dfrac{\pi}{180}^{\blacksquare}$

$\theta_4 := 90 \, fac^{\blacksquare}$

$t := 0, 0.0001 sec \dots 0.05 sec$

$f := 20 Hz$ Rotational rate

$\omega := f \cdot 2\pi = 125.664 \dfrac{1}{s}$ Angular Velocity

$\theta_2(t) := \omega \cdot t$ Crank Angle over time

$\dfrac{1}{20} = 0.05$

$\theta_2(0.5 sec) = 62.832$

$\theta_3(t) := asin\left(\dfrac{a \cdot \sin(\theta_2(t)) - c}{b}\right)$ Angle between strap and horizontal over time

$d(t) := -\left[(a \cdot \cos(\theta_2(t)) - b \cdot \cos(\theta_3(t))) + 0.098 m\right]$ Cam Plate Position Over time
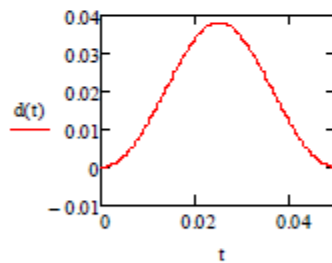
$vel(t) := \dfrac{d}{dt} d(t)$
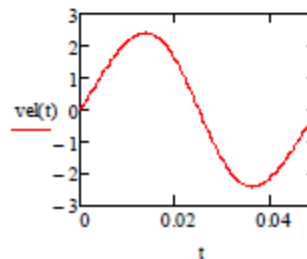
Cam Plate Velocity

$$acc(t) := \frac{d}{dt}\,vel(t)$$
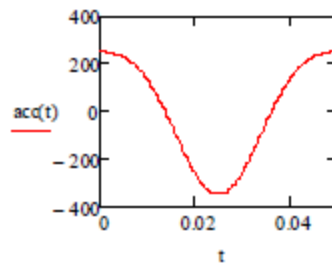
Cam Plate Acceleration

$mass := 2lb$ $mass = 0.907kg$

$$F_i(t) := mass \cdot acc(t)$$

$$-317N = -698.865\frac{m}{s^2} \cdot lb$$

Cam Profile Coefficients

$C3 := 22.335$

$C4 := -253.190$

$C5 := 148\llcorner$

$C6 := -4177.\,$

$C7 := 4341.\,$ $DC := 0.5$

Cam profile with high dwell and low dwell

$$x(t) := \begin{vmatrix} 0 & \text{if } d(t) < (2{\cdot}a - 0.21{\cdot}2{\cdot}a){\cdot}(1 - DC) \\ 39[d(t) - (2{\cdot}a - 0.21{\cdot}2{\cdot}a){\cdot}(1 - DC)]{\cdot}\dfrac{1}{m} & \text{if } (2{\cdot}a - 0.21{\cdot}2{\cdot}a){\cdot}(1 - DC) < d(t) < (2{\cdot}a - 0.21{\cdot}2{\cdot}a){\cdot}(1 - DC) + 0.21{\cdot}2a \\ 0.31 & \text{if } d(t) > (2{\cdot}a - 0.21{\cdot}2{\cdot}a){\cdot}(1 - DC) + 0.21{\cdot}2a \end{vmatrix}$$

Cam profile and normal Vector of Cam Profile

$$\text{Poly}(t) := C3{\cdot}x(t)^3 + C4{\cdot}x(t)^4 + C5{\cdot}x(t)^5 + C6{\cdot}x(t)^6 + C7{\cdot}x(t)^7$$

$$\text{Norm}(t) := \left(\text{atan}\left(3{\cdot}C3{\cdot}x(t)^2 + 4{\cdot}C4{\cdot}x(t)^3 + 5{\cdot}C5{\cdot}x(t)^4 + 6{\cdot}C6{\cdot}x(t)^5 + 7{\cdot}C7{\cdot}x(t)^6\right) + \frac{\pi}{2} \right)$$
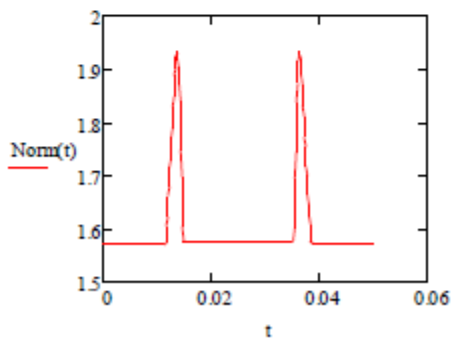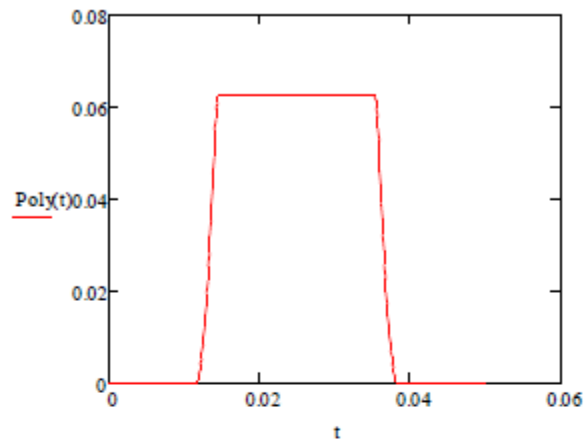
$$CS := 0.6mm \qquad CS = 6 \times 10^{-4} m$$

$$k := 170 \cdot lbf$$

Spring Compression over Time

$$Fspring(t) := \begin{vmatrix} 0 & \text{if } Poly(t) < 0.024 \\ [4 \cdot (Poly(t) - 0.024) \cdot k] & \text{if } Poly(t) > 0.024 \end{vmatrix}$$
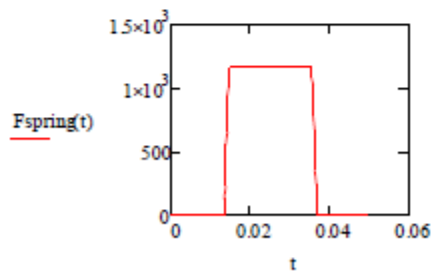
$$Xspring(t) := Fspring(t) \cdot tan\left(Norm(t) - \frac{\pi}{2}\right)$$

X Spring Component
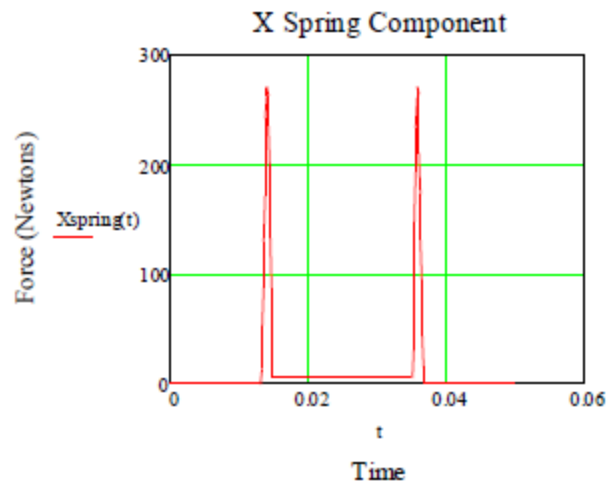
$$F_T(t) := F_s(t) + Xspring(t)$$

$$F_{rod}(t) := \frac{F_T(t)}{\cos(\theta_3(t))}$$

$$F_{rod}(0) = 51.362 lbf$$

Force on Eccentric Strap

$-31 \text{IN} = -69.916 \text{lbf}$

Torque Analysis

$\omega := 40 \cdot \pi \dfrac{1}{\sec}$

Crankangle $\theta2(t) := \omega \cdot t$
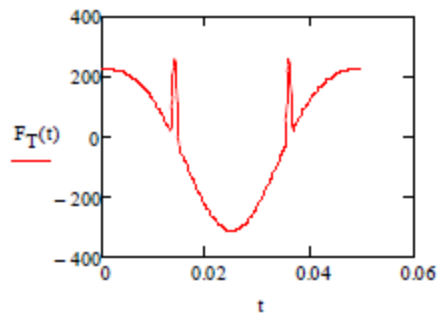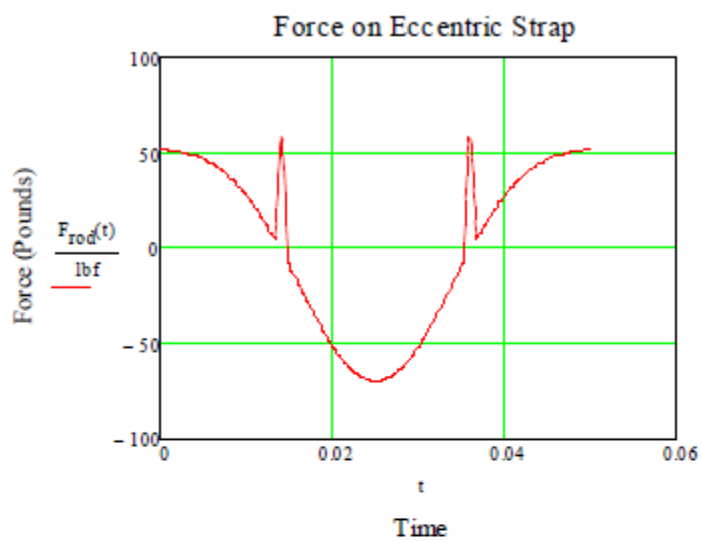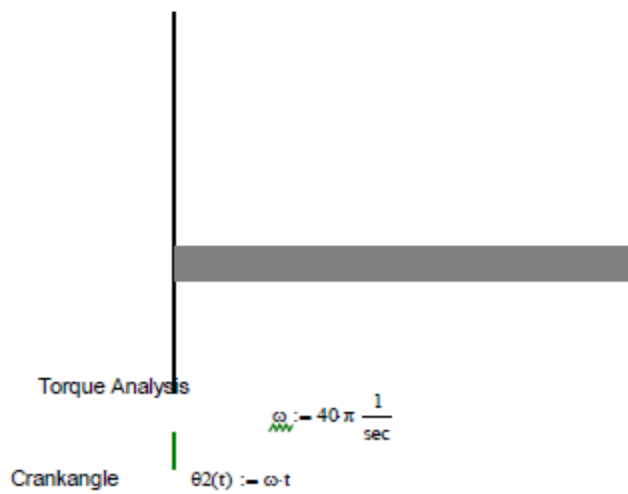
$T\theta(t) := \pi - \theta2(t) - \theta_3(t)$ Angle Between Strap and line between eccentric center and offset position
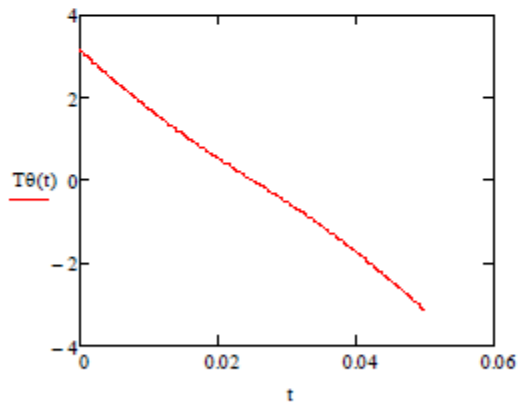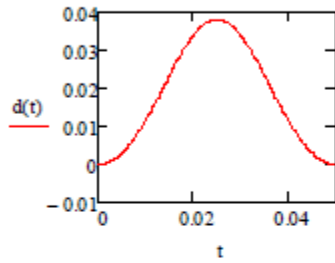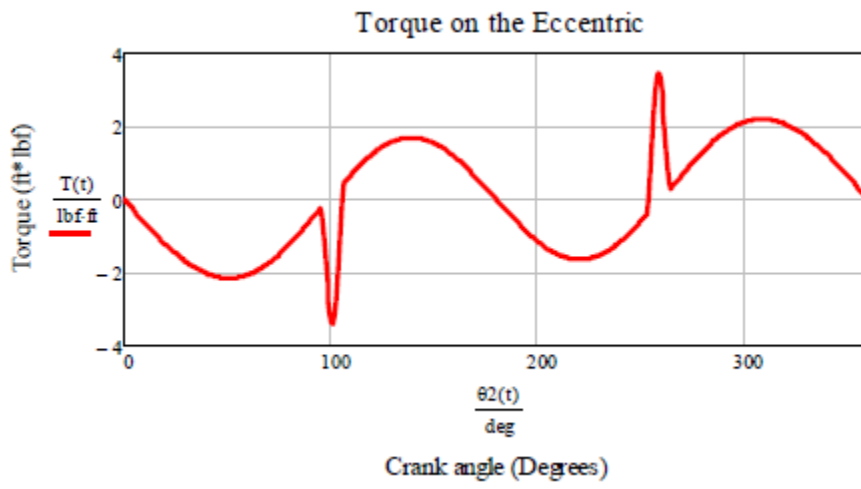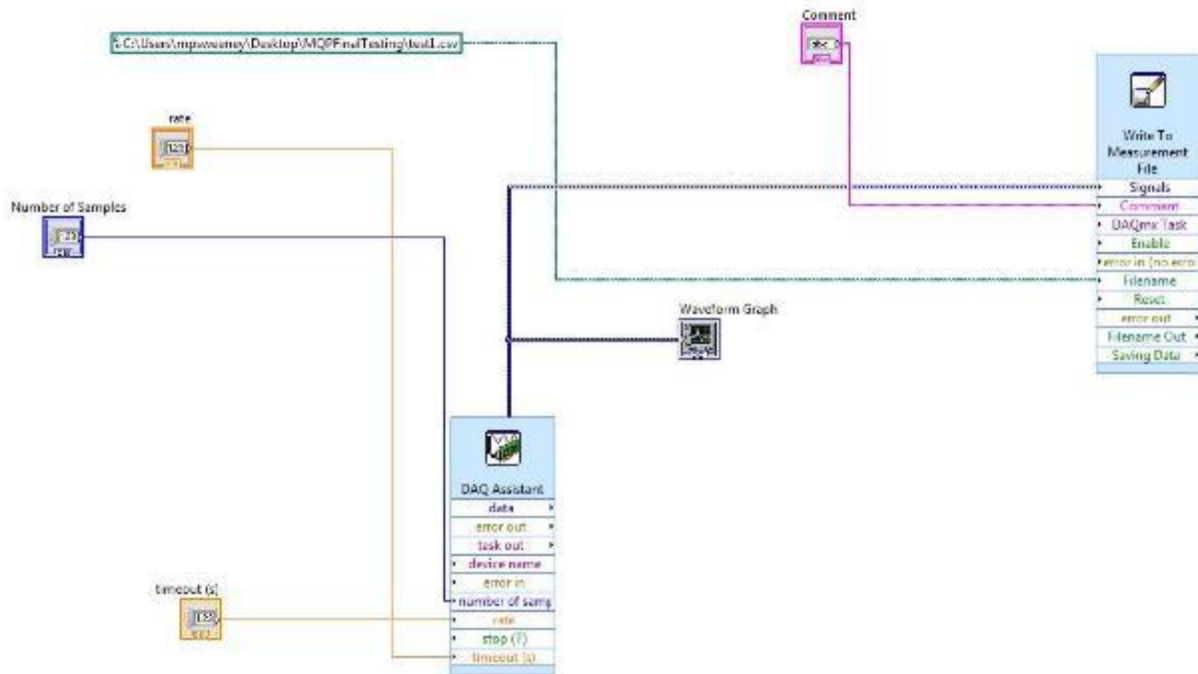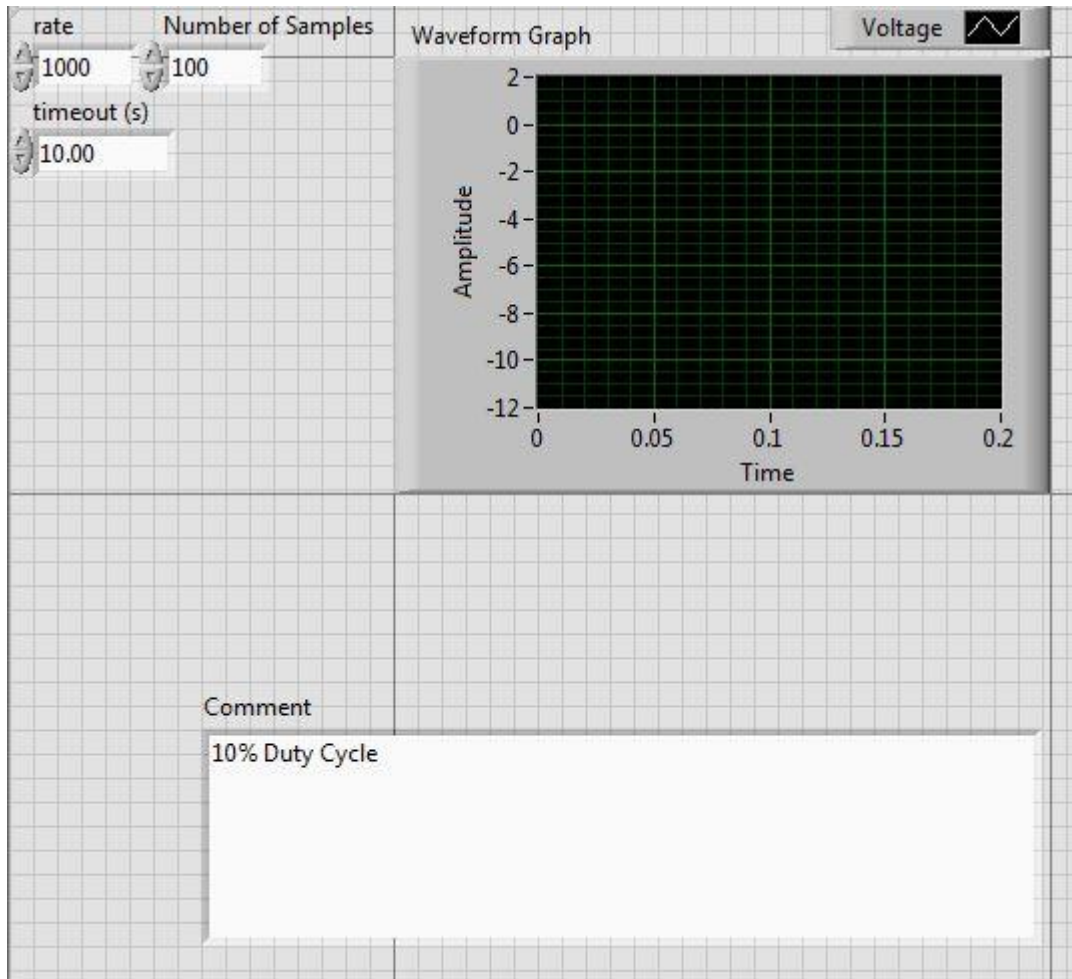
$T(t) := -F_{rod}(t) \cdot \sin(T\theta(t)) \cdot 0.75 in$

Torque on the Eccentric

Crank angle (Degrees)

Appendix F - LabVIEW Program

rate

Number of Samples

Waveform Graph

Voltage

1000

100

timeout (s)

10.00

Amplitude

2 –
0 –
-2 –
-4 –
-6 –
-8 –
-10 –
-12 –

0   0.05   0.1   0.15   0.2

Time

Comment

10% Duty Cycle

Appendix G – Load Cell Response Graphs

0% Duty Cycle
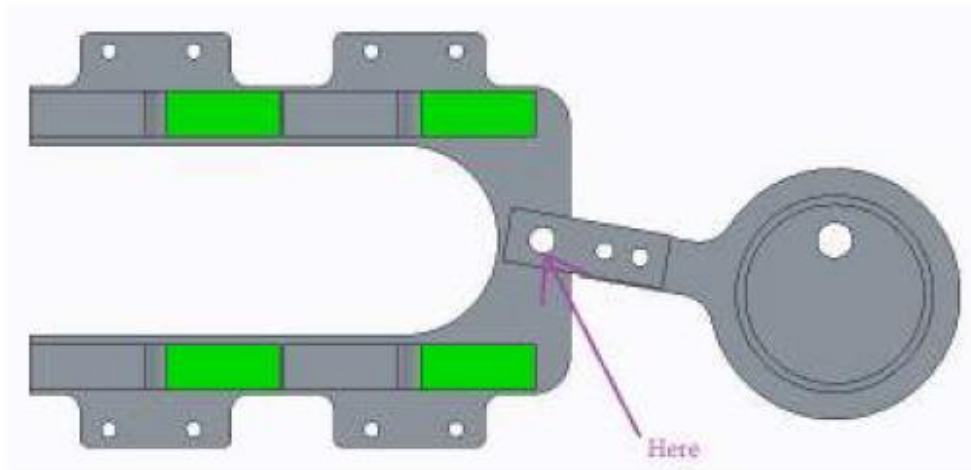

10% Duty Cycle

20% Duty Cycle

30% Duty Cycle

98

40% Duty Cycle

50% Duty Cycle

60% Duty Cycle

Force (Pounds) vs. Time [seconds]

70% Duty Cycle

Force (Pounds) vs. Time [seconds]

80% Duty Cycle

90% Duty Cycle

100% Duty Cycle
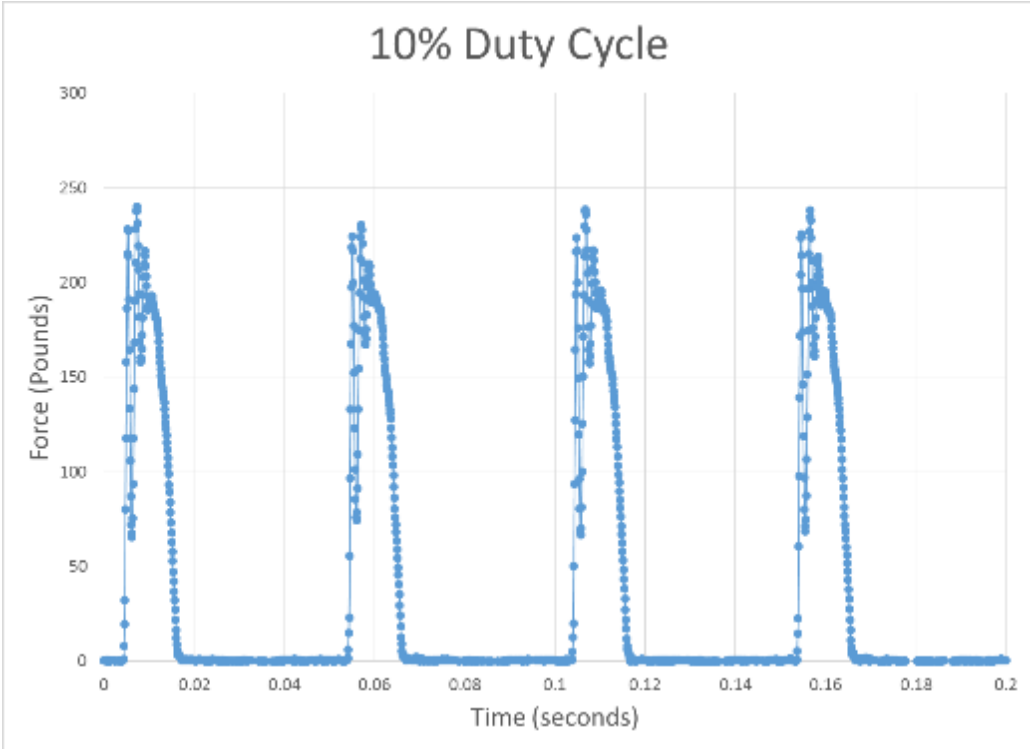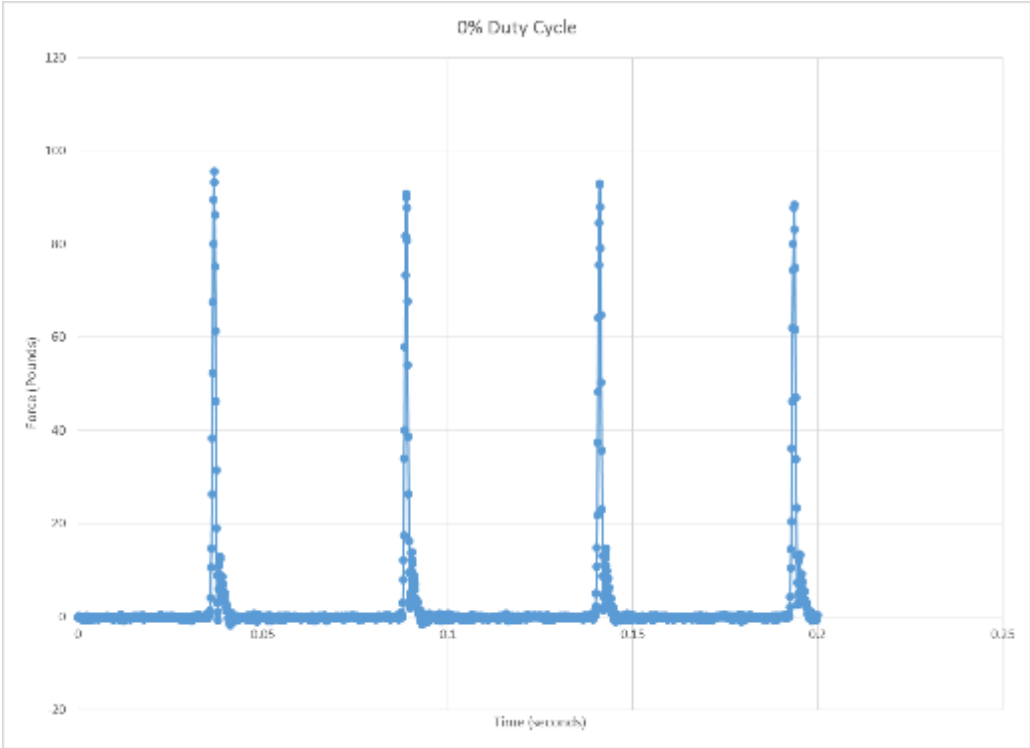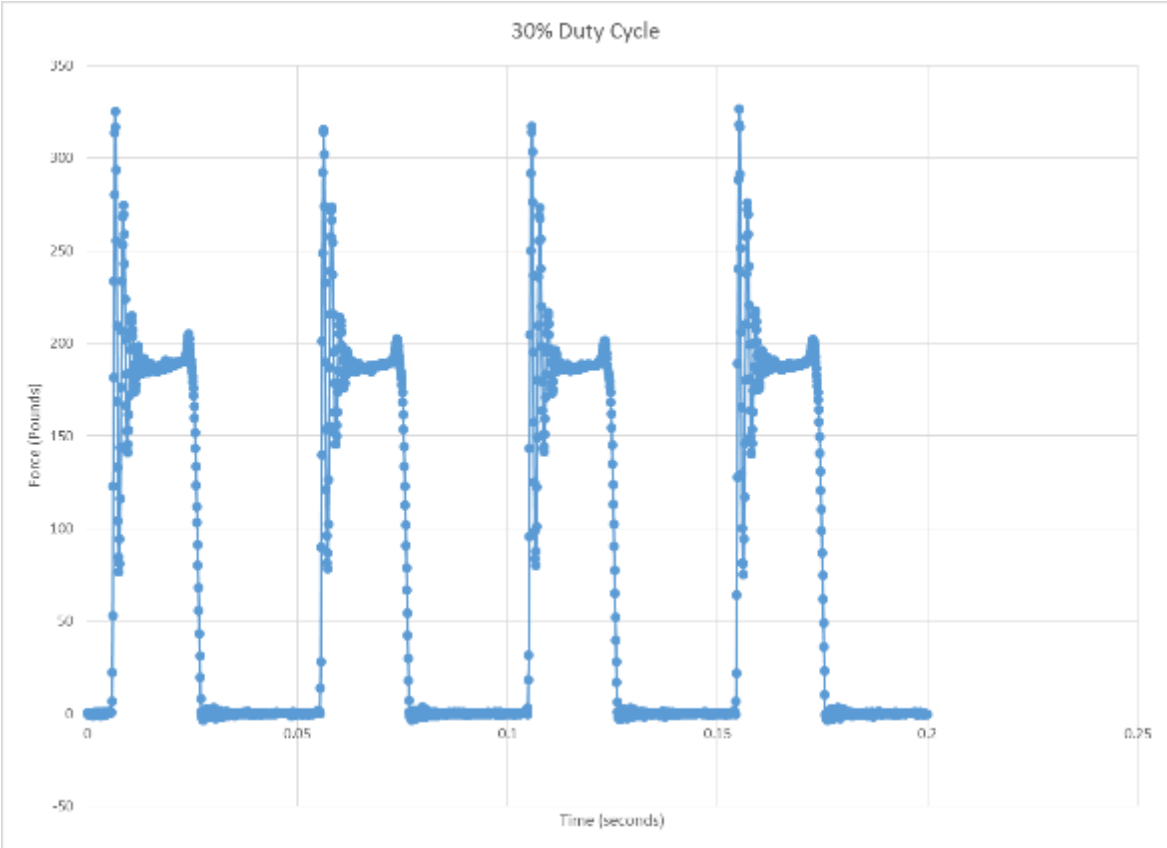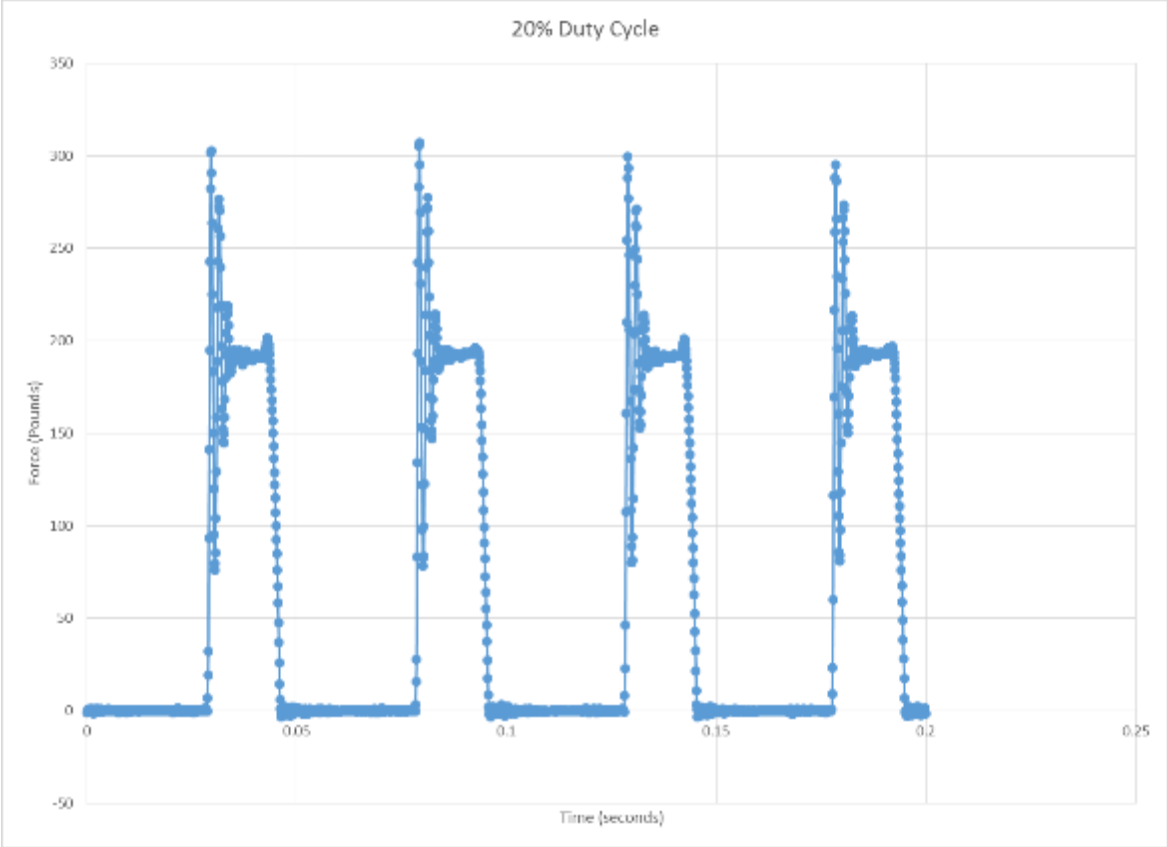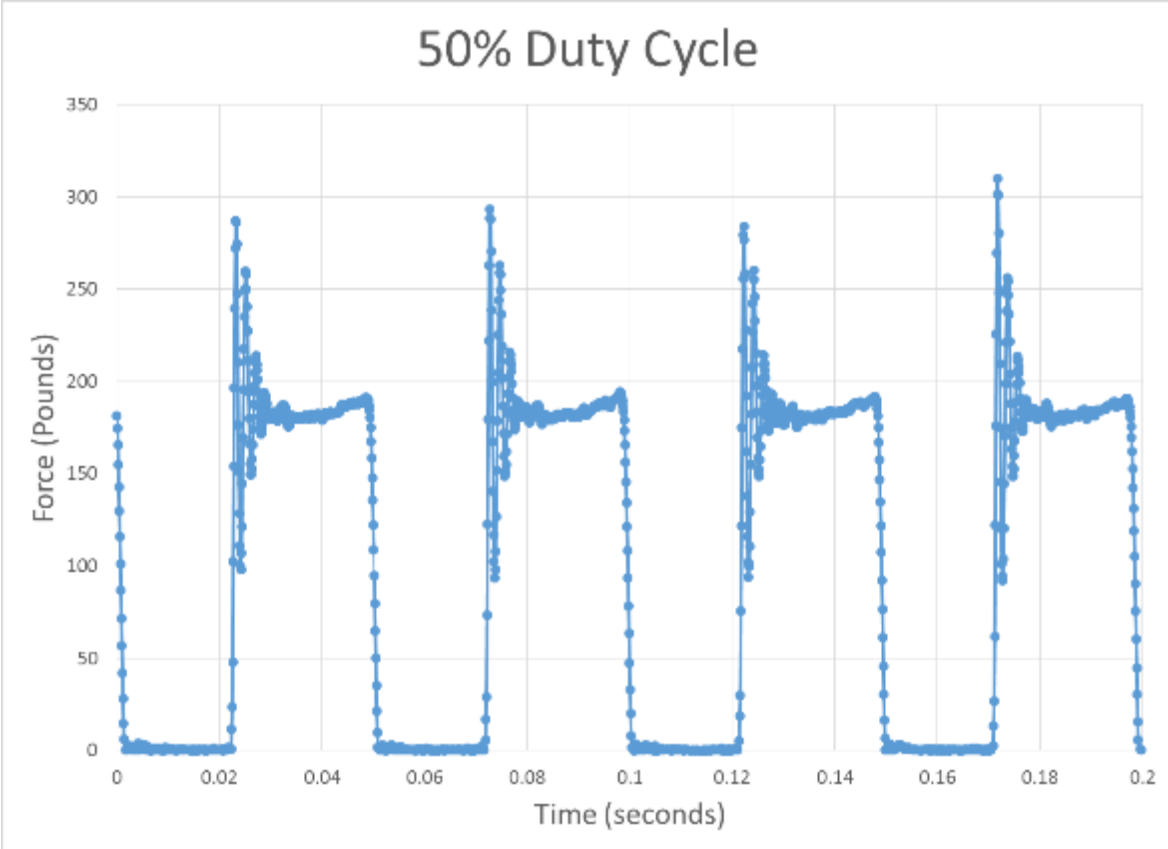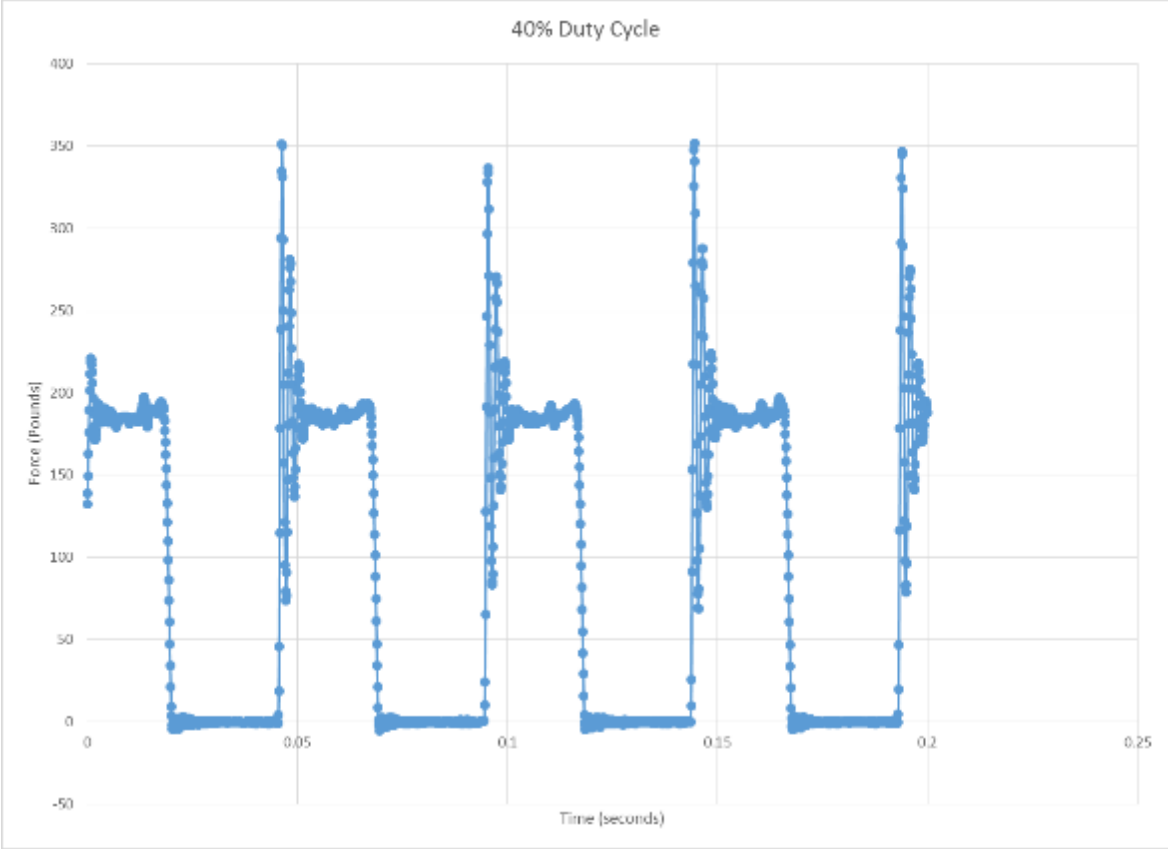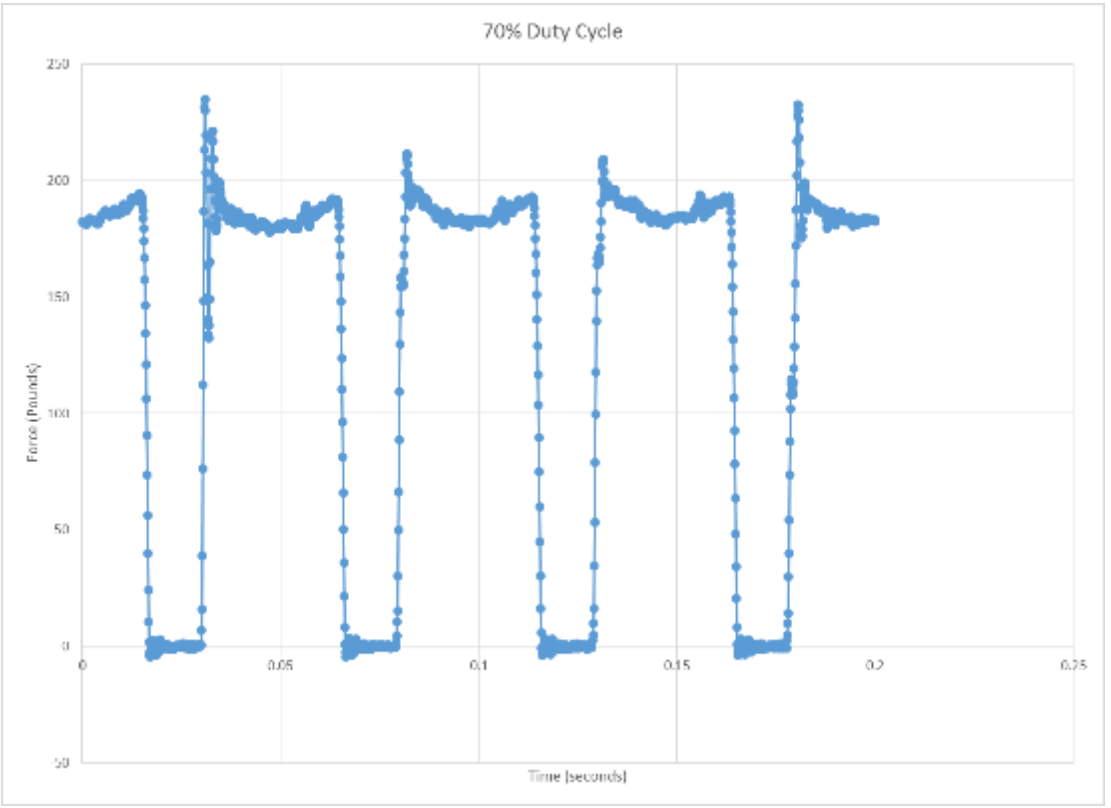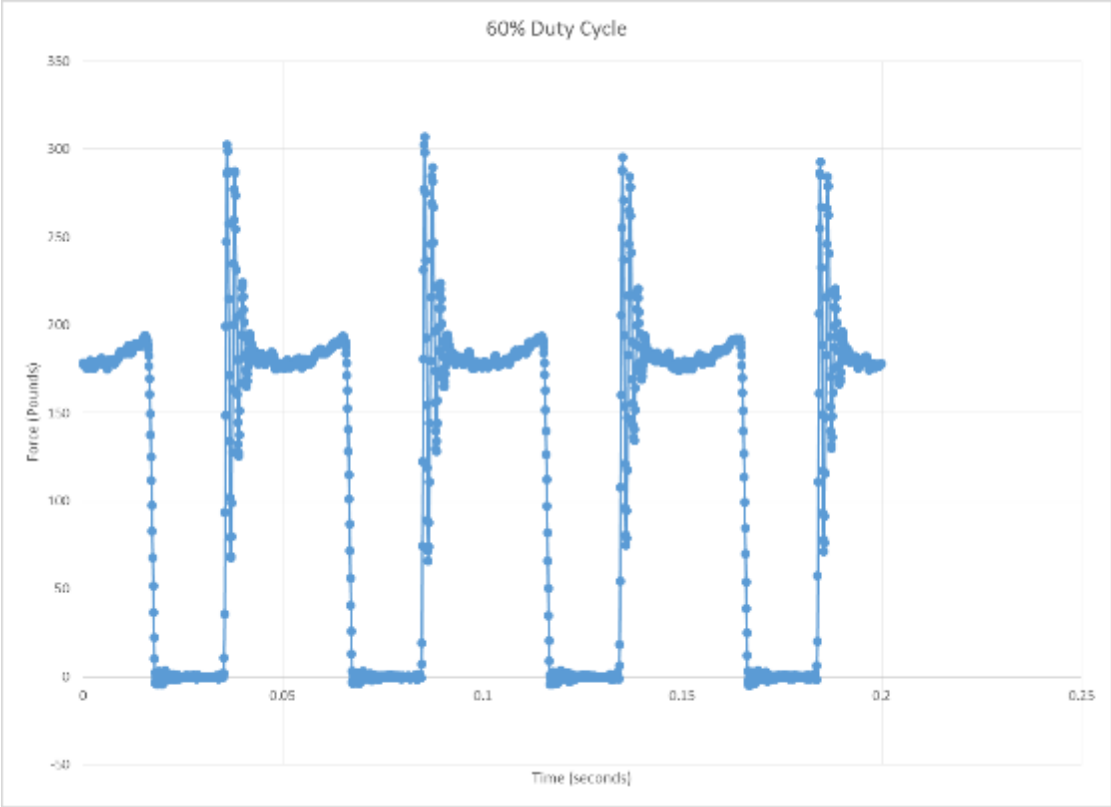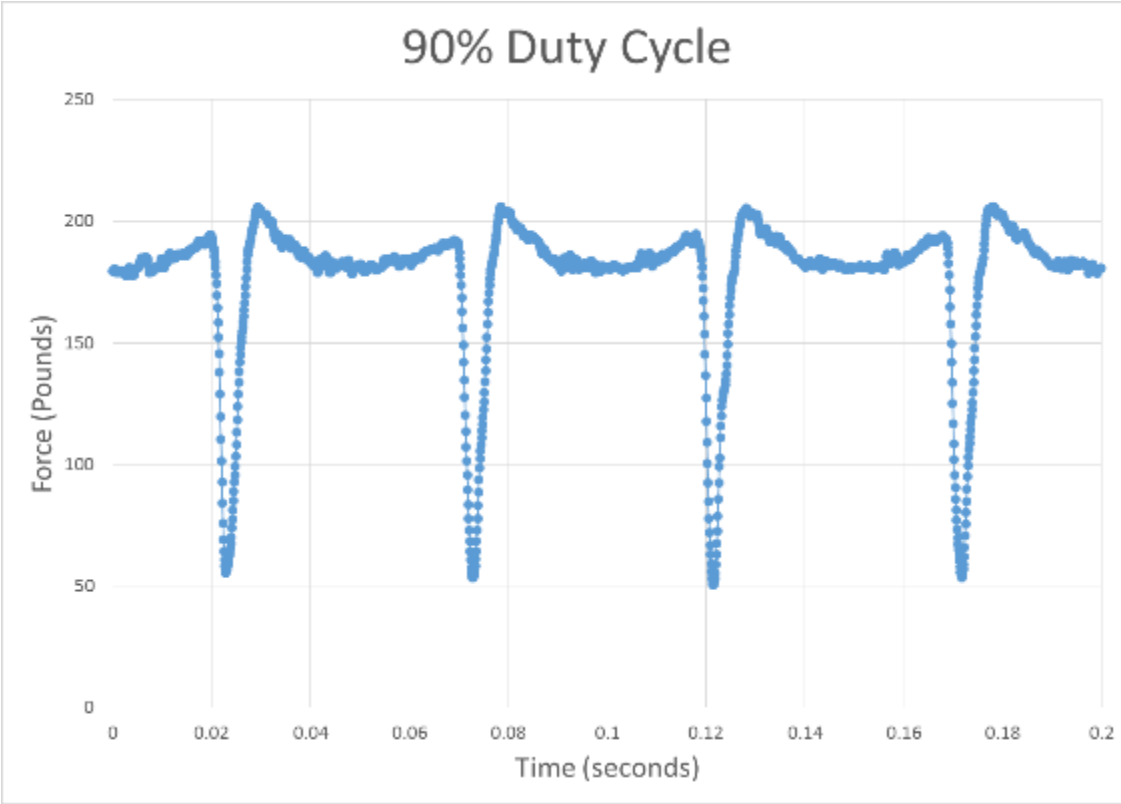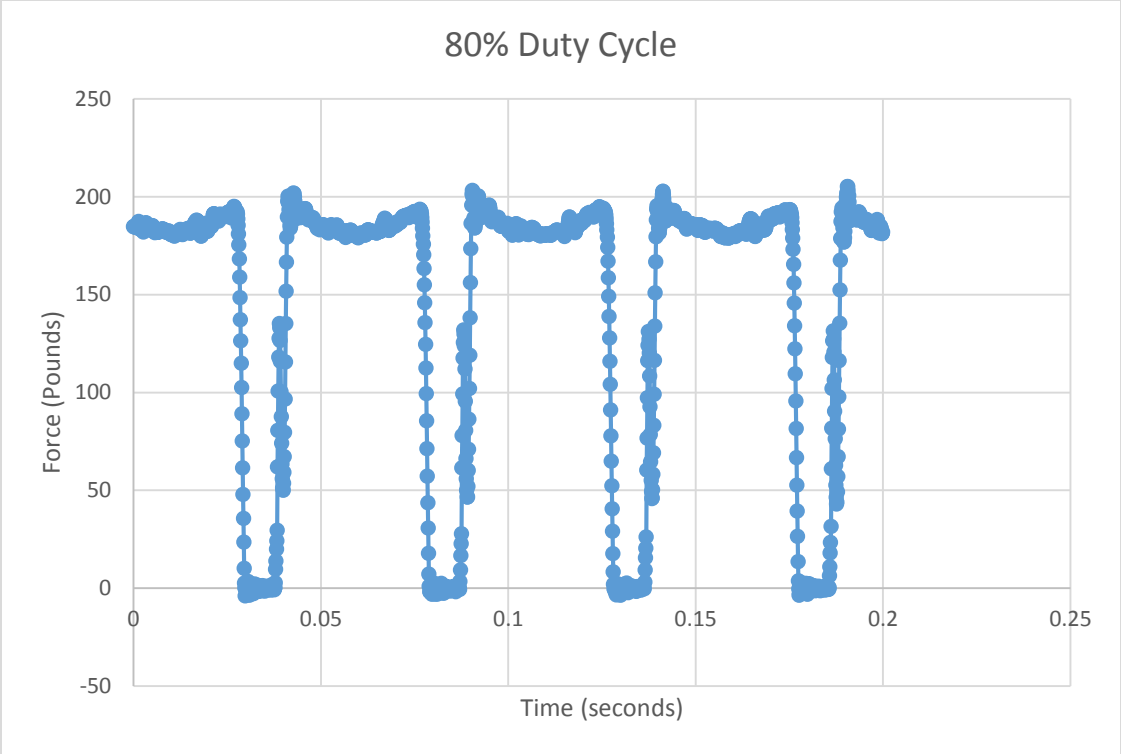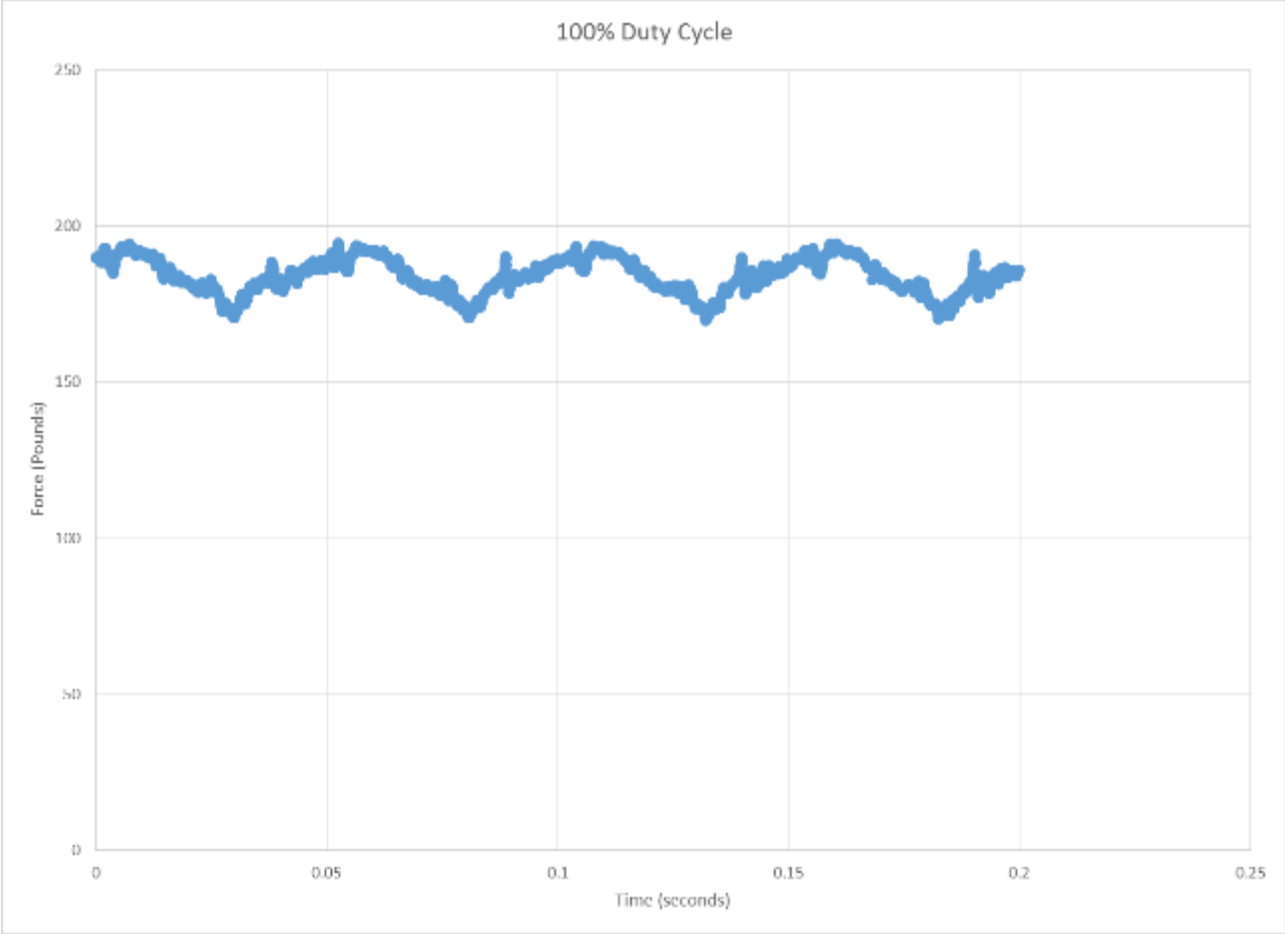
Our eccentric strap is designed to connect to the cam holder with McMasterCarr pin #**92390A893**.

Here

The relevant hole in the cam holder is $D_{ch} := 0.375in$

The center of this hole is placed $x_{ch} := 0.380in$ away from the edge.

The cam holder thickness is $t_{ch} := 0.250in$

The hole in the strap tab is $D_{st} := 0.375in$

The center of this hole is placed $x_{st} := 0.495in$ away from the edge.

The strap tab (where the hole is) has a thickness of $t_{st} := 0.250in$

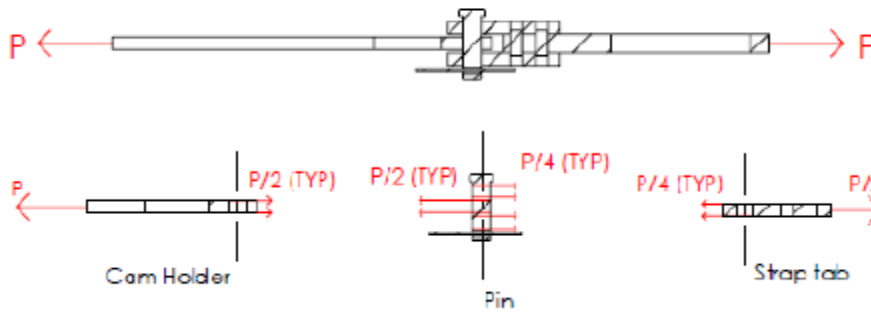They're made of aluminum $S_{yAl} := 40ksi$ $E_{Al} := 10000ksi$

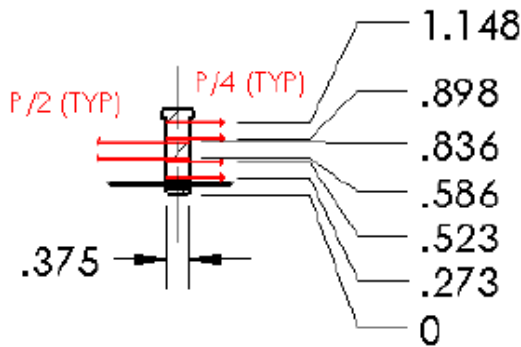The pin has $D_p := 0.375in$ $A_p := \frac{\pi}{4} \cdot D_p^2 = 0.11in^2$ and is $L_p := 1.250in$ long.

It's made of 18-8 STST $S_{ystst} := 42.100ksi$ $S_{utstst} := 90.1ksi$ $E_{stst} := 28000ksi$

The maximum axial force placed on the eccentric strap represents the maximum shear force of this pin.

This junction is basically is pivot in double shear

Cam Holder

Pin

Strap tab

Pin:

$$E := \frac{E_{stst}}{psi} = 2.8 \times 10^7$$

$$I := \frac{\pi}{64}\left(\frac{D_p}{1in}\right)^4 = 9.707 \times 10^{-4}$$

Singularity function:

$$sf(power, a, x) := \begin{vmatrix} \text{if } power = -2 \\ \quad \begin{vmatrix} \text{return } 1 \text{ if } x = a \\ \text{return } 0 \end{vmatrix} \\ \text{if } power = -1 \\ \quad \begin{vmatrix} \text{return } 1 \text{ if } x = a \\ 0 \end{vmatrix} \\ \text{if } power = 0 \\ \quad \begin{vmatrix} \text{if } x \ge a \\ \quad \begin{vmatrix} \text{return } 0 \text{ if } x = a = 0 \\ \text{return } 1 \end{vmatrix} \\ \text{return } 0 \end{vmatrix} \\ \text{if } power \ge 1 \\ \quad \begin{vmatrix} \text{return } (x-a)^{power} \text{ if } x > a \\ \text{return } 0 \end{vmatrix} \end{vmatrix}$$

Mathcad guesses for unknowns:

$C_1 := 8 \quad C_2 := 9 \quad C_3 := 10 \quad C_4 := 11$

$$P := \frac{P}{lbf} = 71$$

104

Load

$$q(x) := \frac{P}{4} \cdot sf(-1, 0.273, x) + \frac{P}{4} \cdot sf(-1, 0.523, x) - \frac{P}{2} \cdot sf(-1, 0.586, x) - \frac{P}{2} \cdot sf(-1, 0.836, x) \ldots$$
$$+ \frac{P}{4} \cdot sf(-1, 0.898, x) + \frac{P}{4} \cdot sf(-1, 1.148, x)$$

Shear

$$V(x) := \frac{P}{4} \cdot sf(0, 0.273, x) + \frac{P}{4} \cdot sf(0, 0.523, x) - \frac{P}{2} \cdot sf(0, 0.586, x) - \frac{P}{2} \cdot sf(0, 0.836, x) \ldots$$
$$+ \frac{P}{4} \cdot sf(0, 0.898, x) + \frac{P}{4} \cdot sf(0, 1.148, x) + C_1$$

Moment

$$M(x) := \frac{P}{4} \cdot sf(1, 0.273, x) + \frac{P}{4} \cdot sf(1, 0.523, x) - \frac{P}{2} \cdot sf(1, 0.586, x) - \frac{P}{2} \cdot sf(1, 0.836, x) \ldots$$
$$+ \frac{P}{4} \cdot sf(1, 0.898, x) + \frac{P}{4} \cdot sf(1, 1.148, x) + C_1 \cdot x + C_2$$

Slope

$$\theta(x) := \frac{1}{E \cdot I} \cdot \left(\frac{P}{4} \cdot sf(2, 0.273, x) + \frac{P}{4} \cdot sf(2, 0.523, x) - \frac{P}{2} \cdot sf(2, 0.586, x) - \frac{P}{2} \cdot sf(2, 0.836, x) \ldots \right.$$
$$\left. + \frac{P}{4} \cdot sf(2, 0.898, x) + \frac{P}{4} \cdot sf(2, 1.148, x) + \frac{C_1}{2} \cdot x^2 + C_2 \cdot x + C_3 \right)$$

Deflection

$$y(x) := \frac{1}{E \cdot I} \cdot \left(\frac{P}{4} \cdot sf(3, 0.273, x) + \frac{P}{4} \cdot sf(3, 0.523, x) - \frac{P}{2} \cdot sf(3, 0.586, x) - \frac{P}{2} \cdot sf(3, 0.836, x) \ldots \right.$$
$$\left. + \frac{P}{4} \cdot sf(3, 0.898, x) + \frac{P}{4} \cdot sf(3, 1.148, x) + \frac{C_1}{6} \cdot x^3 + \frac{C_2}{2} \cdot x^2 + C_3 \cdot x + C_4 \right)$$

Boundary conditions

Given $M(0^-) =$

$$0 = \frac{P}{4} \cdot sf(1, 0.273, 0) + \frac{P}{4} \cdot sf(1, 0.523, 0) - \frac{P}{2} \cdot sf(1, 0.586, 0) - \frac{P}{2} \cdot sf(1, 0.836, 0) \ldots$$
$$+ \frac{P}{4} \cdot sf(1, 0.898, 0) + \frac{P}{4} \cdot sf(1, 1.148, 0) + C_1 \cdot 0 + C_2$$

$$C_2 := Find(C_2) = 0$$

Given $V(0^-) =$

$$0 = \frac{P}{4} \cdot sf(0,0.273,0) + \frac{P}{4} \cdot sf(0,0.523,0) - \frac{P}{2} \cdot sf(0,0.586,0) - \frac{P}{2} \cdot sf(0,0.836,0) \ldots$$
$$+ \frac{P}{4} \cdot sf(0,0.898,0) + \frac{P}{4} \cdot sf(0,1.148,0) + C_1$$

$C_1 := Find(C_1) = 0$

Given $y(0^-) =$

$$0 = \frac{1}{E \cdot I} \cdot \left(\frac{P}{4} \cdot sf(3,0.273,0) + \frac{P}{4} \cdot sf(3,0.523,0) - \frac{P}{2} \cdot sf(3,0.586,0) - \frac{P}{2} \cdot sf(3,0.836,0) \ldots \right.$$
$$\left. + \frac{P}{4} \cdot sf(3,0.898,0) + \frac{P}{4} \cdot sf(3,1.148,0) + \frac{C_1}{6} \cdot 0^3 + \frac{C_2}{2} \cdot 0^2 + C_3 \cdot 0 + C_4 \right)$$

$C_4 := Find(C_4) = 0$

Given $y(L_p^+) =$

$$0 = \frac{1}{E \cdot I} \cdot \left[\frac{P}{4} \cdot sf\left(3,0.273,\frac{L_p}{in}\right) + \frac{P}{4} \cdot sf\left(3,0.523,\frac{L_p}{in}\right) - \frac{P}{2} \cdot sf\left(3,0.586,\frac{L_p}{in}\right) - \frac{P}{2} \cdot sf\left(3,0.836,\frac{L_p}{in}\right) \ldots \right.$$
$$\left. + \frac{P}{4} \cdot sf\left(3,0.898,\frac{L_p}{in}\right) + \frac{P}{4} \cdot sf\left(3,1.148,\frac{L_p}{in}\right) + \frac{C_1}{6} \cdot \left(\frac{L_p}{in}\right)^3 + \frac{C_2}{2} \cdot \left(\frac{L_p}{in}\right)^2 + C_3 \cdot \frac{L_p}{in} + C_4 \right]$$

$C_3 := Find(C_3) = -9.004$

Maximums

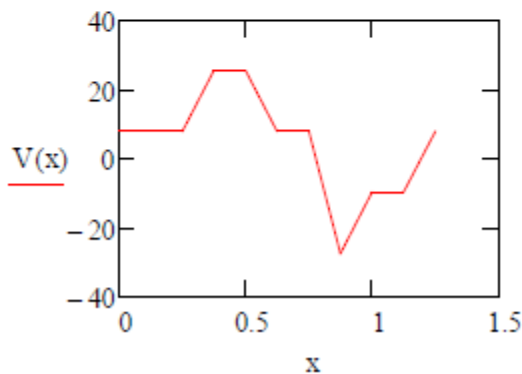$$x := 0, \frac{L_p}{10\,in} \; .. \; \frac{L_p}{in}$$

   Load

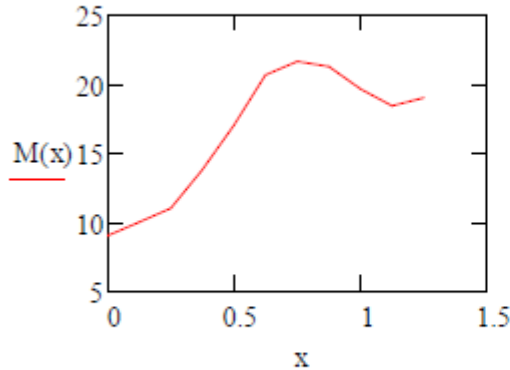The load is equally large at x = 0.586 and 0.836, where q(x) = -34.966.

   Shear

Guess $x_v := 0.875$

Given $\; 0 \le x_v \le 1.25$

$x_{vmin} := \text{Minimize}(V, x_v) = 0.875$

$V_{max} := \left| V(x_{vmin}) \right| \cdot psi = 27.5\,psi$

Moment

Guess $x_m := 0.875$

Given $\; 0 \le x_m \le 1.25$

$x_{mmax} := \text{Maximize}(M, x_m) = 0.836$
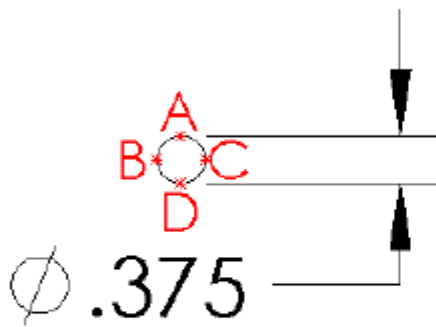
$M_{max} := \left| M(x_{mmax}) \right| \cdot in \cdot lbf = 1.863\,ft \cdot lbf$
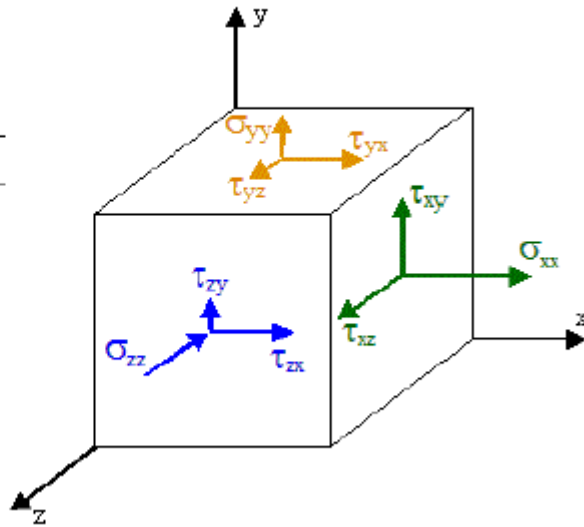
Critical section could happen at x = 0.875 or 0.836.

Bending stress

$$\sigma_{max} := \frac{M_{max} \cdot \dfrac{D_p}{2}}{I \cdot in^4} = 4.319 \times 10^3 \, psi$$

Critical points

Stress cube

$$r := \frac{D_p}{2 \text{in}} = 0.187 \qquad A_{pin} := \frac{A_p}{\text{in}^2} = 0.11 \qquad J := \frac{\pi}{32}\left(\frac{D_p}{\text{in}}\right)^4 = 1.941 \times 10^{-3}$$

$$M_{836} := M(0.836) = 22.362 \qquad V_{836} := |V(0.836)| = 27.5 \qquad T_{836} := 0$$

$$M_{875} := M(0.875) = 21.289 \qquad V_{875} := |V(0.875)| = 27.5 \qquad T_{875} := 0$$

When x = 0.836

$$\sigma_{bendmax836} := \left|\frac{M_{836} \cdot r}{I}\right| = 4.319 \times 10^3 \qquad \tau_{transmax836} := \left|\frac{2 \cdot V_{836}}{A_{pin}}\right| = 497.978$$

$$\tau_{tormax836} := \frac{T_{836} \cdot r}{J} = 0$$

At Point A

$$\sigma_{xx836A} := \sigma_{bendmax836} = 4.319 \times 10^3 \qquad \sigma_{yy836A} := 0 \qquad \sigma_{zz836A} := 0$$

$$\tau_{xy836A} := 0 \qquad\qquad\qquad \tau_{yx836A} := 0 \qquad \tau_{zx836A} := 0$$

$$\tau_{xz836A} := \tau_{tormax836} = 0 \qquad\qquad \tau_{yz836A} := 0 \qquad \tau_{zy836A} := 0$$

Principle normal stresses

$$\sigma_{836A}^3 - C_{2A} \cdot \sigma_{836A}^2 + C_{1A} \cdot \sigma_{836A} - C_{0A} \qquad = 0$$

$$C_{2A} := \sigma_{xx836A} + \sigma_{yy836A} + \sigma_{zz836A} = 4.319 \times 10^3$$
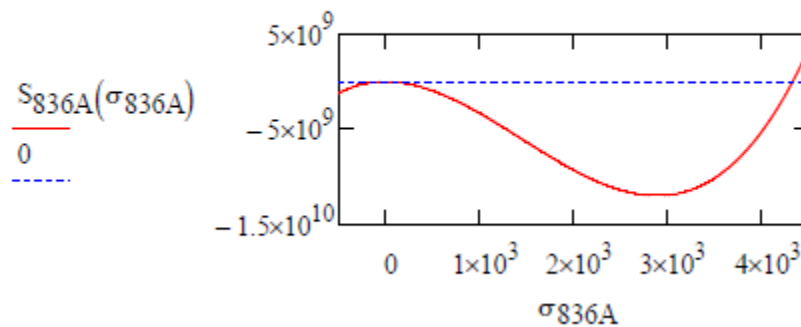
$$C_{1A} := \sigma_{xx836A} \cdot \sigma_{yy836A} + \sigma_{yy836A} \cdot \sigma_{zz836A} + \sigma_{zz836A} \cdot \sigma_{xx836A} \cdots = 0$$
$$+ -\tau_{xy836A}^2 - \tau_{yz836A}^2 - \tau_{zx836A}^2$$

$$C_{0A} := \sigma_{xx836A} \cdot \sigma_{yy836A} \cdot \sigma_{zz836A} + 2 \cdot \tau_{xy836A} \cdot \tau_{yz836A} \cdot \tau_{zx836A} \cdots \qquad = 0$$
$$+ -\sigma_{xx836A} \cdot \tau_{yz836A}^2 - \sigma_{yy836A} \cdot \tau_{zx836A}^2 - \sigma_{zz836A} \cdot \tau_{xy836A}^2$$

$$S_{836A}(\sigma_{836A}) := \sigma_{836A}^3 - C_{2A} \cdot \sigma_{836A}^2 + C_{1A} \cdot \sigma_{836A} - C_{0A}$$

Guess   Root

$$\sigma_{836A} := -1 \qquad r_{836A1} := \text{root}(S_{836A}(\sigma_{836A}), \sigma_{836A}) = -1.334 \times 10^{-5}$$

$$\sigma_{836A} := 1 \qquad r_{836A2} := \text{root}(S_{836A}(\sigma_{836A}), \sigma_{836A}) = 1.333 \times 10^{-5}$$

$$\sigma_{836A} := 3500 \qquad r_{836A3} := \text{root}(S_{836A}(\sigma_{836A}), \sigma_{836A}) = 4.319 \times 10^3$$

$$\sigma_{836A1} := r_{836A3} = 4.319 \times 10^3$$

$$\sigma_{836A2} := r_{836A2} = 1.333 \times 10^{-5}$$

$$\sigma_{836A3} := r_{836A1} = -1.334 \times 10^{-5}$$

Principle shear stresses

$$\tau_{836A13} := \frac{\left| \sigma_{836A1} - \sigma_{836A3} \right|}{2} = 2.16 \times 10^3$$

$$\tau_{836A21} := \frac{\left| \sigma_{836A2} - \sigma_{836A1} \right|}{2} = 2.16 \times 10^3$$

$$\tau_{836A32} := \frac{\left| \sigma_{836A3} - \sigma_{836A2} \right|}{2} = 1.333 \times 10^{-5}$$

$$\tau_{836Amax} := \max\left(\tau_{836A13}, \tau_{836A21}, \tau_{836A32} \right) = 2.16 \times 10^3$$
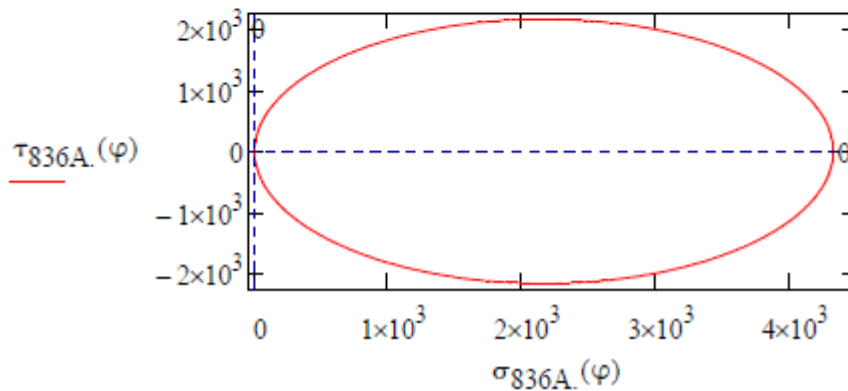
Mohr's Circle

$$r_{836A} := \sqrt{\left(\frac{\sigma_{836A1} - \sigma_{836A2}}{2} \right)^2 + \tau_{836Amax}} = 2.16 \times 10^3$$

$$\varphi := 0, 0.01 .. 2\pi$$

$$\sigma_{836A}(\varphi) := \frac{\sigma_{836A1} + \sigma_{836A3}}{2} + r_{836A} \cdot \cos(\varphi)$$

$$\tau_{836A}(\varphi) := r_{836A} \cdot \sin(\varphi)$$

Mohr's Circle, x = 0.836, Point A

...

The same method was used for points B, C and D at x = 0.836

...

When x = 0.836, stresses are equal at points A and C, and points B and D.

Von Mises stresses at A and B when x = 0.836:

$$\sigma_{vm836A} := \sqrt{\sigma_{836A1}^2 - \sigma_{836A1} \cdot \sigma_{836A2} + \sigma_{836A2}^2} = 4.319 \times 10^3$$

$$\sigma_{vm836B} := \sqrt{\sigma_{836B1}^2 - \sigma_{836B1} \cdot \sigma_{836B2} + \sigma_{836B2}^2} = 497.978$$

...

The same method was used for points A, B, C and D at x = 0.875.

...

When x = 0.875, stresses are equal at points A and C, and points B and D.

Von Mises stresses at A and B when x = 0.875:

$$\sigma_{vm875A} := \sqrt{\sigma_{875A1}^2 - \sigma_{875A1} \cdot \sigma_{875A2} + \sigma_{875A2}^2} = 4.112 \times 10^3$$

$$\sigma_{vm875B} := \sqrt{\sigma_{875B1}^2 - \sigma_{875B1} \cdot \sigma_{875B2} + \sigma_{875B2}^2} = 497.978$$

The largest Von Mises stress is at x = 0.836 (the critical section) at point A (the critical point).

$$\sigma_{pinmax} := \sigma_{vm836A} \cdot psi = 4.319 \times 10^3 \, psi \qquad N_{pin} := \frac{S_{ystst}}{\sigma_{pinmax}} = 9.747$$